University of Cape Town

Doctoral Thesis

pQCD Energy Loss and Thermal Field Theory in Small Systems

Author:
Isobel Kolbé

Supervisor:
Dr. W. A. Horowitz

A thesis submitted in fulfillment of the requirements for the degree of Doctor of Philosophy

in the

Department of Physics

University of Cape Town

May 31, 2019

The copyright of this thesis vests in the author. No quotation from it or information derived from it is to be published without full acknowledgement of the source. The thesis is to be used for private study or non-commercial research purposes only.

Published by the University of Cape Town (UCT) in terms of the non-exclusive license granted to UCT by the author.

University of Cape Town

Declaration of Authorship

I, Isobel Kolbé, declare that this thesis titled, "pQCD Energy Loss and Thermal Field Theory in Small Systems" and the work presented in it are my own. I confirm that:

- This work was done wholly while in candidature for a research degree at this University.
- Where any part of this thesis has previously been submitted for a degree or any other qualification at this University or any other institution, this has been clearly stated. In particular, please see the comment to part II.
- Where I have consulted the published work of others, this is always clearly attributed.
- Where I have quoted from the work of others, the source is always given.
- I have acknowledged all main sources of help.
- Where the thesis is based on work done by myself jointly with others, I have made clear exactly what was done by others and what I have contributed myself. For details, please see the comments to parts II and III.

Signed: Signed by candidate

Date: 11/06/2019

UNIVERSITY OF CAPE TOWN

Abstract

Faculty of Science

Department of Physics

Doctor of Philosophy

pQCD Energy Loss and Thermal Field Theory in Small Systems

by Isobel KOLBÉ

In recent years, experiments at the Large Hadron Collider and the Relativistic Heavy Ion Collider have discovered that many of the signatures that are traditionally ascribed to the presence of a quark-gluon plasma (QGP) in central heavy-ion collisions also manifest in certain classes of peripheral heavy-ion collisions as well as in smaller colliding systems. The glaring exception to this list of observations of QGP signatures in small systems is the partonic energy loss. However, current theoretical descriptions of partonic energy loss are ill-adapted to small systems. This thesis first presents a numerical analysis of an analytical small system extension of a standard energy loss formula, and finds that major inconsistencies in the description of small system energy loss persist, motivating a need for a first principles calculation of the properties of a small droplet of QGP. Thereafter, a first step toward such a calculation is presented by considering a single, massless, scalar field that has been geometrically confined by means of Dirichlet boundary conditions. This toy model reveals, via thermal field theoretic techniques, that quantum fields are very sensitive to the presence of a boundary, presenting significant deviations from the Stefan-Boltzmann limit and revealing a geometrically driven phase transition at the scale of the medium.

Acknowledgements

Studying fundamental physics has always been something I wanted to do, but no amount of imagination could ever have predicted the spectacular life I've lived the last four years. It is without a doubt almost entirely A/Professor W. A. Horowitz's fault that my life has become a fairy tale. I don't think I could ever adequately express my gratitude to Will for the endless list of privileges he has hurled at me for four years, from sending me to conferences and schools all over the world, to teaching me how best to use my time, and the extreme care and dedication to my physics education. Thank you Will, for all the things you have done, and continue to do to guide and teach me.

There is another person who contributed significantly to my physics education and without whom this thesis cannot exist in its current form. Dr. Sylvain Mogliacci's supervision and support has been invaluable. Sylvain, thank you for showing me that it is possible to not lose factors of two. Thank you for teaching me much of the physics in this thesis, for always being willing to discuss physics with me, and for becoming both a supervisor and a friend. I have truly enjoyed working with you.

I'm not at all sure how people who don't have their own Cobi manage to cope with anything in life, let alone a Ph. D., but I certainly would not have been able to make use of the opportunities that Will created for me had it not been for my now-husband, Jacobus Botha. It is true that having someone at home who did the washing and the cooking while I worked was extraordinarily useful, but the real value was in the encouragement when the path ahead seemed impregnable, in the celebrations of small victories and the unfailing faith in me. Cobi, sonder jou sou ek nooit die moed gehaad het hiervoor nie en ek sou dit virseker nie kon doen nie. Baie dankie dat jy my trane af gevee het, 'n glimlag op my gesig gesit het en saam met my hierdie pad gestap het.

The physics department at UCT created an environment in which I was able to thrive. Thank you Andy for always being willing to listen and help, thank you Jill for impeccable administrative support, and thank you to the lecturers and students in the department for welcoming me and always answering my questions. I have two friends who also provided shoulders for my tears and endless support, even though neither is in my physics department, Daan Burger and Camille Hall. Daan, dankie vir al die koppies koffie en die lekker moans, hulle het baie van die moeilikke tye draaglik gemaak. Cam, thank you for the after-work drinks and long voicenotes, they meant the world to me. I am also grateful to the friendship from Catch22, for making me feel welcome in Cape Town.

Finally, I'm indebted to my family. Thank you to my parents, who always encouraged me to pursue my dream of becoming a physicist, for always being willing to help in whichever way they could, and thank you to my sister for being a constant anchor and a close friend. Ma en Pa, baie dankie vir alles wat ma'le al deur die jare gedoen het. Lies, dankie vir die lang kuiers en al jou ondersteuning.

Contents

List of Figures

Aan my splinter nuwe man.

Preface

Apart, perhaps, from Power, it is mankind's incessant desire to understand itself and its own context, that has driven the greatest of its endeavors. Though we might cower at the thought of our own insignificance, we are fundamentally curious. As a little girl I found myself, flat on my back in the family churchyard, staring up at the stars - frustrated because I had not been able to read the text accompanying pictures of the planets in my mother's books. I vowed to one day know everything there is to know about the great big universe. Although the language has since changed, the basic questions of my illiterate childhood mind have remained the same, and today my interest still lies in decrypting the structure of the universe.

The study of nature has long been the exclusive endeavor of those individuals favored by the inevitable structural inequalities of society. It has been a particularly fantastic honor to count myself among those fortunate enough to have the opportunity and means to undertake the task of peeling back the veil of ignorance and glimpsing the mind of God. But modern science does not place individuals on ridiculous pedestals, glorifying arrogance and, oftentimes, blatant theft. Instead, it advances through truly gigantic, multinational endeavors that bring anything from dozens to thousands of great minds together to wrestle the secrets of Nature from Her stubborn grip. In this thesis you will find my tiny contribution to what is the largest scientific endeavor of all time.

Part I

The phenomenology of small systems

"Darkness crept back into the forests of the world. Rumour grew of a shadow in the East, whispers of a nameless fear..."

- Galadriel, The Lord of the Rings, *J. R. R. Tolkien*

Chapter 1

Evidence, and lack thereof

The discovery by Ernest Rutherford of the structure of the atom [1] ushered in an unprecedented era of discovery, but, since then, physicists have developed precious few techniques that differ appreciably from Rutherford, who proclaimed to Freeman Dyson: "We're like children who always want to take apart watches to see how they work" [2]. Perhaps that is simply because, armed with enough money, these methods work exceptionally well, and have led to remarkable discoveries about the structure of nature. Inspired by the success of the apparently brutish approach of rather violently breaking up objects, scientists around the world have built ever larger particle colliders. Today, the largest of these is the Large Hadron Collider (LHC) at CERN in Switzerland, followed closely by the Relativistic Heavy Ion Collider (RHIC) at Brookhaven National Laboratory (BNL) in the United States.

RHIC and LHC collide a myriad of particles, ranging from protons to lead nuclei, at such high energies that the produced material has a temperature 100 000 times that of the center of the sun [3]. The produced densities are ten times higher than normal nuclear matter; the very smallest constituents of the every-day objects around us are forced into a state with properties not unlike the properties of the universe a few micro-seconds after the big bang [4] – the quark-gluon plasma (QGP).

The story of the discovery of the QGP, although replete with drama, was not a single dramatic discovery, but rater an amalgamation of observables that are best understood collectively as resulting from the production of a QGP. The experiments at these super-colliders have yielded colossal amounts of data that have been analyzed by thousands of experimentalists around the world, resulting in half a dozen monumental discoveries, a Nobel prize, and countless fatal blows to tentative theories of nature. But, in the wake of the discovery of the Higgs boson, as the LHC enters an era of precision measurements of known particles and phenomena, a shadow stirs in the results from calibration experiments.

The reader will not find an exhaustive review of heavy-ion experiments in this section, but it is hoped that, by the time the reader reaches the end of it, the results presented here will provide the reader with some idea of the unease within the field, fueled by the desperate need for theoretical control over small colliding systems.

1.1 The experimental checklist

The idea that the quarks that are confined in normal nuclear matter can be forced into a free state by very high temperatures or densities has been around since the late seventies [5–7]. Today we understand this material to be a quantum-chromodynamical (QCD) analogue to the electromagnetic plasma phase of ordinary matter, in which partons carrying color charge are able to move freely within a localized volume while in near thermal equilibrium. However, eluding understanding, and with a $\$1,000,000$ prize on its head, a major hurdle to "observing" the QGP is the phenomenon of confinement. Although we currently do not understand precisely why, the fact is that no single, free quark has ever been observed. Quarks appear in well-documented groupings as hadrons, but the QGP is an entirely new phase of matter in which the quarks and gluons are able to move beyond the confined structures of the hadrons. As such, any observation of the QGP through detectors that can only measure photons, leptons, and hadrons, must be, in some sense, indirect.

In 2004, an empirical answer to the question "How will we know if we've created a QGP?" was proffered [8], a conclusion which was drawn from years of theoretical study and data from experiments at BNL and CERN. The suggestion was that, if experiments could simultaneously offer evidence of the bulk, long-range characteristics of the QGP, along with the short-range perturbative properties of individual elements of the medium, and do so in the presence of a well-understood control experiment in which neither the bulk nor the short-range signatures were observed, then one might safely claim the discovery of a QGP.

Of course, in practice, this meant that far more than three observations needed to be made, since each requirement (the bulk properties, the individual properties, and a control experiment) led to more than one experimental consequence; from a bulk perspective, one might expect to see a large energy density, an increase in the entropy (as the hadronic degrees of freedom give way to QCD degrees of freedom), strangeness enhancement, and long-range particle correlations, perhaps manifesting in radial and elliptic flow or the famous "ridge" structure. Meanwhile, from a short-range perspective, one would look for evidence of modification of particle properties due to the presence of the medium, such as the modification of particle widths or abundances due to color screening, or the energy loss of a particle as it traverses the medium. The control experiment is meant to bring under control effects due to the fact that a large nucleus, like that of gold or lead, will have dramatically different properties to a proton, even in the absence of a QGP, and it is imperative that such "cold nuclear matter" effects are well understood before studies of the QGP may commence in earnest. One approach to constraining cold nuclear matter effects is to apply the analyses that lead to the observation of QGP signatures in nucleus-nucleus (AA) collisions to proton- or deuteron-nucleus ($pA\,/\,dA$) collisions, so that the properties of a nucleus might be studied without the risk of creating a QGP.

1.2 Control experiments

It is perhaps prudent to start with the control experiment and a discussion of its necessity. Apart from the obvious scientific requirement of a control experiment in any measurement, the observation of the QGP is marred by a range of known and unknown pitfalls that need to be brought under control; by trying to study the QGP, we are attempting to study the strong force in an asymptotically free environment that, we believe, has not existed in the known universe since a microsecond after the big bang[1], and we are attempting to do so by colliding hundreds of nucleons, all interacting through the strong force while still *confined*. Although the strong force is known to have a short range, it is also known that the strong force is modified by the presence of other nucleons (for instance, the energy required to separate the proton from the neutron in deuterium is 2 MeV while one would need 30 MeV to separate the nucleus of a ^{4}He atom in four [10, Ch.6.1]; even the mass of the proton far exceeds the combined masses of its three constituent quarks [11, Ch. 4.5]).

Furthermore, at the energies provided by modern-day accelerators, we are no longer "simply" dealing with a superposition of nucleons all modifying the strong force, but instead must consider the presence of a cloud of valence quarks and gluons, the latter (due to gluon splitting and fusion) possibly precipitating into the color-glass condensate [12, 13], to which we can add the energy density fluctuations of nucleons [14], all before a single drop of QGP has been created. In any given AA collision, we have precious little information about the initial state that evolves into a QGP and we may ask a great many questions, including: What is the energy-density profile of the nucleus before the collision? What is the probability of an interaction occurring between two quarks? How many times can one quark interact with the quarks of another nucleus? How close do two nuclei have to get to interact? In short, how is the nucleus modified by the presence of hundreds of nucleons at relativistic energies and how does an AA collision, in the absence of a QGP, differ from, say, a pp collision?

Some of these questions may be answered by colliding a proton or a deuteron into a heavy nucleus, probing the nucleus much as Rutherford probed the atom. It is in this attempt to quantify the properties of the nucleus before the production of the QGP, that a range of pA/dA experiments at RHIC and the LHC were performed [15, 16]. RHIC has added a wider range of collision systems to the pot of evidence, including ^3HeAu as well as an energy scan of dAu. Along with the pp runs of the LHC and peripheral AA collisions, these events became collectively known as the "small colliding systems", and they are challenging many accepted ideas in heavy-ion physics.

[1] There is some evidence that quark matter may exist at the centers of neutron stars [9], but the recent discoveries of neutron stars with masses of up to, and even above, two solar masses have constrained the known equations of state (EsOS) to such a degree that the majority of EsOS that include quark matter have been ruled out. Nevertheless, the possibility exists, although it has not yet been conclusively proven and, in any event, the necessarily "cold" quark matter that would exist at the center of a neutron star is a different beast from the hot and thermal primordial soup.

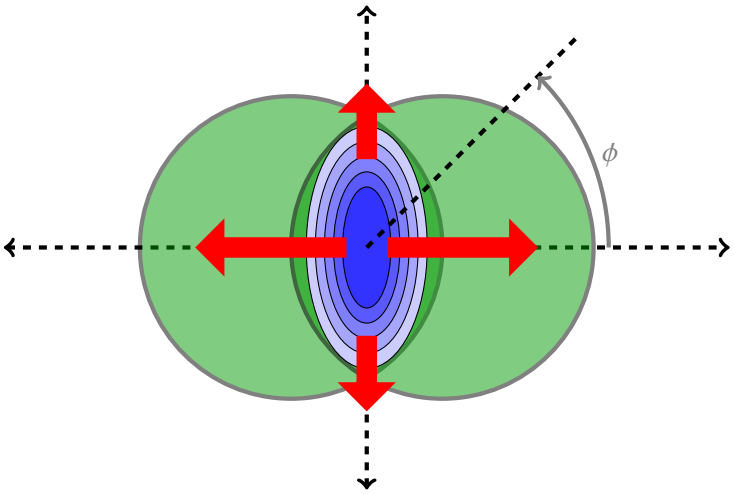

FIGURE 1.1: (Drawn by the author) The reaction plane in a typical heavy ion collision, showing the almond shaped overlap, pressure gradients, and direction of momentum transfer, as well as the azimuthal angle, ϕ.

1.3 Bulk, collective observables

This section will not provide an exhaustive list of bulk observables, but will provide some background on two crucial observables that both motivate the present thesis and are considered necessary observations in any claim of the presence of a QGP.

It was originally thought that the QGP would behave like a gas of free quarks and gluons [17]. However, RHIC discovered that that their data is best described by the presence of a perfect fluid [13]. The discovery of the perfect fluidity is an inference made from the fact that hydrodynamical models describe the manner in which the collective behavior of the fluid propagates an initial spatial anisotropy into final state momentum anisotropy [18][2]. Since many nucleus-nucleus collisions are off-center, the overlap region is most often almond-shaped (not spherical). Therefore, the difference in pressure gradients in the short direction of the almond as compared to the pressure gradients in the long direction provide particles with more momentum in the short direction than in the long direction [26], see fig. 1.1.

One may quantify this momentum anisotropy by considering the coefficients of the Fourier expansion of the angular distribution (in azimuthal angle in the event plane, equivalently ϕ or $\Delta\phi$) of produced particles (which my also depend on the transverse momentum p_T and the rapidity y), leading to what is known as the "flow" coefficients [27], v_1, v_2, v_3, etc:

$$\frac{d^3N}{d\phi dp_T dy} \propto \left[1 + 2v_1(p_T, y)\cos(\phi) + 2v_2(p_T, y)\cos(2\phi) + \cdots\right]. \tag{1.1}$$

[2] Although hydrodynamics has been immensely successful in its description of collective behavior (see for instance [19], but also virtually any experimental collective behavior result that compares to theory), it does not monopolize the field. There are, for instance, kinetic and transport models that reproduce some of the results as well (for example [20–25]), even though the underlying physics is fundamentally different. As such, we know only that observables such as v_2 appear to be most sensitive to the initial condition and not too sensitive to the mechanism whereby the initial geometry and fluctuations are propagated into momentum anisotropies.

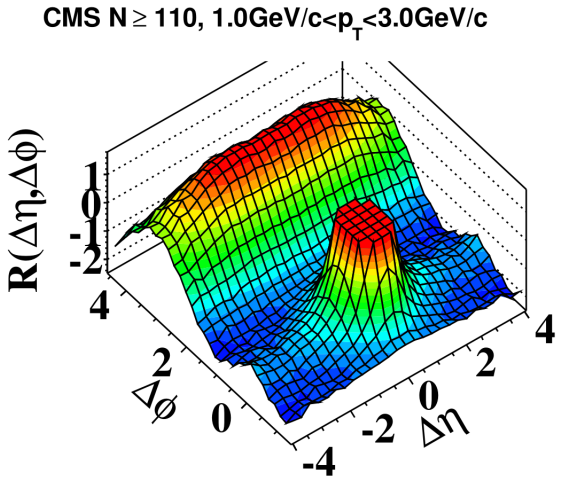

FIGURE 1.2: The 2010 CMS result that inspired a closer look at small systems, showing the two particle correlation function as a function of azimuthal angle ($\Delta\phi$) and pseudorapidity ($\Delta\eta$) and revealing the small, but noticeable, ridge structure along $\Delta\phi = 0$ [48].

While there are infinitely many such coefficients, it is easy to interpret the second, v_2, as an elliptical flow coefficient, and the third, v_3, as a triangular flow coefficient, as their magnitude can be interpreted as a signal of both the initial distribution of the energy density and the bulk evolution [27]. In this way, one might quantify the effect of collective flow

There is a wealth of experimental data on the flow coefficients in AA collisions, at a range of beam energies, nucleus- and hadron species, transverse momenta, rapidities, and centralities (see for instance [28–40]). The mass dependence of the flow coefficients (see for instance [33, 38–43]) is understood to imply that the effect is due to "early time" dynamics (by which is meant that the flow effect is due to the collective partonic behavior of a QGP rather than some effect at the later, hadronic stages) [44], and coefficients higher than v_2 and v_3 have been measured along with higher order cumulants [45–47], which investigate correlations between higher numbers of particles.

The first signs of trouble came in the form of "the ridge." In 2010, the CMS collaboration published a result that hinted at the presence of a structure in the two particle correlation function in very high multiplicity pp collisions [48] that was highly reminiscent of heavy ion collisions, and is shown in fig. 1.2. The LHC ran pPb experiments in 2011 and a positive cascade of measurements of the ridge and flow coefficients followed, both from reevaluations of RHIC data and from the other experiments at the LHC. Figure 1.3 shows the ridges that were seen by CMS, ALICE and ATLAS in pPb, but all manner of long range correlations have also been measured [33, 47, 49–56] and the need for a more precise understanding has brought to the forefront precision ideas such as energy density fluctuations in the proton [57].

Complimenting the ridge results was a slew of measurements of flow coefficients in small systems, two of which are shown in fig. 1.4. In fig. 1.4a, we see the pronounced v_3 in ^3HeAu collisions, which forms part of a collection of measurements performed at RHIC meant to probe the effect of the initial geometry by creating differently shaped initial energy density distributions through choice of projectile, in this case, a decidedly triangular ^3He nucleus.

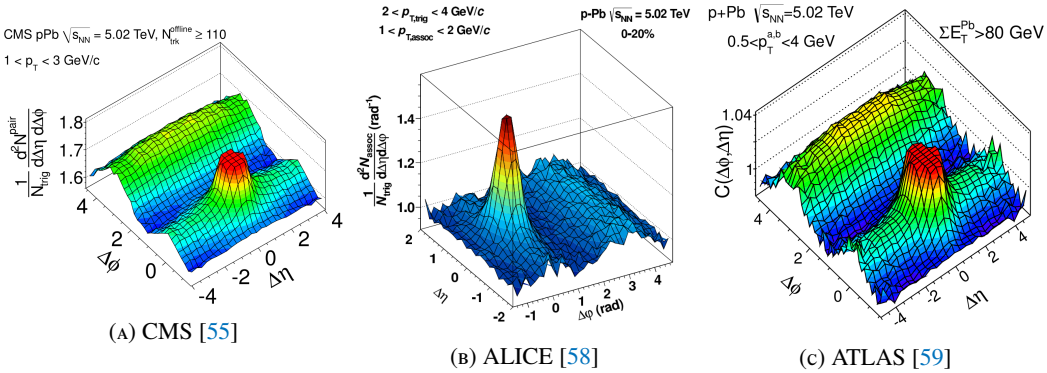

(A) CMS [55] (B) ALICE [58] (C) ATLAS [59]

FIGURE 1.3: Two particle correlation functions in high multiplicity *pPb* collisions at the LHC, showing the ridge at $\Delta\phi \sim 0$. The CMS and ALICE results express the correlation function $C(\Delta\phi, \Delta\eta)$ of ATLAS in terms of the associated yield, but the interpretation is the same.

The striking feature of fig. 1.4b is that all the higher cumulants of v_2 appear to be identical, a very strong motivation for collective behavior [51].

A second important observable that may be ascribed to the statistical and large scale nature of the QGP is strangeness production. In principle, due to the temperature of the QGP being higher than the mass of the strange quark, strange quarks are produced in much larger numbers in the QGP than in normal, cold nuclear matter; thus, in the presence of a QGP, one expects to see an excess of strange hadrons (hadrons containing at least one strange quark)[60]. This, in fact, was the measurement that prompted the first declaration of the discovery at CERN of the QGP [61]. It should be noted that the study of strangeness enhancement is complex, the production being subject to a range of effects, including, for instance, "canonical suppression," whereby the production of strangeness in small systems is subject to strangeness conservation. Strangeness conservation suppresses the number of strange quarks produced in small volumes, so that a false enhancement may be observed by simply increasing the interaction volume and making the effect of strangeness conservation negligible [62, 63]. Questions surrounding the thermodynamic limit become crucial here, but it appears as though very high-multiplicity *pp* might well reach a region in which one finds ensemble equivalence [64] and is therefore not hindered by canonical suppression.

Strangeness production is most easily seen from particle ratios or yields per participating nucleon (see, for example, [65–67])[3]. Strangeness enhancement had already been measured in *AA* at NA49 [68] and WA97 [65] in the '90's, but at the time the interpretation was not that this enhancement was due to the presence of a QGP. (This time-period in strangeness study has been extensively reviewed; see, for instance, [69] and in the modern perspective

[3] Some measurements show the strangeness enhancement using an "Enhancement Ratio" of the yield in a particular phase space window Y, for example [66]

$$E = \frac{\left(\frac{Y}{\langle N_{wound}\rangle}\right)_{PbPb}}{\left(\frac{Y}{\langle N_{wound}\rangle}\right)_{pBe}}, \tag{1.2}$$

but again, $E \nsim 1$ would indicate the presence of an effect not taken into account by a simple nucleonic scaling.

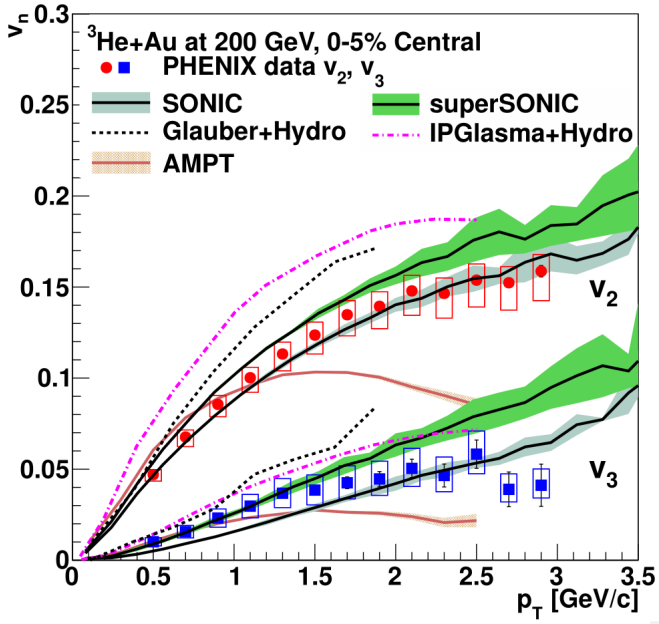

(A) PHENIX measurement of v_2 and v_3 in ^3HeAu as a function of transverse momentum, comparing to a number of theoretical predictions [54].

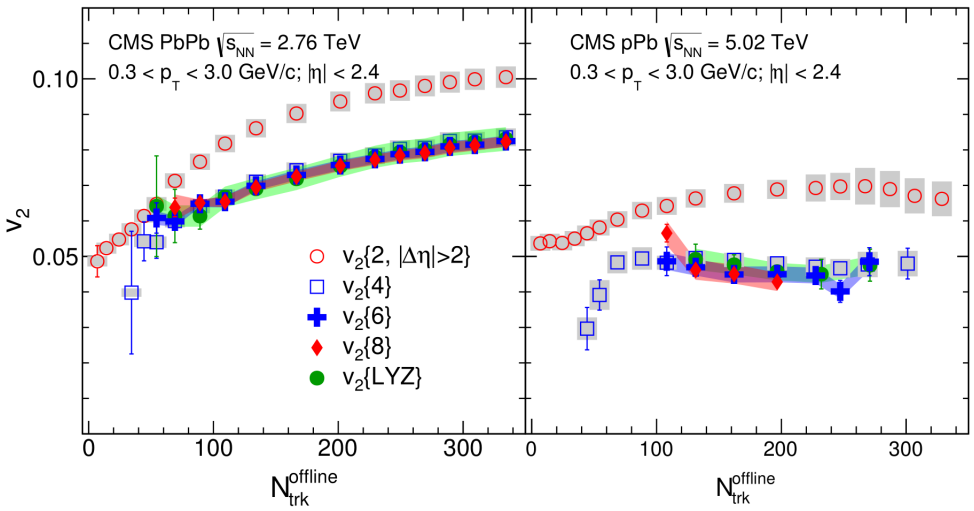

(B) CMS measurement of N-particle v_2 cumulants. Notice that, in pPb, as in $PbPb$, the higher cumulants are identical [51].

FIGURE 1.4: Two striking flow harmonic results from small systems.

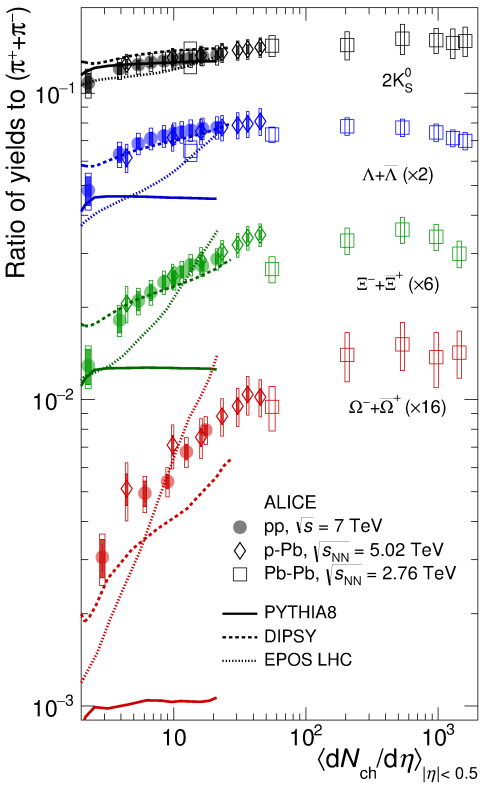

FIGURE 1.5: Particle yields for various strange and multi-strange hadrons at ALICE, showing the relatively smooth transition from *pp* through *pPb* and into *PbPb*[73].

[70].) However, the very recent discovery by the ALICE collaboration of strangeness enhancement in *pp*-collisions, meriting a spot in Nature Physics [71], has certainly bolstered other measurements of strangeness enhancement in small colliding systems [71–76]. The plot in fig. 1.5 shows a particularly striking result from the ALICE collaboration; presented are the particle yields of a range of strange hadrons as a ratio of other very abundant particles, showing that the strangeness enhancement depends on the multiplicity of the event, the data smoothly flowing from *pp* through *pPb* and into *PbPb*.

The presence of strangeness enhancement and directed flow[4] constitute a convincing argument for the observation of the bulk properties of the QGP in high multiplicity events in small systems – one could argue that one of the three experimental boxes has been ticked.

1.4 Short range observables

Again, this section will not present an exhaustive list of short range observables, but will aim to present those results that represent (a very subjective and biased list of) important motivations for the heavy-ion community's interest in partonic energy loss in small systems: one of the major predictions for the way in which partons are modified due to the presence of the medium, which played a crucial role in the discovery of the QGP in central *AA*-collisions, is ominously absent in smaller colliding systems.

[4]For more comprehensive reviews, see for instance [77, 78]

The first observable in this section is the phenomenon of jet-quenching and particle suppression. The first prediction came from Bjorken [79], but in the years since, a wide range of calculations have appeared that predict the manner in which a hard parton produced along with the medium will lose energy due to color interactions as it traverses the medium. These may be broadly categorized by the way that the distribution of gluon radiation is computed and approximated [80] and are commonly known for their original authors; the DGLV (for Djordjevic, Gyulassy, Lévai and Vitev) approach (focused on in part II of this thesis and elaborated on more there) [81–88], as well as BDMPS-Z (for Baier, Dokshitzer, Mueller, Peigné, Schiff, and, independently, Zakharov) [89–97], ASW (for Armesto, Salgado, and Wiedemann) [98–101], AMY (for Arnold, Moore, and Yaffe)[102–104] and Higher-Twist [105–108]. In the presence of a QGP, one expects to observe both the quenching of back-to-back jets and the suppression of partons with high transverse momentum.

The second is screening. The idea that the well-known effect in electromagnetic plasmas of charge (or Debye) screening must have an analogue in a plasma of free color charges led to the prediction that certain kinds of mesons would dissociate in the QGP [109], thereby lowering their expected abundances. More precisely, if the plasma reaches a temperature that is higher than the binding energy of, say, the J/ψ-meson, which consists of a charm and an anti-charm quark bound together (a $c\bar{c}$-pair), not only will the $c\bar{c}$-pair melt, but the individual quarks will be screened from each other in the plasma, preventing the pair from reforming. In this way, the abundance of J/ψ was predicted to be suppressed in the presence of a QGP, when compared to an appropriately normalized pp result[5].

An extraordinarily useful quantity for measuring the modification of a parton due to the presence of a medium is the nuclear modification factor, R_{AA} [110, 111]:

$$R_{AA} = \frac{d^2\langle N_{AA}\rangle/dydp_T}{N_{coll}\cdot d^2d\sigma_{pp}/dydp_T} \tag{1.3}$$

allowing for the quantitative analysis of the difference between an AA-collision and a pp-collision, by dividing the yield of a particular rare event of incoherent production (say, the number of jets, or J/ψ particles) in an AA-collision, by the yield of the same event in a pp-collision, and normalizing appropriately using the mean number of binary collisions, $\langle N_{coll}\rangle$ [6] . It is precisely this normalization that needs to be done carefully, at first simply involving a Glauber calculation of the number of binary collisions (see, for instance, early measurements at RHIC [112]), but later involving a slightly more involved nuclear overlap function, $\langle T_{AA}\rangle$

[5] This effect is also applicable to other quarkonia like the Y-meson, which consists of a $b\bar{b}$ pair, as well as to higher excited states of quarkonia.

[6] One often sees a slightly different quantity that also goes by the name of "nuclear modification factor", but is defined

$$R_{CP} = \frac{\langle N_{coll}\rangle_{peripheral}}{\langle N_{coll}\rangle_{central}}\frac{\left(\frac{d^2N}{dp_Td\eta}\right)_{central}}{\left(\frac{d^2N}{dp_Td\eta}\right)_{peripheral}}, \tag{1.4}$$

which compares the yield in a central event to that in a peripheral event of the same colliding system, thereby avoiding the need for a reference pp data set, which often does not exist at the same energy and therefore needs to be extrapolated, increasing the systematic error. Nevertheless, the interpretation is the same; $R_{CP} \sim 1$ in the absence of a medium.

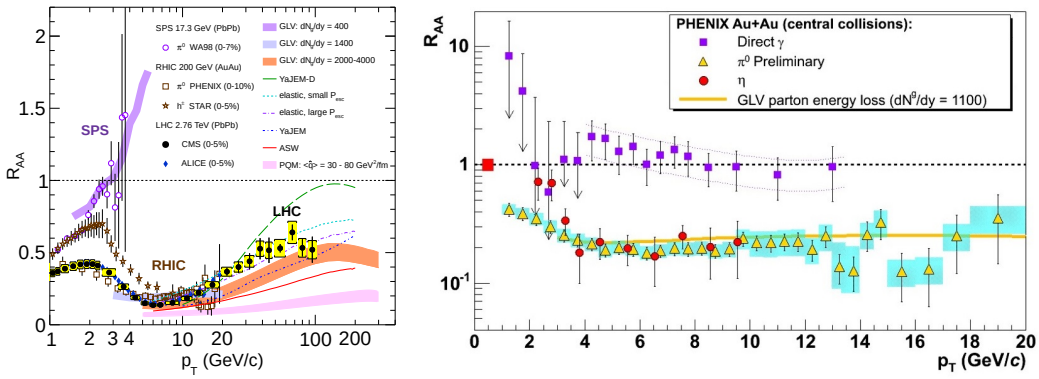

(A) [113] (B) [114]

FIGURE 1.6: Nuclear modification factors as a function of transverse momentum of charged hadrons ($h^{\pm}$), neutral pions π^0, charged particles, η-mesons and photons at (A) a range of different center-of-mass energies and (B) showing the transparency of the medium to photons, along with a number of theoretical calculations. See [113, 114] and references therein for origin of data and theory.

(as in [113].) This evolution of the normalization comes on the back of an ever deeper understanding of the nature of the cold nucleus and how it differs appreciably from a simple superposition of nucleons. An $R_{AA} \sim 1$ would indicate the absence of any modification so that one may conclude that the particular measurement being scrutinized in AA is simply a well-normalized superposition of pp events with all cold nuclear matter effects under control.

A note on multiplicity: Multiplicity is an inherently problematic parameter. Most importantly for the purposes of the present thesis, theoretical models have as an input, not the multiplicity of the event, but rather, the number of participants, N_{part}, easily related to the size of the interaction region or the volume of interacting nucleons. At the multiplicities involved in central AA-collisions at the LHC ($\sim$ 25000 particles [115]), one may neglect non-geometrical fluctuations of multiplicities, and Glauber models therefore offer a simple relationship between N_{part} and the multiplicity of the event. However, in small colliding systems, even high multiplicity events can only ever hope to produce a hundred or so particles [74], causing far more pronounced fluctuations in the geometry, as well as significant fluctuations in the energy density profile within the fluctuating geometries. In this regime then, the relationship between N_{part} and the multiplicity is far less direct [116]. The problem arises from an inherent bias when choosing high multiplicity events - one cannot know whether the 100 particles are produced by a dozen soft interactions, or a handful of hard interactions that have decayed into a hundred soft particles. It is therefore difficult to determine how central the event was and therefore, how many participants there were and, crucially, whether or not enough particles were created to form a free, thermalized, QCD medium [117]. Furthermore, the number of participant nucleons and the number of binary nucleon-nucleon collisions, N_{coll}, are not necessarily the same and, in fact, their relationship scales with the energy of the collision. The ALICE collaboration has shown striking results [118], showing how biases from event selection and collision geometry can cause an apparent suppression.

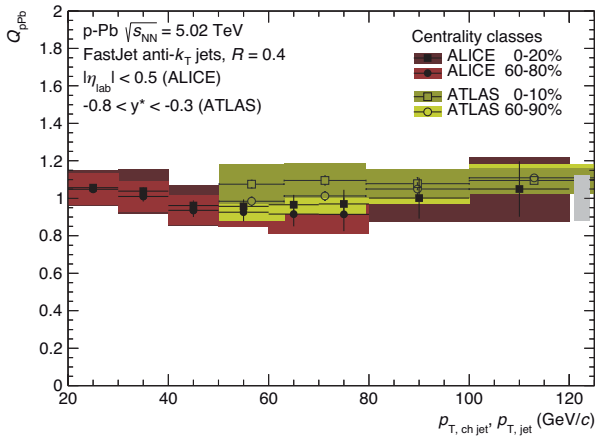

FIGURE 1.7: The nuclear modification factor for charged and full jets as measured by ATLAS [157] and ALICE [158] as function of p_T in different centrality classes of pPb, where Q_{pPb} is an observable which corrects for a number of biases and is to be interpreted in the same way as R_{pPb}.

Nevertheless, the ALICE collaboration [116] has put in a tremendous effort to overcome the afore mentioned biases, including using detectors that are virtually on the beam (the zero-degree calorimeter) to determine how "bruised" the nucleus is after it has collided with a proton, thereby inferring the centrality (and therefore the number of participants) of the event without relying on the raw multiplicity. Their endeavors allow for crisper discussions of centrality dependent measurements.

In AA-collisions, R_{AA} has been extremely useful, providing clear evidence of both jet-quenching (see, for example, [113, 114, 119–132]) and J/ψ (and $\psi(2S)$) screening (for instance, [133–139]). As examples of this body of experimental results concerning short range effects of the medium, consider fig. 1.6, showing the remarkable success of theoretical predictions and abundance of experimental data available for measurements of R_{AA} [7].

After the first observations of non-zero v_2 of low momentum particles in small colliding systems, the natural next step was to search for jet-quenching and quarkonia melting in these same data sets. In small colliding systems at CERN [144–154], and BNL [155], tantalizing evidence exists for J/ψ, Y, and their excited states' suppression in the A-going direction in pA. Although it is not possible from the suppression patterns of J/ψ to conclude whether or not cold nuclear matter (CNM) effects are responsible[8], the additional suppression of $\psi(2S)$ state (a higher excited state of the J/ψ) appears to be inconsistent with CNM descriptions.

However, shockingly, the breadcrumb trail of the QGP in small systems stops here. There is no conclusive evidence for jet quenching or energy loss in small colliding systems. $R_{pA/dA}$, and any bias capturing variation on it, of any number of particle species, as a function of rapidity, transverse momentum, or centrality, at any of the energies available at CERN and

[7] Other examples of the tremendous success of energy loss models in describing partonic energy-loss in central AA collisions include [140–143].

[8] This is because a number of other phenomenological explanations have been put forward, including nuclear absorption, the modification of nuclear parton distribution functions, gluon saturation and in-medium energy loss, reviewed in [156].

BNL, is either consistent with unity or difficult to interpret [118, 121, 157–165]. Just one such result may be seen in fig. 1.7. It is this apparent absence of partonic energy loss in small colliding systems, in the context of the abundance of other QGP signatures, that motivates the calculations performed in this thesis. It is clear that a major part of our understanding of the QGP in small systems has been found wanting: where is the energy-loss?

Chapter 2

Problem identification and thesis outline

Collectively, the experimental results presented in chapter 1 paint a compelling, albeit baffling, picture. Over the last three decades, the heavy-ion community has developed a largely self-consistent picture of deconfined matter, based on a range of observables and phenomena that are best described within the framework of a rapidly expanding fireball, with a critical temperature of $\sim 120 - 160$ MeV[166]. There is little to no objection to the idea that matter has been brought into this state in central AA-collisions, but the observation of many QGP phenomena in small colliding systems is starkly juxtaposed against the absence of partonic energy loss. Where is the energy loss?

Part I explored the available experimental evidence and pointed out the major inconsistency in our current understanding of the QGP by presenting evidence of the presence of a number of traditional signatures of the QGP and confronting the reader with the absence of partonic energy loss. Is there no QGP in small colliding systems? Do we know what we're trying to measure? If there's no QGP, why are all the other observables popping up? Is the energy loss perhaps too small? Do we even know what we expect the energy loss to be in small systems?

All are valid questions, many are difficult to answer. This thesis will attempt to address the following problem:

> *Can we systematically and rigorously either rule out or realize the possibility that the energy loss in small systems is simply too small to measure?*

Part II presents a first attempt to compute the small system corrections to pQCD energy loss, revealing that a range of common assumptions about the nature of the medium are inconsistent at early times and small separation distances. This motivates a need to go beyond the small system corrections to energy loss and insist upon a first principles investigation into the small system-size corrections to the properties of the medium.

Part III provides such a first principles investigation, by considering a single, massless, scalar field that has been confined geometrically by means of Dirichlet boundary conditions. The phenomenology of such a geometrical confinement is rich, presenting substantial corrections to standard thermodynamical quantities as well as revealing a novel, geometrically driven, phase transition.

The main conclusions of the thesis are summarized in chapter 15.

Part II

A pQCD approach to energy loss

"The Creator had a lot of remarkably good ideas when he put the world together, but making it understandable hadn't been one of them."

- Mort, *Terry Pratchett*

Comment to Part II

In February of 2015 I enrolled at the University of Cape Town in a Masters program, and in December of 2015, was awarded a Masters degree in Theoretical Physics. That thesis [167] is freely available and the degree was awarded for the calculation contained in its appendices. Much of what follows is based on the calculation for which I was awarded a Masters degree.

However, the work presented here is a substantial addition and represents a significant effort to investigate the numerical nature of the result presented in [167] in order to better understand its implications. In the years since the presentation of [167] for the degree of Master of Science in Theoretical Physics, A/Professor W. A. Horowitz and I have subjected the energy loss formula to rigorous and extensive interrogation, and present here the methods and conclusions of that investigation.

In order to facilitate the reading of the current thesis, a brief revision of the methods and processes leading to the result (eq. (4.7)), from which the analysis in this part is done, is given in section chapter 4. The interested reader will find more details of the derivation of eq. (4.7) in [167]. The new work relevant to the current thesis is presented in chapter 5 and section 6.4.

Furthermore, the contents of part II of the present thesis is presented in the style of an academic publication since much of it has been submitted to Physical Review C for publication, with only minor revisions for the purposes of the current thesis. My contributions to this paper have been substantial. Apart from having derived the small separation distance correction term (for my Masters thesis), I also produced the Mathematica code that performs all the numerical calculations presented here and I offered the physical interpretations of the truncation versions. With the exception of parts of the introduction and the initial derivation of the asymptotic formula (which I rederived independently), I wrote the version of the paper that is presented here, and I have WAH's permission to present the paper here.

Chapter 3

Introduction

In section 1.4, the claim was made that, although immensely successful in the central AA arena, partonic energy-loss appears to be wholly absent in small colliding systems. Not only does there not appear to be a single measurement from a small colliding system of partonic energy-loss, but the experimental collaborations have insisted [116, 157] that the inherent biases present in measurements of high-multiplicity events in small systems are critical. Alarmingly, there is a second major problem in the consideration of energy-loss in small systems: theoretically, *all* derivations of energy-loss based on pQCD use simplifying assumptions [168] that make them inapplicable to small systems.

The first complication makes it difficult to properly normalize the usual observable adopted in tomographic studies, the nuclear modification factor R_{AB}. R_{AB} is the ratio of a spectrum in A+B collisions to the same particle spectrum in p+p collisions suitably normalized such that $R_{AB} = 1$ for particles unaffected by the presence of a QGP. Because of the aforementioned bias, properly normalizing R_{AB} in high-multiplicity p+p and p/d+A events is problematic. One solution may be to divide the spectrum of interest by a known unaffected electroweak spectrum with the same event selection criteria, forming a γ_{AB}, W_{AB}, or Z_{AB}. Another is to use a different centrality estimator [116].

The work of part II was motivated by the second complication. Although predictions of jet energy loss in small systems have been put forward [169, 170], they consistently over predict the observed suppression. Such small system energy loss predictions utilize energy loss derivations that are derived for large systems and it is therefore difficult to interpret the resultant discrepancy between theory and data as the absence of a hot thermal medium. In the usual DGLV (Djordjevic, Gyulassy, Levai, Vitev) opacity expansion [85, 87], the energy loss derivation assumes a large separation distance $\Delta z \equiv z_1 - z_0 \sim \lambda_{mfp} \gg 1/\mu$ between the initial production position z_0 of the hard parent parton and the position z_1 where it scatters off a QGP medium quasiparticle, characterized by the Debye screening length $1/\mu$ or $1/\mu_D$. This large separation allows one to 1) safely assume a factorization between the hard production process and the interaction of a nearly on-shell parton with a well-defined scattering center and 2) neglect several terms in the energy loss derivation. The mean free path of the high-p_T particle is $\lambda_{mfp} = 1/\rho\sigma \sim 1-2$ fm while the Debye mass in an infinite, static thermal QGP of temperature $T \sim 350$ MeV is $\mu = gT \sim 0.5$ GeV, as derived from

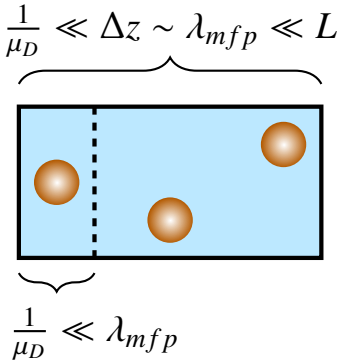

FIGURE 3.1: The usual DGLV setup (full box) compared to the setup used in this article (left of the dashed line), showing a static QGP brick of length L, containing arbitrarily distributed scattering centers (orange balls). Left of the dashed line, no statement is made regarding Δz, the distance between hard production and first scattering, allowing for an application to small systems where $L \sim 1/\mu_D$.

thermal field theory [171]. In the collision of p+p or p/d+A, one expects a system of radius $\lesssim 2$ fm. Therefore, for these small colliding systems, most high-p_T particles have a separation distance between production and scattering that is not particularly large compared to the Debye screening length.

In this article we modify the usual DGLV approach by removing the second implication of the large separation distance assumption: we derive the $N = 1$ in opacity[1] generalization of DGLV, including all previously neglected terms assumed small under the scale ordering $\Delta z \gg 1/\mu$; see Fig. 3.1. Note that the inclusion of smaller separation distances does not affect the scale of the Debye screening length in relation to the mean free path, which is to say that the Gyulassy-Wang model, which describes the interaction with the medium, remains valid. To the extent that factorization, near-on-shellness, and the Gyulassy-Wang model for scattering centers are good approximations even when $\Delta z \lesssim 1/\mu$, we have thus derived the $N = 1$ in opacity generalization of DGLV for *all* separation distances Δz. Since the formation time for a high-p_T particle goes as $\tau_f \sim 1/p_T \lesssim 1/\mu$, our derivation is fully justified for $\Delta z \gtrsim 1/\mu \sim 0.4$ fm for $p_T \gtrsim$ few GeV. Note also that the present short separation distance correction is an additional incorporation of finite size effects, over and above the effects that are due to producing the parent parton at finite time (as opposed to the infinite past), as computed by [172, 173].

Phenomenological energy loss models perform an average over the position(s) at which scattering(s) occur in the given distance that a parton travels in medium, L. Therefore, even though no previous energy loss derivation correctly treated the region $\Delta z \lesssim 1/\mu$, all energy loss models nonetheless used the derived energy loss formulae in this region. One might have hoped that the use of these formulae in the region of violation could be justified either by an argument that the small separation distance corrections are small, or by an explicit *a*

[1] In the reaction operator approach first put forward by GLV [85], it was found that the induced gluon radiation of a hard parton, possibly undergoing multiple scatterings, in a dense medium, is dominated by the first order in opacity result. That is, the gluon radiation is dominated by the $N = 1$ contribution, where N refers to the number of scatterings that the hard parton or radiated gluon undergoes with the medium.

posteriori calculation. What we find from the calculation presented in this work is that the small distance correction can be very large, especially as the momentum of the parent parton becomes large. Worse still, the physics of the early times is not at all clear.

Particular concerns for energy loss phenomenology include the factorization of the hard parton's production in the presence of large fields from its propagation through the fireball, the effect of a boundary on the shape of the Debye screened scattering centers, and the time required for the medium to thermalize and form scattering centers for the hard parton to interact with. In order to investigate the importance of this lack of knowledge, we explore various distributions of scattering centers. We find that the original DGLV is insensitive to the details of the physics at small separation distances $\Delta z \lesssim 1/\mu$. This insensitivity is due to a delicate cancellation of interfering terms, a cancellation beyond formation time effects. On the other hand, the cancellation is not quite so precise for the correction term, which leads to a significant dependence of the correction term on the details of the small distance physics.

The assumption in the DGLV formalism that the formation time of the radiated gluon is much larger than the Debye screening length, the large formation time assumption, will play a crucial role in the derivation of the small separation distance correction term, resulting in a major reduction in the number of diagrams that contribute to the small separation distance correction. We will further show that, not only does the formation time set an important scale for the understanding of the early time physics of the correction term, but also that the large formation time assumption is invalid for much of the relevant gluon emission phase space. Previous work has demonstrated the extreme sensitivity of *all* energy loss calculations to the collinear approximation [168, 174], and therefore the need to move beyond its use in all energy loss models. However, we emphasize that the sensitivity we find from the large formation time approximation is both new and different from the sensitivity to the collinear approximation. As such, all current jet quenching models that include radiative energy loss based on pQCD must individually assess their sensitivity to the large formation time and large system size approximations when making quantitative comparisons with data.

Chapter 4

Setup and calculation

In this paper we use precisely the setup of the DGLV calculation [87], presenting here only an outline of the setup and derivation of the correction term, with more details in [167]. For clarity, we treat the high-p_T eikonal parton produced at an initial point $(t_0, z_0, \mathbf{x}_0)$ inside a finite QGP brick of length L, where we have used $\mathbf{p}$ to mean transverse 2D vectors, $\vec{\mathbf{p}} = (p_z, \mathbf{p})$ for 3D vectors and $p = (p^0, \vec{\mathbf{p}}) = [p^0 + p^z, p^0 - p^z, \mathbf{p}]$ for four vectors in Minkowski and light cone coordinates, respectively. As in the DGLV calculation, we consider the n^{th} target to be a Gyulassy-Wang Debye screened potential [82] with Fourier and color structure given by

$$V_n = 2\pi\delta(q^0)\frac{4\pi\alpha_s}{\vec{q}_n^2 + \mu^2} e^{-i\vec{q}_n\cdot\vec{x}_n} T_{a_n}(R) \otimes T_{a_n}(n). \tag{4.1}$$

The color exchanges are handled using the applicable $SU(N_c)$ generator, $T_a(n)$ in the d_n dimensional representation of the target, or $T_a(R)$ in the d_R dimensional representation of the high-p_T parent parton.

In light cone coordinates the momenta of the emitted gluon, the final high-p_T parton, and that exchanged with the medium Debye quasiparticle are, respectively,

$$\begin{aligned} k &= \left[xP^+, \frac{m_g^2 + \mathbf{k}^2}{xP^+}, \mathbf{k}\right], \\ p &= \left[(1-x)P^+, \frac{M^2 + \mathbf{k}^2}{(1-x)P^+}, \mathbf{q} - \mathbf{k}\right], \\ q &= [q^+, q^-, \mathbf{q}], \end{aligned} \tag{4.2}$$

where the initially produced high-p_T particle of mass M has large momentum $E^+ = P^+ \simeq 2E$ and negligible other momentum components. Notice that we include the Ter-Mikayelian plasmon effect, a color dielectric modification of the gluon dispersion relation, with an effective emitted gluon mass m_g [87, 171]. See fig. 4.1 for a visualization of the relevant momenta.

A shorthand for energy ratios will prove useful notationally. Following [87] we define $\omega \approx xE^+/2 = xP^+/2$, $\omega_0 \equiv \mathbf{k}^2/2\omega$, $\omega_i \equiv (\mathbf{k} - \mathbf{q}_i)^2/2\omega$, $\omega_{(ij)} \equiv (\mathbf{k} - \mathbf{q}_i - \mathbf{q}_j)^2/2\omega$, and $\tilde{\omega}_m \equiv \left(m_g^2 + M^2x^2\right)/2\omega$.

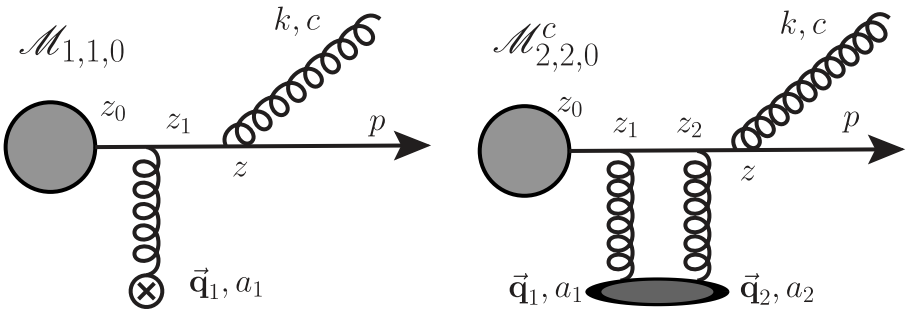

FIGURE 4.1: Following the diagrammatic numbering in [87], $\mathscr{M}_{1,1,0}$ (left-hand panel) and $\mathscr{M}^c_{2,2,0}$ (right-hand panel) are the only two diagrams that have non-zero small separation distance corrections in the large formation time limit. $\mathscr{M}^c_{2,2,0}$ is the double Born contact diagram, corresponding to the second term in the Dyson series in which two gluons are exchanged with the single scattering center.

We will also make the following assumptions: 1) the eikonal, or high energy, approximation, in which E^+ is the largest energy scale of the problem; 2) the soft[1] (radiation) approximation $x \ll 1$; 3) collinearity, $k^+ \gg k^-$; 4) that the impact parameter varies over a large transverse area; and, most crucially for the present article, 5) the large formation time assumption $\omega_i \ll \mu_i$, where $\mu_i^2 \equiv \mu^2 + \mathbf{q}_i^2$.

Note that the above approximations, in addition to allowing us to systematically drop terms that are small, permit us to 1) (eikonal) ignore the spin of the high-p_T parton; 2) (soft) assume the source current for the parent parton varies slowly with momentum $J(p-q+k) \approx J(p+k) \approx J(p)$; 3) (collinearity) complete a separation of energy scales,

$$E^+ \gg k^+ \gg k^- \equiv \omega_0 \sim \omega_{(i\ldots j)} \gg \frac{(\mathbf{p}+\mathbf{k})^2}{P^+}; \tag{4.3}$$

and 4) (large area) take the ensemble average over the phase factors, which become $\langle e^{-i(\mathbf{q}-\mathbf{q}')\cdot\mathbf{b}}\rangle = \frac{(2\pi)^2}{A_\perp}\delta^2(\mathbf{q}-\mathbf{q}')$.

In the original DGLV calculations [87], the large formation time approximation played only a minor role. However, when considering small separation distances between the scattering centers, the large formation time assumption naturally increases in importance.

With the above approximations, we reevaluated the 12 diagrams contributing to the $N = 1$ in opacity energy loss amplitude [87] without the additional simplification of the large separation distance $\Delta z \gg 1/\mu$ assumption.

In the original evaluation of the 12 diagrams contributing to the $N = 1$ in opacity energy loss derivation, the large separation distance approximation $\Delta z \gg 1/\mu$ allowed for the neglect of terms proportional to $\exp(-\mu\Delta z)$. In our reevaluation of these 12 diagrams we retained all terms proportional to $\exp(-\mu\Delta z)$. However, we found an enormous simplification due to the large formation time approximation $\omega_i \ll \mu_i$: all but two of the 12 diagrams' 18 new small separation distance correction pole contributions are suppressed under the large formation

[1] The validity of the soft gluon approximation within the DGLV formalism has recently been confirmed explicitly [175].

time assumption. We show the two diagrams[2] $\mathscr{M}_{1,1,0}$ and $\mathscr{M}^c_{2,2,0}$ with non-zero contributions at the amplitude level in the large formation time approximation in fig. 4.1. See [167] for the computation of all 12 relevant diagrams. One can see from fig. 4.1 that the class of diagrams that contribute to the short distance correction is that for which the radiated gluon is emitted subsequent to the parent parton scattering off the medium.

The reason for the contributing class of diagrams being those for which the scattering occurs prior to the emission of the gluon is the competition between relaxing the large distance approximation $\Delta z \gg 1/\mu$ and keeping the large formation time approximation, $\tau_{form} = xE/\mathbf{k}^2 \gg 1/\mu$. For a diagram to contribute to the small separation distance correction, we require $\Delta z \lesssim 1/\mu$. However, if the gluon is emitted at $\Delta z \lesssim \tau_{form}$, the large formation time approximation dictates that the gluon is not formed before the parent parton encounters a scattering center. The scattering center cannot therefore resolve the gluon independently from the parent parton, and these diagrams' contributions are suppressed. Similarly, the diagram in which the in-medium stimulated radiation is induced by interacting with the vacuum radiation, i.e. the diagram containing a triple gluon vertex, is suppressed since the spontaneously radiated gluon with which the medium is to interact must have enough time to decohere entirely from the parent parton before it can interact with the medium.

The full result for these two amplitudes under our approximation scheme is then

$$\begin{aligned}\mathscr{M}_{1,1,0} \approx & -J(p)e^{ipx_0}2gT_{a_1}ca_1\int\frac{d^2\mathbf{q}_1}{(2\pi)^2}v(0,\mathbf{q}_1)e^{-i\mathbf{q}_1\cdot\mathbf{b}_1} \\ & \times\frac{\mathbf{k}\cdot\boldsymbol{\epsilon}}{\mathbf{k}^2+m_g^2+x^2M^2}\left[e^{i(\omega_0+\tilde{\omega}_m)(z_1-z_0)}-\frac{1}{2}e^{-\mu_1(z_1-z_0)}\right], \qquad (4.4)\\ \mathscr{M}^c_{2,2,0} \approx & J(p)e^{i(p+k)x_0}\int\frac{d^2\mathbf{q}_1}{(2\pi)^2}\int\frac{d^2\mathbf{q}_2}{(2\pi)^2}e^{-i(\mathbf{q}_1+\mathbf{q}_2)\cdot\mathbf{b}_1}\times igT_{a_2}T_{a_1}ca_2a_1v(0,\mathbf{q}_1)v(0,\mathbf{q}_1) \\ & \times\frac{\mathbf{k}\cdot\boldsymbol{\epsilon}}{\mathbf{k}^2+m_g^2+x^2M^2}\times\left[e^{i(\omega_0+\tilde{\omega}_m)(z_1-z_0)}+e^{-\mu_1(z_1-z_0)}\left(1-\frac{\mu_1e^{-\mu_2(z_1-z_0)}}{2(\mu_1+\mu_2)}\right)\right], \qquad (4.5)\end{aligned}$$

where $v(0,\mathbf{q}_1)$ encodes the $\mathbf{q}_1$ dependence of the GW potential. The double differential single inclusive gluon emission distribution is given by [87]

$$\begin{aligned}d^3N_g^{(1)}d^3N_J = & \frac{d^3\vec{\mathbf{p}}}{(2\pi)^3 2p^0}\frac{d^3\vec{\mathbf{k}}}{(2\pi)^3 2\omega} \\ & \times\left(\frac{1}{d_T}\,\mathrm{Tr}\langle|\mathscr{M}_1|^2\rangle+\frac{2}{d_T}\,\Re\,\mathrm{Tr}\langle\mathscr{M}_0^*\mathscr{M}_2\rangle\right), \qquad (4.6)\end{aligned}$$

from which the energy loss, given by the energy-weighted integral over the gluon emission distribution $\Delta E = E\int dx\, xdN_g/dx$, can be calculated from the amplitudes.

Our main analytic result (the derivation of which may be seen in [167]) is then the $N = 1$ first order in opacity all separation distance generalization of the DGLV induced energy loss

[2] We follow the numbering convention of [87], where the subscripts refer to factorizations within the Reaction Operator approach and have no meaning here beyond a useful naming convention.

of a high-p_T parton in a QGP:

$$\begin{aligned}\Delta E^{(1)}_{ind} = \frac{C_R\alpha_s LE}{\pi\lambda_g}\int dx\int\frac{d^2\mathbf{q}_1}{\pi}\frac{\mu^2}{(\mu^2+\mathbf{q}_1^2)^2}\int\frac{d^2\mathbf{k}}{\pi}\int d\Delta z\,\rho(\Delta z)\\ \times\Bigg[-\frac{2\Big(1-\cos\big\{(\omega_1+\tilde{\omega}_m)\Delta z\big\}\Big)}{(\mathbf{k}-\mathbf{q}_1)^2+m_g^2+x^2M^2}\Bigg(\frac{(\mathbf{k}-\mathbf{q}_1)\cdot\mathbf{k}}{\mathbf{k}^2+m_g^2+x^2M^2}-\frac{(\mathbf{k}-\mathbf{q}_1)^2}{(\mathbf{k}-\mathbf{q}_1)^2+m_g^2+x^2M^2}\Bigg)\\ +\frac{1}{2}e^{-\mu_1\Delta z}\Bigg\{\Bigg(\frac{\mathbf{k}}{\mathbf{k}^2+m_g^2+x^2M^2}\Bigg)^2\Bigg(1-\frac{2C_R}{C_A}\Bigg)\Big(1-\cos\{(\omega_0+\tilde{\omega}_m)\Delta z\}\Big)\\ +\frac{\mathbf{k}\cdot(\mathbf{k}-\mathbf{q}_1)}{\Big(\mathbf{k}^2+m_g^2+x^2M^2\Big)\Big((\mathbf{k}-\mathbf{q}_1)^2+m_g^2+x^2M^2\Big)}\Big(\cos\{(\omega_0+\tilde{\omega}_m)\Delta z\}-\cos\{(\omega_0-\omega_1)\Delta z\}\Big)\Bigg\}\Bigg].\end{aligned}\tag{4.7}$$

The second line in Eq. 4.7 (along with the prefactor in the first line) is the original DGLV result (herein after "the DGLV" term). The last two lines are the small separation distance correction (herein after "the correction" or "the small separation distance correction"). In what follows we will refer to the full DGLV + correction in Eq. 4.7 as the "all separation distance" result. The correction term has the properties we expect: 1) the correction goes to zero as the separation distance becomes large, $\Delta z\to\infty$ (or, equivalently, as the Debye screening length goes to 0, i.e., $\mu\to\infty$) and 2) the correction term vanishes as the separation distance vanishes, $\Delta z\to 0$, due to the destructive interference of the Landau-Pomeranchuk-Migdal (LPM) effect.

An immediate surprise is the breaking of color triviality seen to all orders in opacity in the large separation distance approximation [85]; in the small separation distance correction, the color triviality breaking comes from the term proportional to $2C_R/C_A$. We will investigate the effect of this term numerically in Sec. 5.1.

The distribution $\rho(\Delta z)$ of the scattering centers will play a crucial role in our investigation of the short separation distance physics and is treated in great detail in Ch. 6.

Chapter 5

Numerical and asymptotic analyses

Fig. 5.1 is produced by computing the Δz integral in Eq. 4.7 analytically before computing all other integrals numerically (we will refer to this process as the "numerical investigation"). The numerical results use the same values as [87]: $\mu = 0.5$ GeV, $\lambda_{mfp} = 1$ fm, $C_F = 4/3$, $C_A = 3$, $\alpha_s = 0.3$, $m_{charm} = 1.3$ GeV, $m_{bottom} = 4.75$ GeV, and $m_{light} = \mu/2$ [171]. The QCD analogue of the Ter-Mikayelian plasmon effect is taken into account by setting $m_{gluon} = \mu/\sqrt{2}$ [176]. As in [171], kinematic upper limits are used for the momentum integrals such that $0 \leq k \leq 2x(1-x)E$ and $0 \leq q \leq \sqrt{3E\mu}$. The fraction of momentum carried away by the radiated gluon x is integrated over from 0 to 1. The distribution of scattering centers $\rho(\Delta z)$, although originally assumed to be exponential in [87][1], is assumed (in Fig. 5.1) to have the form of a unit step function, since an exponential distribution biases toward short separation distance scattering, lending potentially excessive weight to contributions from short separation distance terms.

In the top left-hand panel of Fig. 5.1 we plot the fractional energy loss of various parent partons of energy $E = 10$ GeV for path lengths up to 5 fm. One sees that the correction has a non-negligible effect even for large path lengths. Although initially unanticipated, the fact that the correction is substantial even for $L \gtrsim 3$ fm (perhaps most easily seen for gluons, but the relative size of the correction is meaningful even for the quarks), is due to the integration over all separation distances between the production point and the scattering position; even for large path lengths, some of the interaction distances between the parent parton and the target occur at separation distances that are small compared to the Debye screening scale. However, as expected, the relative size of the correction term and the leading DGLV result diminishes at fixed energy as the path length grows.

In the top right-hand panel of Fig. 5.1 we show the fractional energy loss of parent partons of varying energy, propagating through an $L = 4$ fm long static QGP brick. Notice first that the small separation distance correction term is generally an energy *gain* due to the sign of the color triviality breaking term and, second, that the size of the correction relative to the large separation distance DGLV result grows with energy.

[1] Choosing an exponential distribution for $\rho(\Delta z)$ was done in order to account for the rapidly expanding medium as well as to allow for clever manipulations leading to a deeper understanding of the asymptotic behavior of the formula, since the exponential form relates well to the cosines in the energy loss formula.

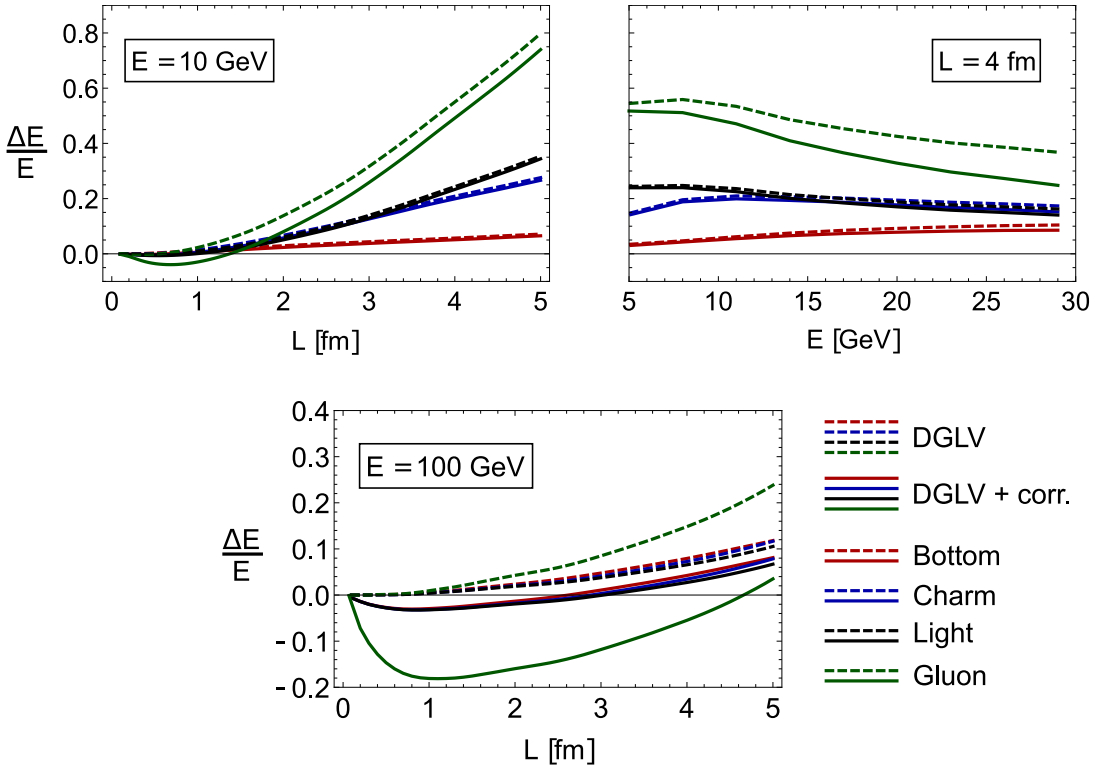

FIGURE 5.1: Fractional energy loss of bottom (red), charm (blue), and light quarks (black), as well as gluons (green) in a QGP with $\mu = 0.5$ GeV and $\lambda_{mfp} = 1$ fm for (top left) fixed energy $E = 10$ GeV, (top right) fixed path length $L = 4$ fm, and (bottom) fixed energy $E = 100$ GeV. Here, DGLV curves (dashed) are computed from the original $N = 1$ in opacity large separation distance DGLV formula while DGLV + corr. curves (solid) are from our all separation distance generalization of the $N = 1$ DGLV result, Eq. 4.7.

In the bottom panel of Fig. 5.1 we show the fractional energy loss of parent partons of energy $E = 100$ GeV. In this $E = 100$ GeV plot one sees that the short separation distance correction term dominates over the DGLV term out to distances of $L \sim 3 - 5$ fm $\gg 1/\mu$. At first glance, it might appear that the negative relative energy loss, or apparent energy gain, is un-physical and might point to an incomplete calculation, since the GW model for the medium models a static medium that does not allow for an energy transfer *to* the parent parton. However, there are several important points to note: The first is that the relative energy loss here measures the difference between the energy lost due to vacuum radiation and the energy lost due to medium-induced Bremmstrahlung. This first point means that a negative relative energy loss would simply imply that the vacuum radiation in suppressed and not necessarily that the parent parton would *gain* energy, although conservation of energy would still require that the negative relative energy loss be less than the energy of the leading parton.

A more technical point is that the two diagrams that contribute to the short separation distance correction have the opposite sign to the diagrams that are suppressed in the short separation distance limit. This fact is already true in the original DGLV calculation, but is amplified in the short separation distance limit due to the energy dependent dominance of the correction term, as will be seen in Sec. 5.2. That the correction term is negative then simply points to the fact that these two diagrams suppress the energy loss. In fact, numerically, even the DGLV large separation distance result exhibits small negative energy loss at very small path lengths.

Note also that, since the energy loss depends on an integration over the $\mathbf{k}$ distribution, a choice of k_{max} was made that guarantees that the final momentum of the parent parton is collinear to the initial momentum of the parent parton, and that the momentum of the emitted gluon is collinear to the momentum of the parent parton. Although we have decided to follow [87] in this choice, it is interesting to note that, even for a very small choice of k_{max}, the correction term remains negative (we have checked this numerically, but we will also see the truth of this statement in the asymptotic analysis presented in Eq. 5.2). We therefore conclude that the negativity of the correction term is not the result of integrating the integrand in a region of phase space in which the collinear assumption is invalid. Nevertheless, the energy dependence of the correction term plays an important role in the dominance of the correction term over the DGLV result. We investigate this persistent domination further in Sec. 5.2.

We lastly point out that one further observes that the color factor in the correction term plays a crucial role, since the gluon energy loss is dramatically different from quark energy loss, especially at high energies (investigated further in Sec. 5.1).

5.1 Color triviality

The color triviality breaking term in the small separation distance correction means the correction for gluons can be an order of magnitude larger than for quarks. To see this difference, consider the first line of the correction term in Eq. 4.7 which contains a term that carries the factor $\left(1 - \frac{2C_R}{C_A}\right)$. For gluons, this factor becomes $1 - 2C_A/C_A = -1$, while for quarks, this

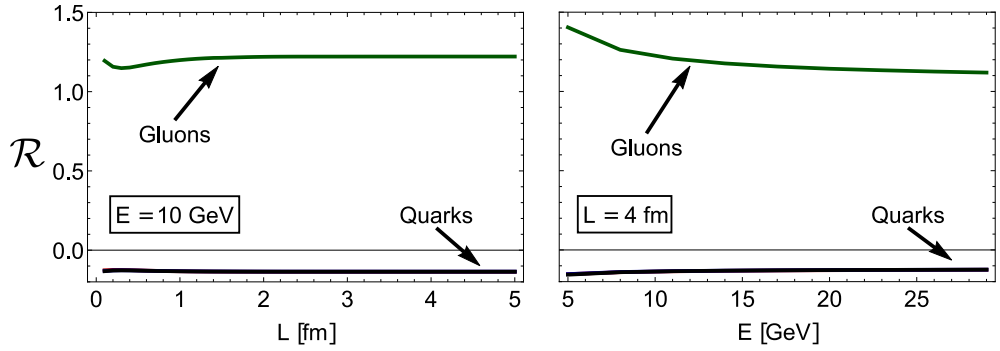

FIGURE 5.2: The ratio $\mathcal{R}$ of the color triviality breaking and the color trivial parts of the correction term in Eq. 4.7, for quarks (C_F) and gluons (C_A), as a function of the length L of the brick for parent partons with $E = 10$ GeV (left-hand panel), and as a function of the energy E of a parent parton moving through a brick of length $L = 4$ fm (right-hand panel).

color factor becomes $1 - \frac{2(C_F)}{C_A} = 1 - \left(\frac{(N_c^2-1)}{2N_c}\right)/N_c = 1 - \frac{2(4/3)}{3} = 1/9$. This factor of ten difference means that, although the gluons have an effective mass (as a result of the way in which the QCD analogue of the Ter-Mikayelian plasmon effect was taken into account) that is only marginally larger than the plasmon mass of the light quarks, the gluons will not necessarily obey the same mass ordering as the quarks.

To illustrate this effect, we have plotted in Fig. 5.2 the ratio $\mathcal{R}$ of the color trivial and color nontrivial terms of the correction term; i.e., we have divided the color triviality breaking part of the correction term, proportional to $\left(1 - \frac{2C_R}{C_A}\right)$, by the color trivial part of the correction term. We show this ratio both as a function of the length L of the brick (left-hand panel) and as a function of the parent parton energy E (right-hand panel). Fig. 5.2 clearly shows the order of magnitude difference between the color trivial and color nontrivial parts of the correction term for parent partons in the fundamental and adjoint representations, the difference in sign of the correction for quarks and gluons, and the persistence of the difference in magnitude of the correction as a function of both L and E.

5.2 Energy dependence and asymptotic analysis

A striking feature of the plot in the bottom panel of Fig. 5.1 is the dominance of the small separation distance correction term at high energies. We see in Fig. 5.1, by comparing the top left-hand panel to the bottom panel, a dominance of the correction term at $E = 100$ GeV, leading to an energy gain, even out to systems with sizes of $L \sim 3$ fm for quarks and $L \sim 5$ fm for gluons. It should be noted that the numerical results for ΔE depend on a choice of k_{max} in the integration over the transverse momentum of the radiated gluons in Eq. 4.7. The choice that has been made in the present thesis ensures collinearity of the momentum of the radiated gluon with the original momentum of the parent parton. In order to better understand this dominance of the correction term at large energies, one may perform an asymptotic analysis. Define $\Delta E^{(1)}_{ind} \equiv \Delta E^{(1)}_{\rm DGLV} + \Delta E^{(1)}_{\rm corr}$, where $\Delta E^{(1)}_{ind}$ is given by Eq. 4.7. Starting with the correction term $\Delta E^{(1)}_{\rm corr}$ and following [85], we take all thermal and quark

masses to zero, and analytically evaluate the integral over the scattering separation distance Δz (using an exponential distribution for analytic simplicity and to connect with the known analytic results of [85]). Then, we remove the kinematic bound on the momentum kick from the medium $q_{max} \to \infty$, shift the momentum integral, analytically evaluate the angular integrals in momentum space, and perform the integrals over k and q. The result is

$$\Delta E^{(1)}_{\text{corr}} = \frac{C_R \alpha_s}{2\pi} \frac{L}{\lambda_g} \left(- \frac{2C_R}{C_A} \right) \frac{1}{2+\mu L} E \int_0^1 dx \log \left(\frac{L k_{max}}{2+\mu L} \right). \tag{5.1}$$

Taking, for simplicity, $k_{max} = 2xE$ we find

$$\Delta E^{(1)}_{\text{corr}} = \frac{C_R \alpha_s}{2\pi} \frac{L}{\lambda_g} \left(- \frac{2C_R}{C_A} \right) \frac{1}{2+\mu L} E \log \left(\frac{2EL}{2+\mu L} \right) \tag{5.2}$$

in the limit of large energy E.

The equivalent asymptotic expression for the large separation distance leading massless DGLV result was derived in [85]. The result, with $k_{max} \to \infty$, is

$$\Delta E^{(1)}_{\text{DGLV}} = \frac{C_R \alpha_s}{4} \frac{L^2 \mu^2}{\lambda_g} \log \frac{E}{\mu}. \tag{5.3}$$

There are several important features of Eqs. 5.2 and 5.3 to note. First, the terms not proportional to the color triviality breaking $2C_R/C_A$ factor in Eq. 5.2 cancel at this level of approximation since $k_{max} \gg q_{max}$, and the correction is purely an *energy gain*. Second, the correction term is log divergent in the upper bound of the perpendicular momentum of the emitted gluon k_{max}, whereas the large separation distance DGLV term is finite for infinite k_{max}. Third, the correction term is linear in L at small L and independent of L at large L, while the DGLV term is proportional to the usual L^2. Fourth, the asymptotic correction term breaks color triviality as its magnitude is proportional to L/λ_R, where λ_R is the mean free path of the parent parton (whether quark or gluon), instead of proportional to L/λ_g, where λ_g is the mean free path for gluons.

Most important, cancellation between the contributions to the large separation distance DGLV result leads to an energy loss that grows only logarithmically with energy E. The small separation distance correction piece does not suffer from a similar interference and grows *linearly* with E. It is precisely this linear in E behavior compared to the log E of the large separation distance DGLV term that leads to the correction term dominating over the leading term at higher energies. The subtle cancellation between terms in the DGLV term, and the absence of such a cancellation in the correction term is discussed in more detail in Sec. 6.3.

The fact that the short separation distance "correction" term can dominate over the leading large separation distance DGLV result even out to path lengths $L \sim 4\mu$ when not relaxing the large formation time assumption (effects that should tend to zero under the large formation time assumption), suggests that the large formation time assumption is invalid in the DGLV

approach. The dependence of the energy loss on the large formation time assumption is explored further in Sec. 6.3 as well.

5.3 Mass ordering and the large formation time assumption

In Fig. 5.1, the all separation distance energy loss can be seen to be mass ordered[2]. The mass ordering of the large separation distance relative energy loss was found in [87], where the explanation was that the effect of increasing the mass of the parent parton was to reduce the relevance of the gluon formation time factor. The formation time physics of the large separation distance DGLV result is encoded in the cosine terms of Eq. 4.7 and a similar dependence on gluon formation times is apparent in the small separation distance correction term.

However, notice that the mass dependence of Eq. 4.7, is also apparent in the massive propagator. The propagator masses lead straightforwardly to a reduction of energy loss. At low energies the propagator mass ordering dominates the energy loss, leading to higher mass partons losing less energy. On the other hand, since the prefactors containing the propagators scale like $1/E^2$ while the formation times scale like $1/E$, formation time physics dominates the mass dependence of the energy loss at high energies; formation times are shorter for more massive parent partons, leading to an enhancement toward incoherent energy loss. We may thus understand the inversion of the mass ordering in the top right- hand panel of Fig. 5.1 (at $E = 10$ GeV) which results from the massive propagator, to the ordering observed in the bottom panel of Fig. 5.1 (at $E = 100$ GeV) where the mass ordering is dominated by formation time physics.

Nevertheless, despite the weak dependence of the mass ordering of the relative energy loss on the gluon formation time at low energies, recall the crucial role that the large formation time approximation $\omega_i \ll \mu_i$ plays in the derivation of the small separation distance correction. Traditionally, the large formation time assumption is considered a restatement of the collinear radiation approximation, but it is already known that the collinear assumption is problematic [168]: it was shown in [174] that a significant fraction of the gluon radiation from $N = 1$ large separation distance DGLV is *not* emitted collinearly, despite the use of the collinear approximation $k^+ \gg k^-$ in the derivation of the result. One may understand this breakdown of the collinear approximation in the DGLV formula by considering the required ordering $k^+ \gg k^-$. From Eq. 4.2, $k^+ \simeq 2xE$ and $k^- \simeq \mathbf{k}^2/2xE$ we require

$$2xE \gg \frac{\mathbf{k}^2}{2xE} \quad \Rightarrow 1 \gg \frac{\mathbf{k}^2}{(2xE)^2}, \tag{5.4}$$

[2]Note that this mass ordering does not hold for the gluons, even though they take on an effective plasmon mass. This is due to the color factor in the correction term; see Sec. 5.1.

which is certainly not true for $k_{max} \sim 2xE$. Similarly, the large formation time approximation requires that

$$\mu_i \gg \omega_i \sim \frac{1}{\tau} = \frac{\mathbf{k}^2}{2xE} \tag{5.5}$$

where the left hand side goes like $\mu \sim 0.5$ GeV, while the right hand side again gives ~ 1 GeV for $k_{max} \sim 2xE$ and typical values of $x_{typ} \sim \mu/E$ [174].

It is important to note that the large formation time assumption is a separate approximation from the collinear approximation; it is only when $|\mathbf{k}| \sim \mu$ that the two approximations are equivalent. Nevertheless, and despite this *a posteriori* understanding, the present calculation was performed making full use of the large formation time assumption.

Chapter 6

Sensitivity to small Δz

There is a lack of theoretical control over the physics of small Δz in heavy ion collisions, including, but not limited to, the factorization of a hard parton in the presence of early time strong fields and the thermalization of the medium. It is therefore valuable to investigate the sensitivity of the energy loss to the details of small Δz physics. In this section, we investigate the small Δz robustness of the energy and mass dependence of the correction term, seen in the previous section.

6.1 Distribution of scattering centers

The energy loss formula in Eq. 4.7 contains an integral over the distribution of scattering centers $\rho(\Delta z)$, which one is free to choose. The original DGLV calculation assumed an exponential distribution, motivated by an attempt to mimic a rapidly expanding medium. We have already alluded to the fact that an exponential distribution biases toward small separation distances, an effect which is exaggerated in small systems. In order to counter this bias and to further explore the sensitivity of the energy loss calculations to early time dynamics, it is useful to consider other distributions of scattering centers.

As a first step, and in order to avoid the complications of biasing toward small separation distances, we start our investigation by considering, as has been done by [172], a step function distribution of scattering centers. This function is a properly normalized Heaviside-theta function which distributes the scattering centers evenly for all $0 \leq \Delta z \leq L$, and we will refer to it as the "full step function" (abbreviated to "F" where necessary) for reasons that will become clear as we start to consider modifications of the simple step function.

Secondly, one might attempt to investigate the sensitivity of the relative energy loss to small separation distances by imposing a lower cut-off for Δz. The medium is modeled by Gyulassy-Wang potentials that explicitly require small $1/\mu$, setting a convenient scale for what "small Δz" might mean. We, therefore, propose a modification of Eq. 4.7 so that $\rho(\Delta z)$ is a properly re-normalized truncated step function in which the scattering centers are evenly distributed between $1/\mu \leq \Delta z \leq L$. The re-normalization needs to be such that the probability of scattering between $1/\mu$ and L is one. Physically, in this instance, we envision

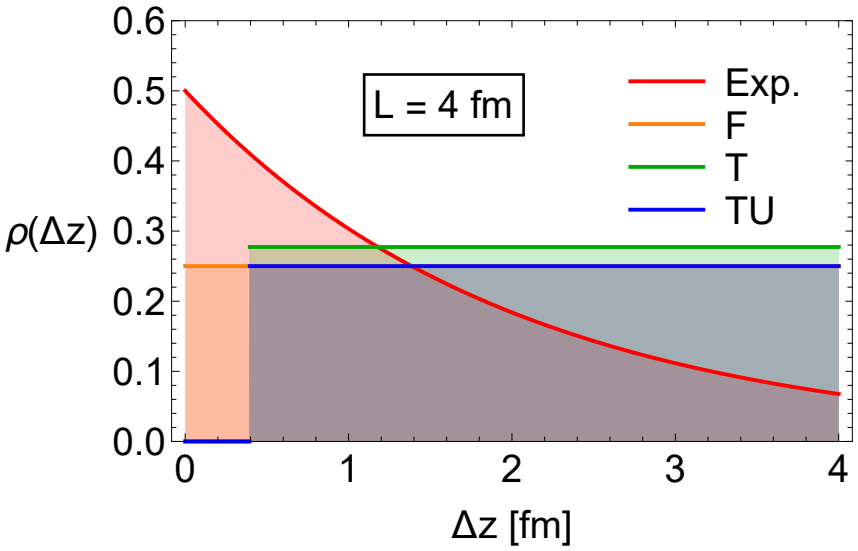

FIGURE 6.1: The four different options for $\rho(\Delta z)$, the distribution of scattering centers, discussed in the present article and described in eqs. (6.1) to (6.4), as a function of Δz. In this particular set of curves we have chosen a system with $L = 4$ fm.

producing a hard parton (its production having been properly factorized) before the medium has thermalized. The parton might, therefore, travel a short $\Delta z \lesssim 1/\mu$ distance through an unthermalized medium that has not yet formed quasiparticle scattering centers, keeping in mind that, since we consider first order in opacity, we require exactly one scattering to take place. We will call this distribution the "truncated step function" (abbreviated to "T" where necessary).

Thirdly, recall that pQCD energy loss formalisms assume that the production of the hard parton may be factorized from its propagation through the medium. The production mechanisms for hard partons in the presence of strong fields, and the scales on which they occur, have not yet been fully explored. However, the present calculation is performed within the framework of DGLV energy loss, which is a static brick problem, and therefore does not take into account the details surrounding the production of hard partons. In order to investigate this lack of information surrounding the factorization of the hard production processes, we propose a distribution of scattering centers which prohibits any energy loss from occurring close to the production. We impose such a cut-off on the energy loss by applying a unit step function to the energy loss formula, while employing the full unit step distribution of scattering centers. In practice, this truncation of the energy loss is implemented by truncating the unit step function distribution of the scattering centers without renormalizing, so that the probability of scattering is constant for $0 \leq \Delta z \leq L$, but the energy loss is zero for $\Delta z \leq 1/\mu$. Physically, this distribution is intended to mimic a hard parton that, having not yet formed properly, will not lose energy for some distance ($0 \leq \Delta z \leq 1/\mu$) even if it should encounter a scattering center. We will call this distribution the "truncated un-renormalized step function" (abbreviated to "TU" where necessary).

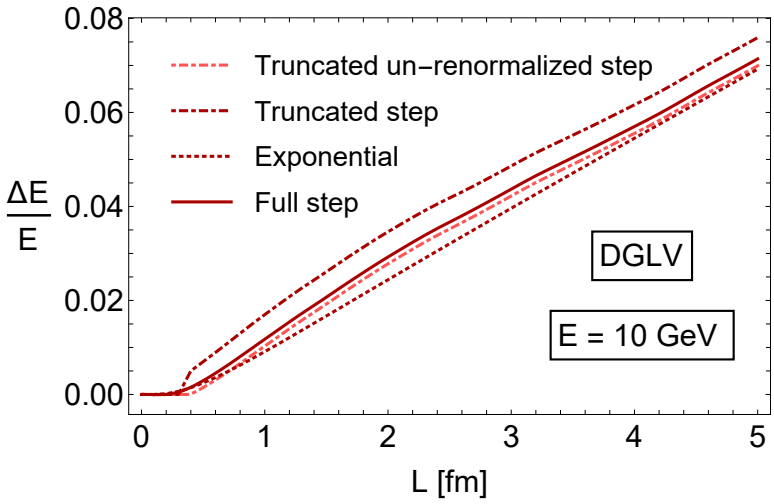

FIGURE 6.2: The relative DGLV energy loss of a bottom quark without small separation distance correction, as computed using the four different distribution functions for the scattering centers described in Eqs. 6.1 - 6.4. This plot is to be compared directly to Fig.2 in [87]. Note that the relative energy loss when using the truncated step function (dot-dashed curve) does not smoothly go to zero as $L \to 1/\mu$ due to the normalization factor in Eq. 6.3.

In summary, the four scattering center distribution functions we consider in this article are given by

$$\rho_{\rm exp}(\Delta z) = \frac{2}{L}\exp\left(-2\Delta z/L\right) \tag{6.1}$$

$$\rho_{\rm F}(\Delta z) = \frac{1}{L}\Theta\left(L-\Delta z\right) \tag{6.2}$$

$$\rho_{\rm T}(\Delta z) = \frac{1}{L-1/\mu}\Theta\left(\Delta z - 1/\mu\right)\Theta\left(L-\Delta z\right) \tag{6.3}$$

$$\rho_{\rm TU}(\Delta z) = \frac{1}{L}\Theta\left(\Delta z - 1/\mu\right)\Theta\left(L-\Delta z\right), \tag{6.4}$$

and are shown in Fig. 6.1 for a brick of $L = 4$ fm.

In Fig. 6.2 we show, having chosen the same parameters as were used in [87], the DGLV relative energy loss of a bottom quark without small separation distance correction, utilizing the four scattering center distributions described in Eqs. 6.1 - 6.4. Fig. 6.2 is to be compared directly to Fig. 2 in [87]. In Fig. 6.2 it can be seen, and we will show in Sec. 6.3 again, that the original DGLV term is not particularly sensitive to the choice of distribution. The distribution with the biggest difference in energy loss is the truncated (renormalized) step. This distribution biases the scatterings to larger Δz, causing the bias toward larger energy loss. Note that the relative energy loss when using the truncated step function (dot-dashed curve in Fig. 6.2) does not smoothly go to zero as $L \to 1/\mu$ due to the normalization (as $L \to 1/\mu$, the normalization diverges like $(L-1/\mu)^{-1}$). The almost complete lack of sensitivity to the differnces in the other distributions can be understood from formation time effects and a subtle cancellation of terms discussed further in Sec. 6.3.

6.2 Energy and mass dependence at small Δz

The sensitivity of Eq. 4.7 to the choice of $\rho(\Delta z)$ may be further investigated by considering more closely the sensitivity of the flavor and energy dependence of the correction to the choice of $\rho(\Delta z)$. To this end, we present a number of plots in Fig. 6.3, showing the relative energy loss $\Delta E/E$ for four different parent parton flavors (grouped in rows) at $E = 10$ GeV (left column) and $E = 100$ GeV (right column). All of these plots show the curves produced by using the full step function (solid curves), the truncated step function (dashed curves), and the truncated un-renormalized step function (dot-dashed curves)[1], for both the large separation distance DGLV result (light curves) and the present all separation distance result (dark curves).

By considering the dark curves of each plot in Fig. 6.3, showing the all separation distance result Eq. 4.7, it is clear that the correction term is sensitive to the choice of distribution of scattering centers. We investigate the reasons for this sensitivity in section 6.3. The dominance of the correction term at high energies (right-hand column) is described in section 5.2. One may understand the crossover of the truncated step function (T) and truncated un-renormalized step function (TU) curves (most easily seen in the $E = 100$ GeV plots, but also present in the $E = 10$ GeV plots) as a result of the fact that the T distribution biases toward larger separation distances so that, at larger L, the characteristic L^2 dependence of the DGLV energy loss overpowers the L^0 dependence of the correction term at a smaller L (see Eqs. 5.2 and 5.3). The column on the right in Fig. 6.3 also clearly shows that, at $E = 100$ GeV, the mass dependence of the relative energy loss of the quarks disappears. This may be understood by recalling that the momentum of the radiated gluon $\mathbf{k}$ is integrated over from 0 to $2x\left(1 - x\,E\right)$, so that masses in both the momentum prefactors and the formation times in Eq. 4.7 are overpowered by the $\mathbf{k}^2$ at large E.

In order to further quantify the sensitivity of the energy loss to early time physics, we plot in Fig. 6.4 ratios of relative energy loss computed using three different scattering center distributions (truncated un-renormalized step function in dashed curves, truncated step function in dot-dashed curves and exponential in dotted curves) to the relative energy loss computed using the full step function, for the large separation distance DGLV result on the left, and the present small separation distance correction on the right, all for an $E = 10$ GeV bottom quark. This ratio is unity for an energy loss formula that is insensitive to the physics of $\Delta z \lesssim 1/\mu$. One immediately notes that, while the DGLV results all tend toward one, the correction term's sensitivity to the early time dynamics is persistent even at large L. One can see that, compared to the unit step, varying the scattering center distribution leads to up to a factor of two reduction, or factor of three enhancement, of the correction term. The large deviation of T away from F for the DGLV result at small L is due to the normalization of T, as well as a very small energy gain and subsequent division by zero for small path lengths.

We may investigate the mass and energy dependence of the differences between scattering center distributions even further by considering the plots presented in Fig. 6.5, where we plot

[1] We have not included the exponential distribution here as it lends little to the present discussion.

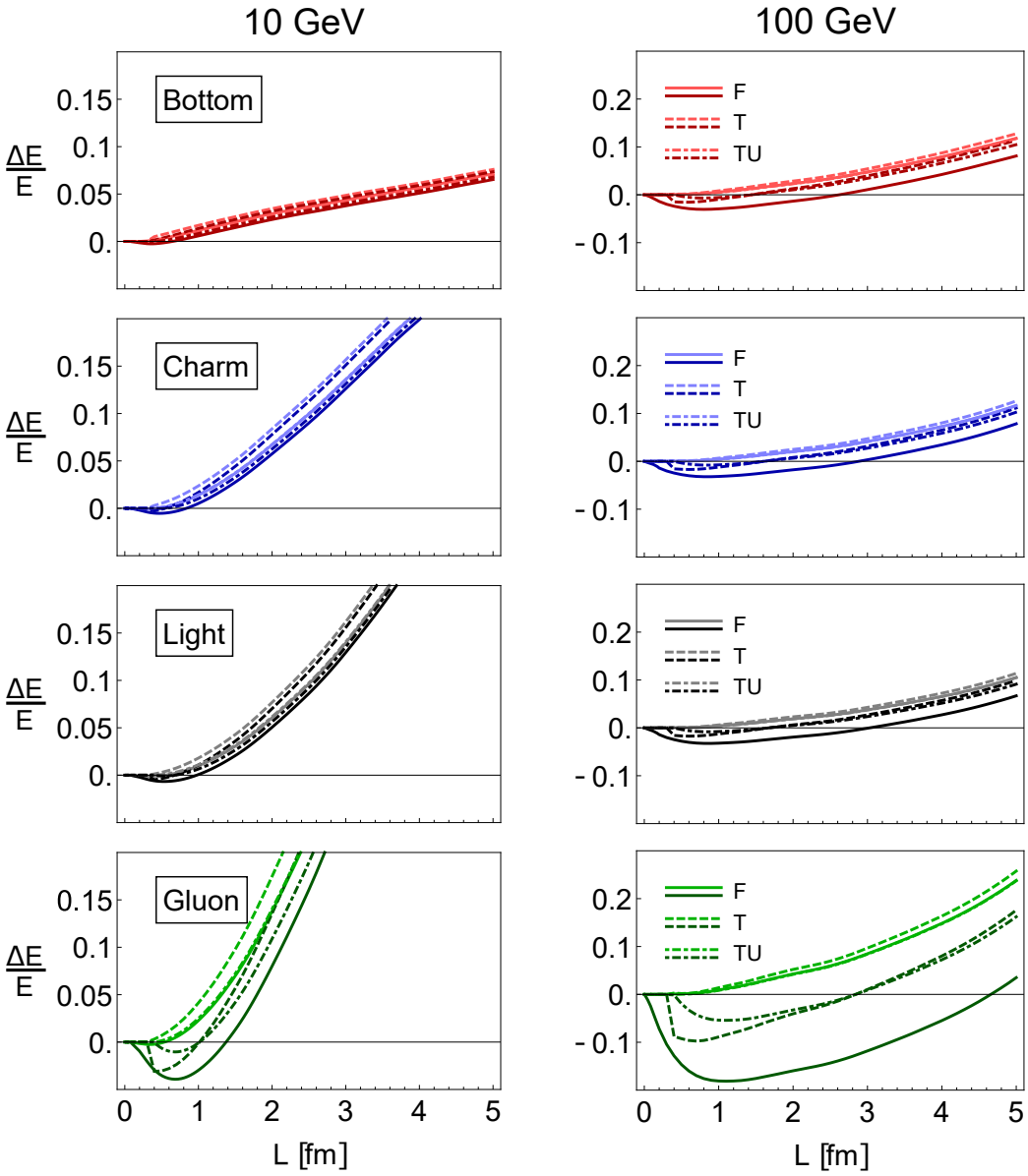

FIGURE 6.3: The relative energy loss of four different parent parton flavors (organized in rows), for parent parton energies of $E = 10$ GeV (left column) and $E = 100$ GeV (right column), for both the original large separation distance DGLV result (light curves) and the present all separation distance result (dark curves), as computed using the full step function (solid curves), the truncated step function (dashed curves) and the truncated un-renormalized step function (dot-dashed curves).

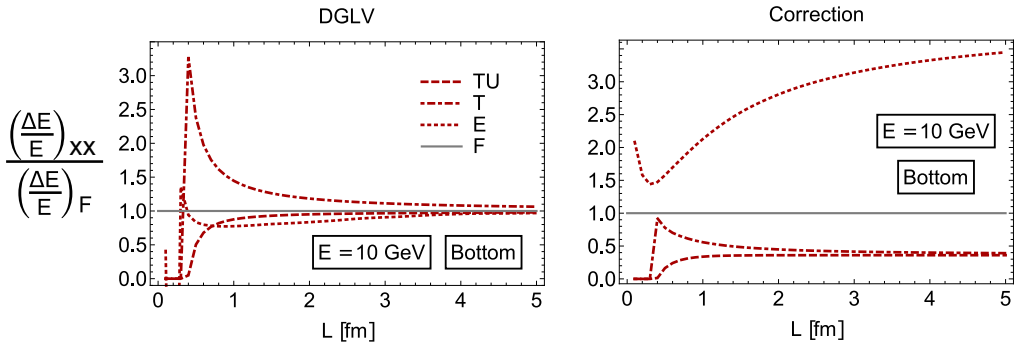

FIGURE 6.4: The ratio of the relative energy loss as computed using various different scattering center distributions (truncated un-renormalized step function in dashed curves, truncated step function in dot-dashed curves and exponential in dotted curves) to that computed using the full step function distribution, for an $E = 10$ GeV bottom quark as a function of the size L of the brick, for the DGLV term (left-hand panel) and the small separation distance correction term (right-hand panel). This ratio is unity for an energy loss formula that is insensitive to the physics of small separation distances.

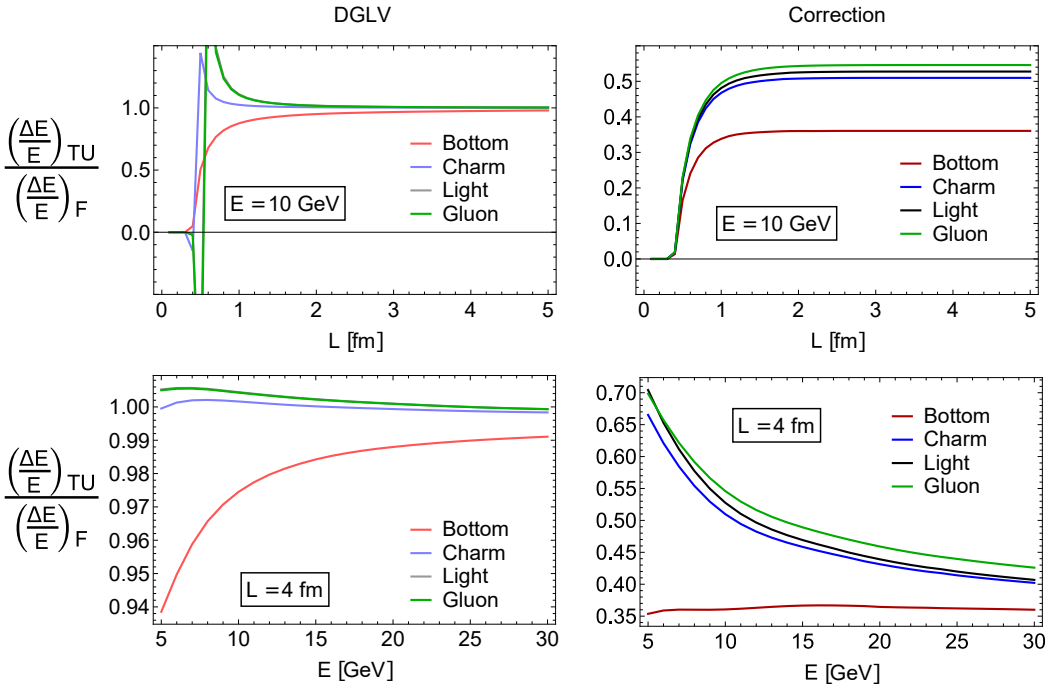

FIGURE 6.5: The ratio of the relative energy loss as computed using the truncated un-renormalized step function to that computed using the full step function. This ratio is shown in the top row as a function of the length of the brick for parent partons with $E = 10$ GeV and in the bottom row as a function of the energy of the parent parton moving through a brick of $L = 4$fm, for DGLV (left column) and for the correction (right column). This ratio is unity for an energy loss distribution that is insensitive to the physics of $\Delta z \lesssim 1/\mu$.

the ratio of the relative energy loss as computed using the truncated un-renormalized scattering center distribution to that computed using the full step function, for the DGLV result (left column) and the correction term (right column). The plots in the left column of Fig. 6.5 show that the insensitivity of the DGLV result to small system dynamics is independent of both mass and energy, particularly for $L \gtrsim 1\text{fm}$. On the other hand, differences of a factor of 2 persist to all path lengths for the correction term. The length dependent DGLV ratio in the top left hand corner of Fig. 6.5 exhibits some fluctuant behavior at small L for some flavors, due, as in Fig. 6.4, to numerical division by zero.

The correction term's sensitivity to small Δz physics is also seen to be mass dependent in Fig. 6.5, with the bottom quark most affected by the truncation of the scattering center distribution. Although the overall mass dependence of the relative energy loss at low energies is mostly due to the mass dependence of the propagators in Eq. 4.7 (discussed in Sec. 5.3), the ratio of relative energy losses divides out any mass dependence that is not coupled to the separation distance. We may therefore understand the mass dependence of the ratio shown in Fig. 6.5 from a formation time perspective: Consider the formation time of a gluon radiated off a parent parton with mass M, given by

$$\tau_f \equiv \frac{2xE}{\mathbf{k}^2 + x^2M^2}. \tag{6.5}$$

The high mass of the bottom quark will then give the bottom quark the shortest radiated gluon formation time. The shorter the formation time, the more sensitive will the parton be to early time physics. One expects such a mass dependence to disappear at high energies, and indeed, the sensitivity of the relative energy loss to the choice of distribution appears to converge for the different quark masses at high energies, as seen in the bottom left plot of Fig. 6.5. Naively one might expect all the quarks to appear massless (and so to see the ratio in Fig. 6.5 converge to the light quark result rather than that of the bottom quark at high energies). For the DGLV result (bottom left in Fig. 6.5), this intuition holds because the DGLV result is insensitive to small separation distance physics. On the other hand, because of the correction term's sensitivity to small separation distance dynamics, and since higher energies result in shorter radiation formation times, the curves in the bottom right panel of Fig. 6.5 tend toward the bottom quark result, since it is the bottom quark that already has the shortest formation time.

6.3 Origins of small Δz sensitivity

In Eq. 4.7 we see that both the DGLV terms and the correction terms contain formation times; i.e., the terms are proportional to cosines of argument $\omega_i \Delta z$ such that ΔE_{DGLV} and ΔE_{corr} go to zero for $\Delta z \lesssim 1/\omega_i$. It is therefore difficult to understand the sensitivity of the correction term to early time physics, in conjunction with the *insensitivity* of the DGLV term, from a formation time perspective. Investigating the DGLV term further numerically, one finds a subtle cancellation that occurs in the DGLV term that does not occur in the

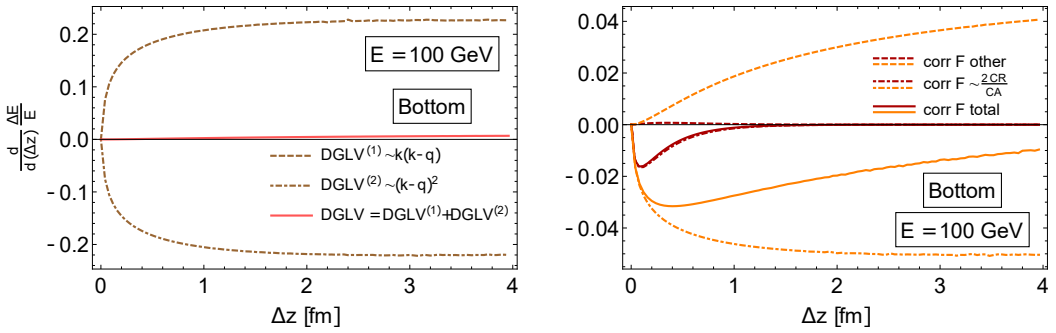

FIGURE 6.6: The DGLV term (left-hand panel) and correction term (right-hand panel) contributions to the $d(\Delta z)$ differential of the relative energy loss of an $E = 100$ GeV bottom quark moving through a brick of $L = 4$ fm, showing the contributions from individual terms in Eq. 4.7. in the panel on the left, the dashed and dot-dashed curves show the two terms in brackets in the second line of Eq. 4.7, while the solid curve shows their sum (the full DGLV result). In the right-hand panel the dashed curves show the sum of the two terms that cancel in the high energy limit (see Sec. 5.2 for details), the dot-dashed curves show the color carrying term and the solid line their sum. For the correction term in the right-hand panel, the red curves show the full result while the orange curves show what the contributions to the correction term would be without the $\exp(-\mu\Delta z)$ factor (see Sec. 6.3 for details).

correction term. In the DGLV term, the two terms in the brackets in the second line of Eq. 4.7 ($DGLV^{(1)} \sim k(k-q)$ and $DGLV^{(2)} \sim (k-q)^2$, so that $DGLV = DGLV^{(1)} + DGLV^{(2)}$) are very large but almost equal in magnitude and opposite in sign. As such, the two contributions to the DGLV term cancel almost identically, which may be seen in the left hand panel of Fig. 6.6, where we plot the contributions from $DGLV^{(1)}$ and $DGLV^{(2)}$ separately, along with their sum, for an $E = 100$ GeV bottom quark.

No such cancellation occurs in the correction term, a fact we already alluded to in Sec. 5.2 where we found that two of the three terms in the correction cancel, while the color triviality breaking term remains and is responsible for the bulk of the contribution. To illustrate the dominance of the color triviality breaking term in addition to the cancellation of the remaining terms of the correction, we present the red curves in the right-hand panel of Fig. 6.6, showing the contributions from the two terms that cancel in the high energy limit, the color triviality breaking term, and their sum, for an $E = 100$ GeV bottom quark. One can see in the red curves of the right-hand panel of Fig. 6.6 that the color triviality breaking term controls the correction term's energy loss. Therefore, the DGLV term's insensitivity to the small separation distance physics is due to *both* the destructive LPM effect *and* this subtle cancellation effect, while the absence of such a cancellation in the correction term contributes to the correction term's sensitivity to small Δz.

Additionally, the correction contains a factor of $\exp(-\mu\Delta z)$, which plays the part of suppressing contributions to the correction term from $\Delta z \gtrsim 1/\mu$, enforcing a strong dependence on the physics of $\Delta z \lesssim 1/\mu$. In order to understand the role of the exponential factor in the sensitivity of the correction term to the small separation distance physics, we present the orange curves in the right-hand panel of Fig. 6.6, which show the same three terms of the correction term as are shown in the red curves, but without the factor of $\exp(-\mu\Delta z)$. It is

clear that, upon integrating over Δz, the bulk of the contributions to the integral comes from the region $\Delta z \lesssim 1/\mu$ due to the presence of the $\exp(-\mu\Delta z)$ factor.

6.4 Conclusions

The original DGLV derivation of the energy loss of a hard, potentially massive parton via radiation (of potentially massive quanta), while traversing a static brick of weakly coupled QGP, assumed a large path length for the parent parton. In this paper, we generalized the first order in opacity of DGLV by including the short path length terms that were neglected in the original derivation. We have thus analytically derived a small separation distance correction to the first order in opacity of DGLV. Our result constitutes an important step toward the understanding of partonic energy loss in small colliding systems.

The main result of our paper is the all separation distance first order in opacity energy loss formula Eq. 4.7. In our derivation we retained the scale ordering of $1/\mu \ll \lambda_{mfp}$, justifying the use of the Gyulassy-Wang model, as well as the soft and collinear assumptions, and we have retained the usual assumption of large formation time. We found that the majority of terms that are exponentially suppressed under the large path length assumption are additionally suppressed under the large formation time assumption at the amplitude level, meaning that only two diagrams out of twelve contribute to the small separation distance correction. We performed an extensive numerical analysis of the correction term and found that, surprisingly, the correction term dominates over the original DGLV result at high energies. This energy dependence may be understood from an asymptotic analysis that revealed an $E \log E$ energy dependence of the correction term, in contrast to the $\log E$ dependence of the large separation distance DGLV. We further found that the correction term depends on the distance traveled through the medium as L for small L and L^0 for large L, again deviating from the L^2 dependence of the DGLV term. Therefore, the effects of the correction term persist to arbitrarily large paths. Interestingly, the correction term also breaks color triviality.

Naively one might expect aspects such as the factorization of the production of the hard parton from the scattering, the behavior of a Debye screened scattering center near the edge of a thermalized medium, etc., to play a role in small system modeling. In order to explore the effect of the physics of small systems and early times on our correction term, we proposed a number of distributions of scattering centers, attempting to take into account the factorization of the production of the hard parton from its propagation through a medium, as well as the formation of that medium. We showed that the short separation distance correction is sensitive to early time physics explored by these distributions, while the original large separation distance DGLV result is not. We found that the DGLV term's insensitivity to the physics of small Δz is due to both the known formation time physics and a subtle cancellation of terms. This cancellation does not persist in the correction term, which accounts for the sensitivity of the correction term to small Δz physics.

Our derivation revealed that the formation time of a gluon radiated off a hard parent parton is of crucial importance. Already at the amplitude level of the all separation distance derivation, we found that the naive application of the large formation time assumption leads to a dramatic reduction of terms present in the correction. We also demonstrated that the large formation time assumption is violated for much of the phase space of the emitted radiation.

Since all energy loss formalisms, DGLV, BDMPS-Z-ASW, AMY, and HT (see [177] and references therein) exploit the large formation time approximation, we are faced with a need to assess the applicability of the large formation time assumption in any description of energy loss. While the influence of the assumption of collinearity was relatively easy to quantify across formalisms by simply varying the maximum allowable perpendicular momentum of the emitted gluon, estimating the importance of the large formation time approximation will likely be a challenge. Similarly, deriving expressions that do not rely on either the collinear or large formation time approximations is formidable.

The physics of formation times is also relevant to the mass ordering of the energy loss at high parent parton energies. However, we found that the mass ordering is additionally subject to competing effects from the massive propagator, so that the mass dependence of the relative energy loss at low energies is dominated by the propagator. Our results show that, if one is to consider a system in which the separation distances are on the order of the Debye screening length, one will have to understand the in-medium production mechanisms as well as the nature of a Debye screened scattering center near the edge of a thermalized medium, in addition to the validity of the large formation time assumption in small systems. Due to these large uncertainties, the quantitative effect of the correction on observables is unclear. Further, the lack of theoretical control over these assumptions calls into doubt the quantitative extraction of medium parameters through the use of jet quenching [142]. We leave addressing these issues for future work.

Chapter 7

Interlude

"No good sittin' worryin' abou' it," he said. "What's comin' will come, an' we'll meet it when it does."

- Rubeus Hagrid, Harry Potter and the Goblet of Fire,
J. K. Rowling

If the reader is predisposed to such things, let them now settle down with a glass of fine South African wine and reflect upon the current state of affairs.

If a droplet of QGP that is similar in nature to that formed in central AA-collisions is indeed formed in small colliding systems, then it is a logical imperative that the absence of the energy loss be understood. It may well be that the energy loss is simply too small to be measured, or that no energy loss can occur because the system is too small to develop those properties that are traditionally understood to encourage energy loss.

However, we have seen that a simple – yet valid – small system adjustment of a common energy loss model, one that has traditionally been both phenomenologically successful and is consistent within the framework of similar models, highlights the need for stricter theoretical control of all the model assumptions that produce a phenomenological result. Let us review briefly the major ideas that have brought us thus far:

1. A perturbative QCD calculation must be appropriately factorized. This is because, unlike in QED, the asymptotic states of a QCD amplitude are not directly related to the objects involved in experiments: hadrons are collided, and hadrons (and photons and leptons, *but not quarks or gluons*) are measured [177]. We therefore do not have QCD ${}_{in}\langle\psi|$ and $|\psi\rangle_{out}$ states that are prepared in the infinite past and future, but rather, a QCD ${}_{in}\langle\psi|$ state that is the product of some non-perturbative production process, and a QCD $|\psi\rangle_{out}$ state that is the input for a non-perturbative hadronization process. While such a factorization of non-perturbative production // perturbative scattering // non-perturbative hadronization is understood and well-studied in the case of scattering that occurs in vacuum, it is a fundamental assumption in medium, and remains wholly unproven. We must therefore ensure that any process, that may be

perturbatively expanded in powers of α_s, which is used to model energy loss in the medium, is "sandwiched" between a process of production and a process of hadronization, both of which might occur in the presence of a medium. The process of production occurs on very small time scales (a $p_T = 10$ GeV parton will be produced on a length scale $\Delta x \sim 1/p_T = \hbar c/10\,\text{GeV} \sim 0.02\,\text{fm}$, while the medium scales are $1/T \sim \hbar c/200\,\text{MeV} \sim 1\,\text{fm}$). The assumption that the hadronization of the hard parton occurs in vacuum may be justified if the parton is hard enough [168, Sec. D.4]. We are therefore left only with the assumption that the production of the hard parton, as well as its modification by the presence of the medium, does not interfere with the perturbative scattering process[1].

2. Even in AA collisions the energy loss has always been known to have a strong dependence on the distance traveled through the medium, and so we can hardly be surprised that there is system size dependence[2], but it has been shown [178, 182] that simply taking L small (note that, in principle, is invalid in these schemes since both [178, 182] use BDMPS-Z-like energy loss, which requires $L \gg 1/\mu$), overestimates the suppression seen experimentally.

3. In an attempt to ensure that we are fully justified in applying the energy loss formulae to small systems, one may compute the small separation distance correction to DGLV energy loss. We have seen that the effect of the correction is not only dominant at high energies, but is also very sensitive to the nature of the medium at early times – how and when is energy lost at the smallest distance scales? Do we understand the properties of the medium at early times[3]?

By varying the distribution of scattering centers in the DGLV formalism, one sees that the energy loss in an all separation distance energy loss formalism is highly sensitive to the dynamics of early times and short separation distances. One might hope to be able to constrain the scattering center distribution function through a better understanding of the properties of the medium, either subjected to a boundary or at early times. Of particular interest to the DGLV formalism and the GW model is the behavior of the Debye screening length in the presence of a boundary.

Unfortunately, the reader will not find in this thesis a computation of the finite size corrections to the Debye mass. However, we have developed a consistent framework in which to consider the finite size corrections to the basic thermodynamic properties of a toy model (a single, massless, scalar field theory, confined by spatial Dirichlet boundary conditions) and we have

[1] Of course, all of the models mentioned here consider the production to occur at $t = 0$ and then include the off-shell vacuum radiation and its interference pattern (except AMY, but even there extensions have been performed to include interference with the vacuum [178]), so some manner of finite medium *is* taken into account, but even calculations in "finite media" are always careful to ensure that radiation factors from production.

[2] In fact, this has been explored experimentally at RHIC through various channels. One way is to vary the collision system and consider, for instance, *CuCu* collisions [179, 180]. Another, perhaps more successful method, is to consider the nuclear modification factor as a function of the angle at which partons are emitted [181], although one then encounters problems with hydrodynamical flow [177, Sec. 6.4.5].

[3] Some work has been done on the evolution of the medium from a highly non-equilibrated initial state to a hydrodynamic state (see for instance [183–188]).

discovered a number of fascinating consequences of introducing a spatial boundary. This calculation constitutes a first step toward computing the Debye mass.

The remainder of this thesis explores the thermodynamics of small systems, presenting a rigorous derivation of the thermal field theoretic partition function of our toy model.

Part III

A thermal approach to the small medium

"Our future was so completely unknown, and I think that the unknown and the awful always bring a man nearer to his Maker."

- King Solomon's Mines, *H. Rider Haggard*

Chapter 8

Comment to Part III

Part III of this thesis is an almost verbatim reproduction of the paper submitted to the journal Nuclear Physics B for publication (the only exceptions being the omission of a few introductory paragraphs, and the inclusion of section 11.6 and its relevant appendix). At the time of submission of this thesis, the article has not yet been accepted by the editor for publication. This paper was written in collaboration with Dr. W. A. Horowitz and Dr. S. Mogliacci and I have their permission to reproduce that work here.

My contributions to this paper include the following; It was my initial idea to compute small system corrections within the dynamical formalism that led to the thermal field theoretic computation performed here. While I did not initialize the geometric confinement, I reproduced the initial derivation of the partition function and exact form of the plates case (originally derived by SM and WAH), before independently computing the exact forms of the tube and box cases, all in what is called here the "canonical" or "usual" approach[1]. I computed all analytic expressions for the thermodynamic quantities as well as independently produced Mathematica code to perform all numerical calculations presented here. I also independently derived the matrix elements of the Hessian matrix presented in section 11.6 as well as the additional periodic boundary condition results. The novel phase transition was first noticed by WAH, but, using the expressions from the canonical approach, I independently performed all analytic and numerical calculations leading to the boson results in chapter 13. I did not perform the fermion calculations. Although all the plots in this paper were produced by SM (except for fig. 11.3), I have independently derived and produced all of the results (except Fermion results). The derivations in appendices A.2.2 and A.2.3 are my own, although they, as with my other contributions here, were inspired by many discussions with SM and WAH.

[1] I did not perform the "alternative derivation" of the partition function, put forward by SM, but include it here since it has been valuable for the cross-checking of my results.

Chapter 9

Introduction

9.1 Motivation and goals

The present work is motivated by the pressing need for a better understanding of small droplets of QGP, including a quantification of the small system size corrections to the usual approximation of using dynamics derived in systems of infinite size. In terms of QGP phenomenology, our goals are modest. As a first step, we concentrate on the finite size corrections to thermodynamic quantities such as the equation of state (EoS) computed in thermal field theory in the usual Stefan-Boltzmann limit of an ideal gas of infinite size in all directions. As a further simplification, we consider only noninteracting fields. Of the various types of boundary conditions one might use, we focus on Dirichlet boundary conditions (BC) for simplicity and, as we will argue below, because these are the most natural BC when considering a finite-sized QGP.

Despite the simplicity of our model, we will find a suggestive phenomenology. In our derivation of thermodynamic quantities, we use two independent methods that yield analytic formulae with different numerical convergence properties: one which converges exponentially fast when the dimensionless scale of the temperature times the system size is small, $T \times L \lesssim 1$, and one that converges exponentially fast for $T \times L \gtrsim 1$. A careful application of these two formulae allows us to numerically investigate to arbitrary accuracy the various thermodynamic quantities such as the pressure, energy, entropy, and heat capacity for our model. Of particular importance to the heavy ion community, the introduction of Dirichlet instead of periodic BC leads to significant small system corrections to the usual infinite size results of the equation of state even out to fairly large system sizes $L \sim 10/T$.

However, our work is of potential interest beyond heavy ion physics. In some sense there is a long history of investigating finite size effects in (thermal) field theory. Most famously at $T = 0$ a noninteracting field between two parallel plates induces an attractive force between the plates, which may be interpreted as a negative pressure, the well-known Casimir effect [189–193]. The original Casimir effect of a free scalar field between two slabs has been extended to systems with nontrivial geometries and to Fermi fields [194]. For $T > 0$, one encounters a number of interesting fundamental questions, many of which have only begun to be explored recently [195–199]. First, if all spatial dimensions are of finite size, the system

may not be in the thermodynamic limit [200]. When not in the thermodynamic limit one is no longer guaranteed that the different statistical ensembles, i.e. microcanonical, canonical, etc., agree [196, 201–203]. It is then very important to consider the physical setup for an experimental measurement and use the appropriate ensemble; in particular, isolated systems may behave very differently from systems in contact with a heat bath. Second, phase transitions are notoriously difficult to rigorously identify. This difficulty is only compounded in finite-sized systems [203–206] with some authors claiming that phase transitions in systems of finite size are impossible. Third, in finite-sized systems, one loses extensivity in thermodynamics [207], where, by extensivity, we mean that the entropy is positively homogeneous of degree 1, i.e. $S(\lambda E, \lambda X_1, \lambda X_2, \ldots) = \lambda S(E, X_1, X_2, \ldots)$. This lack of extensivity then leads to questions about the use of the Tsallis distribution [208, 209] and the minimal set of assumptions required for a consistent thermodynamics [210]. Fourth, once a system is of finite size, then thermal fluctuations can be important, which has begun to be explored in the heavy ion hydrodynamic community [211].

We also find a connection between our work and the study of phase transitions. Phenomenologically, one finds substances for which a phase transition can be driven by a change of pressure at constant temperature, for example the liquid-gas phase transition for water above 0°C. We are aware of only one example of a phase transition driven by the size of the system [206], in which case the transition is due to the self interactions of the system. What we will show is that for an isolated ideal gas constrained within parallel plates, the system resists compression until the separation of the plates is on the order of the thermal wavelength; at this critical length $L_c \sim 1/T$ the susceptibility diverges and the system collapses. This divergence of the susceptibility indicates a second order phase transition driven by the size of the system, which is conjugate to the pressure on the system. Unlike other works that draw a connection between Bose-Einstein condensation between parallel plates [212] and a first order phase transition in a finite volume box [213], the phase transition found here is second order and also exists for Fermionic fields.

9.2 Geometric confinement for HIC

There have been a number of studies of finite size effects using periodic boundary conditions [214–222]. Consider, however, that a boundary-less manifold, e.g. a three-dimensional sphere, is entirely decoupled from the rest of the universe: there is no possibility for any signal or information to come through the QGP and reach the detectors. Therefore, spatial boundary conditions—other than periodic ones—should be considered for a more realistic approach to the finite size corrections of the EoS[1].

Consider now a QGP system inside of which the quarks and gluons are color deconfined and propagate relatively freely while outside of this QGP system the quarks and gluons are color

[1]Note that the EoS of QCD relevant to the early universe QGP potentially lacks such a requirement of a boundary.

confined into hadrons. Inside the system the quark and gluon fields, then, are weakly coupled while these same quark and gluon fields are strongly coupled outside the system. There is further some very small region of space over which the fields transform from weakly to strongly coupled. For our purposes here, we are most interested in the dynamics inside the QGP system. And if we approximate the small transition region from weak to strong coupling as a decoupling, we must impose a boundary condition that prevents an inside weakly coupled field from propagating outside of the geometric region defining the QGP system. We refer readers to [223–225] for related investigations that demonstrate the need for such more realistic boundaries. We also refer to [226–230] for somewhat related investigations, as well as to [64] regarding the importance of accounting for finite size effects in the different context of proton-proton collisions. While such a decoupling might seem irrelevant from a perturbative point of view, since this change of degrees of freedom across the two regions must involve nonperturbative physics, our system appears to be analogous to the Quantum Electrodynamics (QED) Casimir effect [189, 193], which can be reproduced by imposing Dirichlet Boundary Conditions (DBCs). Such boundary conditions indeed follow the requirement for the fields to vanish at the boundary, and any two-point correlation function connecting the inside part to the boundary would identically vanish, thereby decoupling both sides of the boundary. Thus, DBCs for the QGP can avoid the propagation of QGP particles across the boundary, keeping the relatively free quarks and gluons geometrically confined inside the volume of the QGP system, while at the same time allowing for other fields, e.g. electromagnetic, to freely propagate out from the confined system.

We then introduce the notion of *geometric confinement* for such a system, by implementing appropriate spatial compactifications (depending on the geometry to be characterized). In each of the compactified directions we impose DBCs[2]. It should be noted that such a boundary is not a material boundary, but rather a thin layer subdividing different regions of space with different degrees of freedom. And since we are only interested in the bulk physics away from the boundary (avoiding then possible technical complications [231, 232]), we will not consider the microscopic nature of the boundary. As a result, the physical space is separated into two distinct regions: An inside part of nearly free quarks and gluons characterizing the quark-gluon plasma, and an outside part (of nearly free hadrons composed of strongly coupled quarks and gluons). For the sake of our investigations in this manuscript we ignore the details of color confinement and the microscopic nature of the boundary. Moreover, it should be noted that while DBCs may be implemented in more physically realistic geometries, for the sake of simplicity we choose to work here with simple rectangular geometries, that is planar pairwise parallel spatial boundaries forming a cuboid cavity. In three spatial dimensions, we consider two infinite parallel plates, the infinite rectangular tube, and the finite volume box.

We stress that our concept of geometric confinement is in no way related to actual color confinement, for it barely reproduces only one consequence of it (the fact that quark and

[2]Note that by a compactification we do not mean, e.g., the addition of the point at infinity to turn $\mathbb{R}$ into S^1. Rather, we mean that we are considering directions that are compact, i.e. of finite extent (technically, closed and bounded).

gluon fields should not propagate outside of the QGP); we do not address the fundamental mechanism of color confinement. In addition, our concept is different from the MIT bag model [233] since our model is not meant to be relevant for strongly coupled fields, but for weakly coupled ones.

9.3 A model for initial investigations

Recalling that the EoS for a noninteracting gas of gluons is the same, up to a group theory prefactor, as the EoS given by a massless scalar field, for simplicity we choose to consider a single neutral noninteracting massless scalar field at finite temperature under geometric confinement. Further, we will work in the canonical ensemble: we will compute the partition function using thermal field theoretic methods. Even though the quark-gluon plasma created in heavy ion collisions is an isolated system, we choose to work in the canonical ensemble for two reasons. First, we may more readily connect our results to lattice QCD calculations [234–247]; and second, for simplicity.

In the following, we will keep the mass of the field nonzero for convenience during the calculations. At a later stage, we will, however, take the massless limit which is the present case of interest. We will work in D spacetime dimensions with an arbitrary number c of the spatial dimensions compactified with DBCs. The number c here, for "compactified", is not to be confused with c for the speed of light, which will be equal to one as we will employ natural units throughout. We will leave the noncompactified dimensions, if any, in the usual infinite Euclidean form. Each such compactified spatial direction will then have a distinct compactification length L_i, $i = 1, \dots c \leq D-1$. The L_i's do not necessarily have to be equal, which allows us to investigate systems of asymmetric sizes. Our starting point is therefore the free, Wick rotated Euclidean action

$$\mathcal{S}\Big[\phi\left(\tau,\{z_i\},\mathbf{x}\right)\Big] \equiv \int_0^{1/T} \mathrm{d}\tau \int_0^{L_1} \mathrm{d}z_1 \dots \int_0^{L_c} \mathrm{d}z_c \int_R \mathrm{d}^{D-1-c}\mathbf{x} \Big(\mathcal{L}\Big[\phi\left(\tau,\{z_i\},\mathbf{x}\right)\Big]\Big), \tag{9.1}$$

where beside the usual trace induced periodic boundary condition along the Wick-rotated τ direction, and the new geometric confinement inducing DBCs along the z_i spatial directions, the $\mathbf{x}$ coordinates will be momentarily compactified around circles of radius R, i.e. with periodic boundary conditions. At the end of the calculation we will take $R \to \infty$. The free Lagrangian $\mathcal{L}\left[\phi\left(\tau,\{z_i\},\mathbf{x}\right)\right]$ then reads

$$\begin{aligned}\mathcal{L}\left[\phi\right] \equiv & \frac{1}{2}\left(\frac{\partial\phi\left(\tau,\{z_i\},\mathbf{x}\right)}{\partial\tau}\right)^2 + \frac{1}{2}\sum_{i=1}^{c}\left(\frac{\partial\phi\left(\tau,\{z_i\},\mathbf{x}\right)}{\partial z_i}\right)^2 \\ & + \frac{1}{2}\Big(\nabla_{\mathbf{x}}\phi\left(\tau,\{z_i\},\mathbf{x}\right)\Big)^2 + \frac{m^2}{2}\,\phi^2\left(\tau,\{z_i\},\mathbf{x}\right),\end{aligned} \tag{9.2}$$

where we are working in $\hbar = c_{light} = k_B = 1$ natural units.

Chapter 10

Partition function and free energy for parallel plates, a tube, and a box

10.1 Deriving the partition function

In this subsection, we derive the partition function $\mathcal{Z}(T, \{L_i\})$ for a single, neutral, non-interacting, massless scalar field that is geometrically confined within $c \leq D-1$ spatial dimensions.

Formally, the partition function in a theory with Hamiltonian operator $\hat{\mathcal{H}}$ and no globally conserved charges is obtained from the trace of the density matrix

$$\mathcal{Z}(T, V) \equiv \mathrm{Tr}\left[\hat{\rho}(T, V)\right] \equiv \mathrm{Tr}\left[\exp\left\{-\beta \int_V d^{D-1}x\, \hat{\mathcal{H}}\right\}\right], \tag{10.1}$$

where $\beta = 1/T$ is the inverse temperature, V the spatial volume of the system, and the trace represents a summation over all possible physical states. We will employ the Matsubara imaginary time formalism [248] in order to compute the partition function using path integral techniques [249]. For more details on this formalism as well as on thermal field theory, we refer readers to [250–255].

The usual procedure for expressing the partition function as a path integral leads to a path integral with a *periodic boundary condition* on the temporal line which, up to an irrelevant constant, reads

$$\mathcal{Z}(T, V) \propto \int_{\phi(0)}^{\phi(\beta)} [\mathcal{D}\phi] \exp\left\{-\int_0^\beta d\tau \int_V d^{D-1}x\, \mathcal{L}\right\}\Bigg|_{\phi(\beta)=\phi(0)}. \tag{10.2}$$

We now extend the above to a manifold with c compactified spatial dimensions. The procedure will require DBCs for the compactified spatial dimensions, in addition to the periodic boundary condition required by the trace operation. The derivation of the analogue of eq. (10.2) with compactified spatial dimensions closely follows that of the spatially noncompactified case, which we call the Stefan-Boltzmann limit, the details of which can be seen in

the aforementioned textbooks. For pedagogical reasons we will first compactify only one dimension ($c = 1$), which gives the canonical ensemble description for a noninteracting scalar field at temperature T constrained between two infinite parallel plates separated by a distance L_1. Extending the result to c compactified dimensions will be straightforward.

Following the usual procedure, we start by decomposing our field into the relevant Fourier modes. The dimensions that will ultimately be left noncompactified are, as usual, momentarily compactified onto circles of identical sizes R (which means we impose periodic boundary conditions), while the dimension we wish to permanently compactify is done so along a finite interval with length L_1. We choose a convenient normalization constant (see appendix A.2.1 for more details) and express the Fourier decomposition of our field as

$$\phi(\tau, z_1, \boldsymbol{x}) = \sum_{n\in\mathbb{Z}} \sum_{\ell_1\in\mathbb{N}} \sum_{\boldsymbol{k}\in\mathbb{Z}^{D-2}} \sqrt{\frac{2\beta}{L_1 R^{D-2}}} \exp\left\{i\omega_n\tau - i\boldsymbol{\omega}_k\cdot\boldsymbol{x}\right\} \sin\left\{\omega_{\ell_1} z_1\right\} \tilde{\phi}_{n,\ell_1}(\boldsymbol{\omega}_k), \quad (10.3)$$

where the components of $\boldsymbol{x}$ are the spatial components in the non permanently compactified dimensions, z_1 is the spatial component in the compactified dimension, and $\tilde{\phi}_{n,\ell_1}(\boldsymbol{\omega}_k)$ are the dimensionless Fourier modes. The Matsubara, the compactified spatial dimension, and the non permanently compactified spatial dimensions related frequencies are given by $\omega_n = 2\pi nT$, $\omega_{\ell_1} = \pi\ell_1/L_1$ and $\boldsymbol{\omega}_k = 2\pi\boldsymbol{n}_k/R$, respectively, and we also refer to [256] for more details on the derivation of the modes given DBCs. The latter frequencies are to be replaced by a $D-2$ dimensional continuous momentum $\boldsymbol{k}$ (with corresponding momentum integrals), in the asymptotically large R limits.

Setting $c = 1$ and employing eq. (9.2) for the Lagrangian, the partition function eq. (10.2) becomes, after an integration by parts,

$$\mathcal{Z} \propto \int_{\phi_{\text{cond.}}} [\mathcal{D}\phi(\tau, z_1, \boldsymbol{x})] \exp\left\{-\int_0^\beta \int_0^{L_1} \mathrm{d}z_1 \int_R \mathrm{d}^2\boldsymbol{x} \;\; \frac{1}{2}\phi(\tau, z_1, \boldsymbol{x})(\partial_\mu\partial^\mu + m^2)\phi(\tau, z_1, \boldsymbol{x})\right\}, \quad (10.4)$$

where, among others, the periodic boundary condition from the trace is imposed through setting $\phi_{\text{cond.}}$ such that $\phi(\beta, z_1, \boldsymbol{x}) = \phi(0, z_1, \boldsymbol{x})$, and where $\partial_\mu\partial^\mu \equiv \frac{\partial^2}{\partial\tau^2} + \frac{\partial^2}{\partial z_1^2} + \boldsymbol{\nabla}_{\boldsymbol{x}}^2$.

Substituting eq. (10.3) into eq. (10.4), and simplifying the argument of the exponential by performing the integrations (see appendix A.2.1 for more details) [253–255], we obtain

$$\mathcal{Z} \propto \int_{\phi_{\text{cond.}}} [\mathcal{D}\phi(\tau, z_1, \boldsymbol{x})] \exp\left\{-\frac{\beta^2}{2} \sum_{n\in\mathbb{Z}} \sum_{\ell_1\in\mathbb{N}} \sum_{\boldsymbol{n}_k\in\mathbb{Z}^{D-2}} \left|\tilde{\phi}_{n,\ell_1}(\boldsymbol{\omega}_k)\right|^2 \left(\omega_n^2 + \omega_{\ell_1}^2 + \boldsymbol{\omega}_k^2 + m^2\right)\right\}. \quad (10.5)$$

As in the Stefan-Boltzmann case, we are faced with an issue of double counting when performing explicitly the path integral. This problem can be accounted for, in the noninteracting case, by separating the Fourier modes into real and imaginary parts

$$\begin{aligned} \tilde{\phi}_{n,\ell_1}(\omega_k) &= a_{n,\ell_1}(\omega_k) + ib_{n,\ell_1}(\omega_k) \\ \Rightarrow \left|\tilde{\phi}_{n,\ell_1}(\omega_k)\right|^2 &= a^2_{n,\ell_1}(\omega_k) + b^2_{n,\ell_1}(\omega_k), \end{aligned} \tag{10.6}$$

and since the field is required to be real, we obtain the following restrictions

$$\begin{aligned} a_{-n,\ell_1}(-\omega_k) = a_{n,\ell_1}(\omega_k) \qquad &\text{and} \qquad b_{-n,\ell_1}(-\omega_k) = -b_{n,\ell_1}(\omega_k) \\ \Rightarrow & b_{0,\ell_1}(\mathbf{0}) = 0, \end{aligned} \tag{10.7}$$

from which one may choose a set of physically relevant independent ϕ-variables over which to integrate. Following the standard procedure [253–255], one may then perform the infinite set of Gaussian integrals (dropping any T- and L_i-independent factors [257]) to obtain the partition function of a free scalar field in $D-1$ spatial dimensions with $c = 1$ geometrically confined dimension. However, since thermodynamic quantities are straightforwardly related to the logarithm of the partition function, we will find the more useful quantity to be

$$\ln \mathcal{Z}^{(1)}(T, L_1) = \ln \left\{ \prod_{n\in\mathbb{Z}} \prod_{\ell_1\in\mathbb{N}} \prod_{\boldsymbol{n}_k\in\mathbb{Z}^{D-2}} \left[\beta^2\left(\omega_n^2 + \omega_{\ell_1}^2 + \omega_k^2 + m^2\right)\right]^{-1/2} \right\}. \tag{10.8}$$

Formally, eq. (10.8) is our final result for the logarithm of the partition function of a single neutral noninteracting scalar field in between two parallel plates. Extending eq. (10.8) to arbitrary $c \leq D-1$ compactified spatial dimensions is relatively straightforward, and the corresponding logarithm of the partition function with c geometrically confined dimensions is therefore given by

$$\ln \mathcal{Z}^{(c)}(T, \{L_i\}) = -\frac{1}{2} \sum_{n\in\mathbb{Z}} \sum_{\boldsymbol{\ell}\in\mathbb{N}^c} \sum_{\boldsymbol{n}_k\in\mathbb{Z}^{D-1-c}} \left[\ln \left\{ \beta^2 \left((2\pi n T)^2 + \sum_{i=1}^{c} \left[\left(\frac{\pi \ell_i}{L_i} \right)^2 \right] + \omega_k^2 + m^2 \right) \right\} \right], \tag{10.9}$$

where we still have to send R to infinity.

In Appendix appendix A.1.1 and appendix A.1.2 we present two independent methods of evaluating eq. (10.9). We have confirmed numerically that both methods yield the same results. The two methods are mutually complementary as they naturally yield results with different numerical convergence properties. More precisely, the usual method yields a result that is always better suited for small values of the dimensionless parameters ($T \times L_i$). The alternative method yields a result better suited for high values of these dimensionless parameters and thus to recover the usual Stefan-Boltzmann limits. Moreover, the usual result explicitly isolates the T-independent contributions, and one can pass from one compactified

dimension case to the next in an iterative manner; therefore the usual method explicitly yields the known zero temperature Casimir pressure.

10.2 Evaluating the free energy

We now present our final results for the free energy in the massless limit using both eq. (A.19) and results from eq. (A.21). Recall that the free energy density is given by $f \equiv F/V$, F being the total free energy, and therefore reads

$$f(T, \{L_i\}) \equiv -\frac{T}{V} \ln \mathcal{Z}(T, \{L_i\}), \tag{10.10}$$

where $V \equiv \prod_{i=1}^{D-1} L_i$.

10.2.1 Case I: Two infinite parallel plates

In the usual approach, and after considering $D-2 = 2-2\epsilon$, simplifying the summations with Bessel functions, expanding about $\epsilon = 0$, and performing summations using analytic continuation of the Epstein-zeta functions, eq. (A.19) leads to the further refined expression of the free energy density, $f^{(c=1)}(T, L_1)$, of a system geometrically confined in between two infinite parallel plates separated by a distance L_1

$$f^{(1)} = -\frac{\pi^2}{1440 L_1^4} - \frac{T^2}{2L_1^2} \sum_{\ell=1}^{\infty} \left[\ell \, \mathrm{Li}_2 \left(\mathrm{e}^{-\frac{\pi \ell}{T L_1}} \right) \right] - \frac{T^3}{2\pi L_1} \sum_{\ell=1}^{\infty} \left[\mathrm{Li}_3 \left(\mathrm{e}^{-\frac{\pi \ell}{T L_1}} \right) \right], \tag{10.11}$$

where the Li_n are the usual polylogarithm functions.

We can also follow the alternative approach, as presented in appendix A.1.2, to compute the same free energy density. Employing similar techniques and making use of eq. (A.20) in order to analytically continue the Epstein-zeta functions without formally manipulating a divergence, we end up with a similar expression which we further resum using the contour integral representation of the polylogarithm function. We find

$$\begin{aligned} f^{(1)} = &- \frac{\pi^2 T^4}{90} + \frac{\zeta(3) T^3}{4\pi L_1} - \frac{T^2}{8L_1^2} \sum_{\ell=1}^{\infty} \left[\frac{\mathrm{csch}^2 \left(2\pi T L_1 \ell \right)}{\ell^2} \right] \\ &- \frac{\zeta(3) T}{16\pi L_1^3} - \frac{T}{16\pi L_1^3} \sum_{\ell=1}^{\infty} \left[\frac{\coth \left(2\pi T L_1 \ell \right) - 1}{\ell^3} \right], \end{aligned} \tag{10.12}$$

where in the last summation, we kept the -1 explicit—even though there exists a simple closed form for $\coth(x) - 1$—since the less simple form improves the convergence properties of the expression.

As previously mentioned, we see that eq. (10.11) converges exponentially fast for low values of the dimensionless variable TL_1, while eq. (10.12) converges exponentially fast for high values of this dimensionless variable. The latter even has enhanced convergence properties

(due to the additional resummation which we performed), for nearly all TL_1 down to $TL_1 \sim 10^{-6}$.

A similar resummation could have been performed on eq. (10.11), but we will refrain in doing so since the alternative result covers nearly all TL_1 values.

10.2.2 Case II: Infinite rectangular tube

Using the usual approach together with the same type of procedure as in the parallel plates case, we may then set $c = 2$ in eq. (A.19), perform a few more refinements, and obtain the free energy density, $f^{(c=2)}(T, L_1, L_2)$, of a system geometrically confined within an infinite rectangular tube of section $L_1 \times L_2$

$$\begin{aligned} f^{(2)} =& \frac{45\,L_1\,\zeta(3) - \pi^3 L_2}{1440\pi L_2 L_1^4} - \frac{1}{64\pi\,L_1^2\,L_2^3}\sum_{\ell=1}^{\infty}\left[\frac{L_1\left(1-\mathrm{e}^{-\frac{2\pi L_2}{L_1}\ell}\right)+2\pi L_2\ell}{\ell^3}\times\operatorname{csch}^2\left(\frac{\pi L_2}{L_1}\,\ell\right)\right] \\ & -\frac{T}{L_1 L_2}\sum_{\ell,\ell_1,\ell_2=1}^{\infty}\left[\frac{1}{\ell}\sqrt{\left(\frac{\ell_1}{L_1}\right)^2+\left(\frac{\ell_2}{L_2}\right)^2}\,K_1\left(\frac{\pi\ell}{T}\sqrt{\left(\frac{\ell_1}{L_1}\right)^2+\left(\frac{\ell_2}{L_2}\right)^2}\right)\right], \end{aligned} \tag{10.13}$$

where K_n are the usual modified Bessel function of the second kind.

We may also use our alternative approach, in order to compute the very same free energy density, doing so we obtain

$$\begin{aligned} f^{(2)} =& -\frac{\pi^2 T^4}{90} + \frac{\zeta(3)\,T^3(L_1+L_2)}{4\pi L_1 L_2} - \frac{\pi T^2}{24 L_1 L_2} + \frac{\pi T(L_1+L_2)}{96 L_1^2 L_2^2} - \frac{\zeta(3)\,T(L_1^3+L_2^3)}{32\pi L_1^3 L_2^3} \\ & - \frac{T^2}{4L_1^2}\sum_{\ell=1}^{\infty}\left[\ell\,\mathrm{Li}_2\left(e^{-4\pi T L_1\ell}\right)\right] - \frac{T^2}{4L_2^2}\sum_{\ell=1}^{\infty}\left[\ell\,\mathrm{Li}_2\left(e^{-4\pi T L_2\ell}\right)\right] \\ & - \frac{T}{16\pi L_1^3}\sum_{\ell=1}^{\infty}\left[\mathrm{Li}_3\left(e^{-4\pi T L_1\ell}\right)\right] - \frac{T}{16\pi L_2^3}\sum_{\ell=1}^{\infty}\left[\mathrm{Li}_3\left(e^{-4\pi T L_2\ell}\right)\right] \\ & + \frac{T^2}{L_1 L_2}\sum_{n,\ell=1}^{\infty}\left[\frac{n}{\ell}\,K_1\left(4\pi T L_1 n\ell\right) + \frac{n}{\ell}\,K_1\left(4\pi T L_2 n\ell\right)\right] \\ & - \frac{T}{8L_1 L_2^2}\sum_{\ell_1=1}^{\infty}\sum_{(n,\ell_2)\in\mathbb{Z}^2\setminus\{\mathbf{0}\}}\left[\frac{\sqrt{\ell_2^2+(2TL_2)^2n^2}}{\ell_1}\,K_1\left(\frac{2\pi L_1}{L_2}\,\ell_1\,\sqrt{\ell_2^2+(2TL_2)^2n^2}\right)\right] \\ & - \frac{T}{8L_2 L_1^2}\sum_{\ell_2=1}^{\infty}\sum_{(n,\ell_1)\in\mathbb{Z}^2\setminus\{\mathbf{0}\}}\left[\frac{\sqrt{\ell_1^2+(2TL_1)^2n^2}}{\ell_2}\,K_1\left(\frac{2\pi L_2}{L_1}\,\ell_2\,\sqrt{\ell_1^2+(2TL_1)^2n^2}\right)\right]. \end{aligned} \tag{10.14}$$

10.2.3 Case III: Finite volume box

Using, again, the same type of procedure as for the two previously cases, we may set $c = 3$ in eq. (A.19), perform a few more refinements, and then obtain within the usual approach,

the free energy density, $f^{(c=3)}(T, L_1, L_2, L_3)$, of a system geometrically confined in a finite volume box

$$
\begin{aligned}
f^{(3)} =& -\frac{\pi^2}{1440 L_1^4} - \frac{1}{64\pi\, L_1^2 L_2^3} \sum_{\ell=1}^{\infty} \left[\frac{L_1 \left(1 - \mathrm{e}^{-\frac{2\pi L_2}{L_1}\ell}\right) + 2\pi L_2 \ell}{\ell^3} \times \operatorname{csch}^2\left(\frac{\pi L_2}{L_1}\,\ell\right) \right] \\
& - \frac{\pi}{96 L_1^2 L_2 L_3} + \frac{(L_2 + L_3)\,\zeta(3)}{32 L_1^3 L_2 L_3} + \frac{1}{4 L_1^2 L_2 L_3} \sum_{\ell_1,\ell_2=1}^{\infty} \left[\frac{\ell_1}{\ell_2}\, K_1\left(2\pi \ell_1 \ell_2 \frac{L_2}{L_1}\right) \right] \\
& - \frac{1}{2\pi L_1 L_2 L_3} \sum_{\ell_1,\ell_2,\ell_3=1}^{\infty} \left[\frac{1}{\ell_3} \sqrt{\left(\frac{\ell_1}{L_1}\right)^2 + \left(\frac{\ell_2}{L_2}\right)^2}\; K_1\left(2\pi L_3 \ell_3 \sqrt{\left(\frac{\ell_1}{L_1}\right)^2 + \left(\frac{\ell_2}{L_2}\right)^2}\right) \right] \\
& - \frac{\sqrt{2}}{L_1 L_2 L_3} \sum_{\ell,\ell_1,\ell_2,\ell_3=1}^{\infty} \left[\sqrt{\frac{1}{\ell}\left(\frac{\ell_1^2}{L_1^2} + \frac{\ell_2^2}{L_2^2} + \frac{\ell_3^2}{L_3^2}\right)}\; K_{\frac{1}{2}}\left(\frac{\ell}{T}\sqrt{\frac{\ell_1^2}{L_1^2} + \frac{\ell_2^2}{L_2^2} + \frac{\ell_3^2}{L_3^2}}\right) \right]. \qquad (10.15)
\end{aligned}
$$

Introducing a new notation, in order to shorten our next representation, namely the set σ of permutations of L_i,[1] as well as $\Omega = \{L_1,\, L_2,\, L_3\}$, we may also use our alternative approach to compute the same free energy density,

$$
\begin{aligned}
f^{(3)} =& -\frac{\pi^2 T^4}{90} + \frac{T\, \log\left(8 T^3 L_1 L_2 L_3\right)}{24 L_1 L_2 L_3} + \frac{\zeta(3)\, T^3 (L_1 L_2 + L_1 L_3 + L_2 L_3)}{4\pi L_1 L_2 L_3} \\
& - \frac{\pi T^2 (L_1 + L_2 + L_3)}{24 L_1 L_2 L_3} - \frac{\zeta(3)\, T (L_1^3 L_2^3 + L_1^3 L_3^3 + L_2^3 L_3^3)}{48\pi L_1^3 L_2^3 L_3^3} \\
& + \frac{\pi T (L_1^2 L_2 + L_1 L_2^2 + L_1^2 L_3 + L_1 L_3^2 + L_2^2 L_3 + L_2 L_3^2)}{144 L_1^2 L_2^2 L_3^2} \\
& + \frac{T}{4 L_1 L_2 L_3} \sum_{L_i \in \Omega} \sum_{\ell \in \mathbb{N}} \left[\log\left(1 - \mathrm{e}^{-4\pi T L_i \ell}\right) - \frac{T^2 \ell}{6 L_i^2}\, \mathrm{Li}_2\left(\mathrm{e}^{-4\pi T L_i \ell}\right) - \frac{T}{24\pi L_i^3}\, \mathrm{Li}_3\left(\mathrm{e}^{-4\pi T L_i \ell}\right) \right] \\
& + \sum_{\sigma_i \in \sigma} \left[\frac{T^2}{4 L_1 L_2 L_3} \sum_{(n,\ell) \in \mathbb{N}^2} \left[\frac{\sigma_i(1) + \sigma_i(2)\ell}{n}\, K_1\left(4\pi T \sigma_i(3) n \ell\right) \right] \right. \\
& \quad - \frac{T}{16 L_1 L_2 L_3} \sum_{(n,\ell) \in \mathbb{Z}^2 \setminus \{\mathbf{0}\}} \log\left(1 - \mathrm{e}^{-\frac{2\pi\sigma_i(1)}{\sigma_i(2)} \sqrt{\ell^2 + (2\pi T \sigma_i(2))^2 n^2}}\right) \qquad (10.16) \\
& \quad - \frac{T}{24 L_1^2 L_2^2 L_3^2} \sum_{\ell_1 \in \mathbb{N}} \sum_{(n,\ell_2) \in \mathbb{Z}^2 \setminus \{\mathbf{0}\}} \left[\sigma_i(1) (\sigma_i(2))^2 \frac{\sqrt{\ell_2^2 + (2nT\sigma_i(3))^2}}{\ell_1^2} \times \right. \\
& \qquad \left. \left. \times K_1\left(\frac{2\pi\sigma_i(1)}{\sigma_i(3)} \ell_1 \sqrt{\ell_2^2 + (2T\sigma_i(3))^2 n^2}\right) \right] \right. \\
& \quad \left. + \frac{T}{48 L_1 L_2 L_3} \sum_{(n,\ell_1,\ell_2) \in \mathbb{Z}^3 \setminus \{\mathbf{0}\}} \log\left(1 - \mathrm{e}^{-4\pi T \sigma_i(1) \sqrt{n^2 + \frac{\ell_1^2}{(2T\sigma_i(2))^2} + \frac{\ell_2^2}{(2T\sigma_i(3))^2}}}\right) \right].
\end{aligned}
$$

Since the expressions in eq. (10.15) and eq. (10.16) describe fully compactified boxes, it is

[1] Containing six elements. For instance, if the third element of σ is $\sigma_3 = (L_3,\, L_1,\, L_2)$, then $\sigma_3(2) = L_1$.

perhaps prudent to reiterate that we have very specifically not taken the microscopic properties of the boundary into account as we are interested in the bulk properties away from the boundary.

Chapter 11

Thermodynamic expressions, first and third laws of thermodynamics, statistical fluctuations, and nonextensivity

In this section we 1) examine how the First Law of Thermodynamics is altered by the compactified directions, in particular showing how the pressure is no longer a scalar but depends on direction, 2) provide some formal manipulations to arrive at the formulae for the usual thermodynamic quantities such as the EoS that we ultimately evaluate numerically in chapter 12, 3) comment on the effects of geometric confinement on the Third Law of Thermodynamics, 4) quantify the thermal fluctuations of our geometrically confined system, and 5) show explicitly that a thermal system between parallel plates is not extensive.

11.1 Modification of the first law

Recall that the fundamental object that is computed when using the canonical ensemble is the partition function, $\mathcal{Z}(T, \{L_i\})$. The partition function is indeed fundamental in the sense that it allows one to compute any thermodynamic potential, and therefore any thermodynamic quantity of interest. Recall also that the natural potential to use in the canonical ensemble is the Helmholtz free energy $F(T, \{L_i\})$, as previously derived inchapter 10.

Besides being related to the partition function, the free energy is also defined as the Legendre transform [258] of the total energy $E(S, \{L_i\})$ with respect to the total entropy S

$$F(T, \{L_i\}) \equiv E(S, \{L_i\}) - TS, \tag{11.1}$$

where

$$T \equiv \left.\frac{\partial E(S, \{L_i\})}{\partial S}\right|_{\{L_i\}} \tag{11.2}$$

provides a generalization of the definition for the usual Stefan-Boltzmann thermodynamic temperature [259, 260]. Recall also that the Legendre transform in eq. (11.1) is well defined only if E is a convex function of S, at constant lengths L_i, i.e. $E''(S, \ldots) > 0$. We will see below that E is convex for our geometrically confined systems. Furthermore, the total energy as a function of the total entropy S and the lengths L_i, i.e. the entropy as a function of only extensive parameters,[1] is a thermodynamically complete function: $S(E, L_i)$ contains the full thermodynamic information. Other relations such as, e.g., the pressure as a function of T and L_i, $p(T, L_i)$, are *equations of state*, which may only contain partial information about the thermodynamics of the system. See, e.g., [259, 260] for more details on these general concepts.

From both the variable dependence of the total energy and eq. (11.2), we can readily write

$$dE = TdS + \sum_{i=1}^{3}\left[\left(\left.\frac{\partial E}{\partial L_i}\right|_{S,\{L_{k\neq i}\}}\right)dL_i\right]. \tag{11.3}$$

Let us then comment on the subsequent modification of the first law of thermodynamics, recalling that for infinitesimal changes the most general form [259, 260] of the First Law is

$$dE = đQ + đW, \tag{11.4}$$

where $đQ$ and $đW$ are respectively the infinitesimal transfers of heat and work. Considering quasistatic processes, without any loss of generality, and since the only work which can be done is the one coming from a displacement of the boundaries in any of the three directions, we obtain a generalization of the First Law of Thermodynamics to include the possibility of asymmetric pressures:

$$dE = TdS - V\sum_{i=1}^{3}\left[\frac{P_i}{L_i}\,dL_i\right], \tag{11.5}$$

where the P_i are the pressures along each (i) of the three directions and are defined as

$$P_j \equiv -\frac{L_j}{V}\left.\frac{\partial E(S,\{L_i\})}{\partial L_j}\right|_{S,\{L_{k\neq j}\}}. \tag{11.6}$$

The tensor-like structure of the pressure here is not unusual in the context of heavy-ion phenomenology. For instance, the differences in pressure gradients in hydrodynamical simulations with asymmetric initial conditions gives rise to the flow described in section 1.3. The implication here is that the pressure (or force) depends on the compactification length and may differ in different directions.

Equation (11.6) shows explicitly that for asymmetric systems, the pressure may be anisotropic. The above manipulations also allow us to make the temperature and pressure functions of the entropy, S, and the system side lengths, L_i: $T = T(S, \{L_i\})$ and $P_i = P_i(S, \{L_i\})$. Note that in the thermodynamic limit, in which all lengths L_i become asymptotically large, the second

[1] The concept of extensivity being meaningful only in the large size, thermodynamic limit [261].

term of eq. (11.5) reduces to the usual $-PdV$. Thus, in the thermodynamic limit, we recover that the pressure P is thermodynamically complete, an obvious consequence of the relation $PV = -F$, which holds in the thermodynamic limit.

11.2 Thermodynamic expressions

Let us now give some details concerning the practical computation of various thermodynamic quantities. We start from the free energy as derived inchapter 10.

Starting from eq. (11.1), we already have that

$$S\left(T, \{L_i\}\right) \equiv - \left.\frac{\partial F(T, \{L_i\})}{\partial T}\right|_{\{L_i\}}, \tag{11.7}$$

and thus

$$E(T, \{L_i\}) \equiv F(T, \{L_i\}) - T \left.\frac{\partial F(T, \{L_i\})}{\partial T}\right|_{\{L_i\}}. \tag{11.8}$$

In addition, given the proof inappendix A.2.2, we know that eq. (11.6) is equivalent to

$$P_j \equiv -\frac{L_j}{V} \left.\frac{\partial F(T, \{L_i\})}{\partial L_j}\right|_{T,\{L_{k\neq j}\}}. \tag{11.9}$$

Furthermore, using eqs. (11.8) and (11.9), we obtain the trace of the energy-momentum tensor

$$T^{\mu}_{\mu}(T, \{L_i\}) \equiv \varepsilon(T, \{L_i\}) - \sum_{j=1}^{3} P_j(T, \{L_i\}), \tag{11.10}$$

where $\varepsilon \equiv E/V$ is the energy density. Not surprisingly, given that our noninteracting model is indeed conformal, this quantity clearly vanishes. Notice further that it is indeed a generalization of the Stefan-Boltzmann limit result, $T^{\mu}_{\mu} = \varepsilon - 3P$, and encodes the aforementioned system anisotropy.

Coming back now to eq. (11.4), and using the explicit form for the total amount of infinitesimal work that can be done from eq. (11.5), we obtain a heat function Q which admits an exact differential, when all the lengths L_i are kept fixed[2]. More precisely, we have

$$đQ = dE|_{\{L_i\}}, \tag{11.11}$$

which leads to the following definition of the heat capacity at constant sizes (hence volume):

$$C_v(T, \{L_i\}) \equiv \left.\frac{\partial E(T, \{L_i\})}{\partial T}\right|_{\{L_j\}}. \tag{11.12}$$

We keep the usual V index on our heat capacity to emphasize the connection with the usual heat capacity at fixed volume. It is worth noting that given eqs. (11.7) and (11.8), the heat

[2]Hence when the volume is fixed too, even if the latter constraint does not imply the former.

capacity can be re-written as

$$C_v(T, \{L_i\}) = T \left.\frac{\partial S(T, \{L_i\})}{\partial T}\right|_{\{L_j\}}. \tag{11.13}$$

We will see inchapter 12 that our finite-size heat capacity is always positive.

The positivity of the finite size heat capacity means the connection between the pressure, temperature, and entropy is straightforward: the relation $T = T(S, \{L_i\})$ is invertible and hence equivalent to $S = S(T, \{L_i\})$. Thus we may equivalently use $P_i(T, \{L_i\})$ in place of $P_i(S, \{L_i\})$. Further, this statement together with eq. (11.13) imply that $E''(S, \ldots) = T/C_v > 0$, thus making the Legendre transform connecting the free energy with the total energy well defined.

11.3 On the third law

The Third Law of Thermodynamics states that the entropy reduces to a constant value (usually 0) as the temperature of a system goes to 0 [259, 260]. Some implementations of the Lifschitz theory of the Casimir effect in QED claim that in their system the Third Law of Thermodynamics is violated [262]. We first recall that in our system the spatial compactification(s) required for establishing a geometric confinement lead to a zero temperature Casimir-type geometrical contribution to the free energy $F(T, \{L_i\})$. However, given the definition of the entropy eq. (11.7), we expect that this temperature independent contribution vanishes from the expression of the entropy. The numerical value of the entropy can then be assessed by appropriately rescaling S by the dimensionless combination T^3V. Numerical evaluation of this quantity (see chapter 12) clearly shows that $\tilde{s} \equiv \frac{S}{T^3V} \to 0$ as the temperature vanishes. We refer to [263] for another study of the Third Law in the context of QED Casimir systems.

11.4 Fluctuations of the energy

Recall that in the micro-canonical ensemble the total energy is fixed. However, in the canonical ensemble the system is in contact with a heat bath of infinite heat capacity and all energies of the system are accessible through a probability distribution. For the canonical ensemble, then, there is a mean total energy together with a standard deviation (the square root of the statistical variance $\overline{\Delta E^2} = \overline{E^2} - \overline{E}^2$). It is precisely the variance of the energy of the system that we take to provide us with insight into the energy fluctuations of our canonical ensemble system.

One may compute the mean total energy $\overline{E} \equiv E$ in the usual way with partition functions

$$E \equiv \left\langle \hat{H} \right\rangle_{e^{-\beta H}} = \frac{1}{\mathcal{Z}} \frac{\partial \mathcal{Z}}{\partial(-\beta)}, \tag{11.14}$$

where the angular brackets denote the usual ensemble average

$$\langle \ldots \rangle_{e^{-\beta H}} \equiv \frac{1}{\mathcal{Z}} \mathrm{Tr}\left[\ldots \exp\left\{ -\beta \int_V d^{D-1}x \hat{\mathcal{H}} \right\} \right]. \tag{11.15}$$

The standard deviation, $\sigma_E = \sqrt{\overline{\Delta E^2}}$, is then

$$\sigma_E \equiv \sqrt{\left\langle \hat{H}^2 \right\rangle_{e^{-\beta H}} - \left\langle \hat{H} \right\rangle^2_{e^{-\beta H}}} = \sqrt{\frac{\partial E}{\partial(-\beta)}}. \tag{11.16}$$

Therefore, after a little manipulation, the standard deviation may be simply written as

$$\sigma_E = T\sqrt{C_v}, \tag{11.17}$$

where we recall that the heat capacity C_v is defined in eq. (11.12).

Recall that both the heat capacity and the total energy of a system scale with the volume V of the system. Therefore as the system volume increases, the relative size of the energy fluctuations decreases, $\sigma_E/E \sim 1/V^{1/2} \to 0$. Systems that are not compactified in all directions, such as the case of two infinite parallel plates or a rectangular tube of infinite length, have infinite volume and therefore experience *no* fluctuations in their total energy. Crucially, then, for these systems with no fluctuations in total system energy, we conclude that the canonical ensemble must exactly reproduce the results of the microcanonical ensemble. We will exploit this equivalence of ensembles later to demonstrate a phase transition at a critical length (instead of temperature) for isolated systems of finite extent in some (but not all directions) in chapter 13.

In fig. 11.1, we plot the mean total energy and its standard deviation as a function of temperature T (in units of $1/L$) for the case of a massless, noninteracting scalar field geometrically confined in a finite-sized box. The upper left panel shows the results for a symmetric box, with side ratios 1:1:1; the upper right panel shows the same for an asymmetric box of side ratios 1:1:3, a finite volume symmetric tube; the lower panel shows the same for an asymmetric box of side ratios 1:3:3, a set of two finite area parallel plates. One can see that as $T \times L$ grows large, the system approaches the thermodynamic limit, which we denote by "SB," for Stefan-Boltzmann. Even out to relatively large $T \times L \sim 20$, energy fluctuations are on the order of 10%. In the limit that $T \times L \to 0$ the energy density becomes negative, which is the usual case for Casimir-like systems[3].

11.5 Nonextensivity of finite size systems

We show in figure (11.2) the deviation from extensivity for the parallel plates case. The plot shows the difference between the entropy for a massless, noninteracting scalar field between

[3]The negative energy density implies that at some $T \times L$ the energy density is 0. Hence it is not very enlightening to plot the relative fluctuations in energy σ_E/E (as opposed to σ_E/E_{SB} for small $T \times L$.

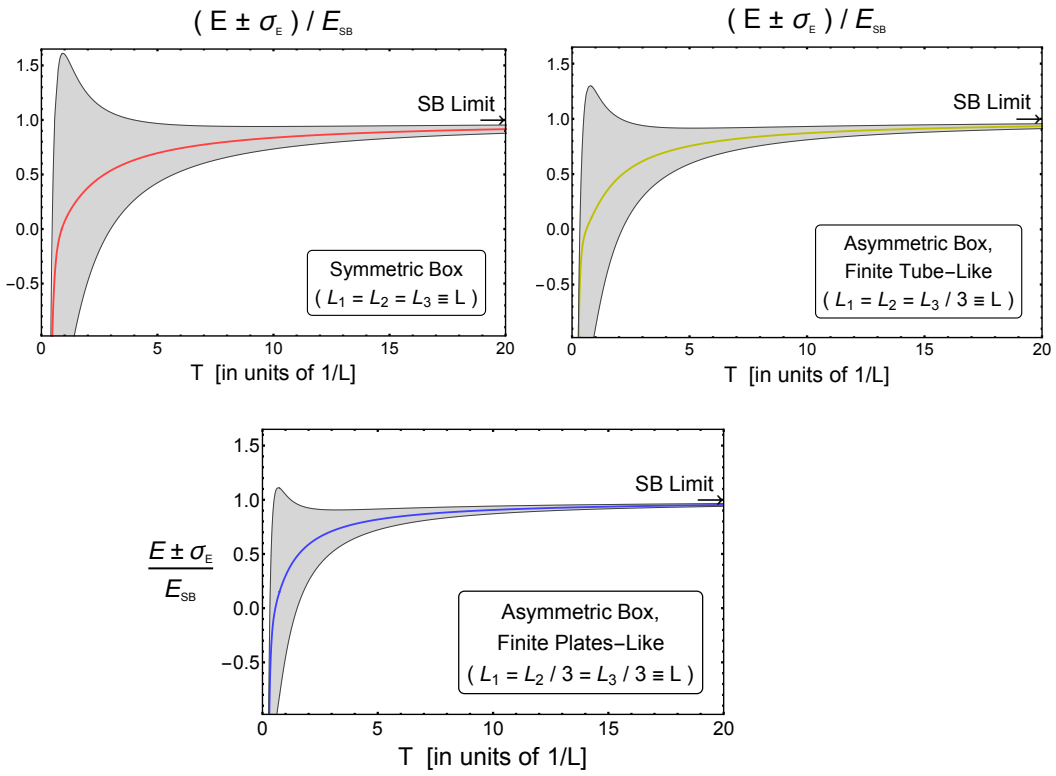

FIGURE 11.1: The mean total energy (solid thick colored lines) with corresponding standard deviation bands describing the fluctuations (whose edges are the solid thin black lines), in different cases of finite volume symmetric and asymmetric boxes, and rescaled to the usual Stefan-Boltzmann limit as a function of the temperature T in units of $1/L$, where L measures the length of the compactified direction(s) for a massless, noninteracting scalar field. The upper left panel accounts for a symmetric box of side ratios 1:1:1, while the upper right panel accounts for an asymmetric box of side ratios 1:1:3, and the lower panel for an asymmetric box of side ratios 1:3:3.

two parallel plates a distance $2L$ apart and twice the entropy for plates a distance L apart scaled by T^3V. For an extensive system, this difference is 0. The nonextensivity goes to zero as $T \to 0$ trivially: the entropy for the parallel plates case falls faster than T^3V for small T, which we show in detail below in the left panel of fig. 12.5. A system with all lengths infinite is extensive. Hence we may understand why the system approaches extensivity as T increases in the figure as follows. As T increases, the thermal de Broglie wavelength decreases, and the effective size of the system becomes larger.

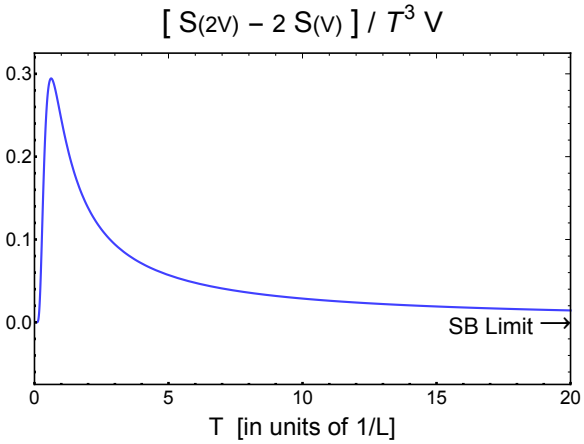

FIGURE 11.2: The difference in entropy for a massless, noninteracting scalar field between parallel plates a distance $2L$ apart and twice the entropy for a system with plates a distance L apart at a temperature T measured in units of $1/L$ scaled by the quantity T^3V.

11.6 On the second law

Recalling that from eqs. (11.2), (11.5) and (11.6), the T and all P_i appear to be functions of S and the L_i, as functions of state should be, and that there exists a one-to-one correspondence

$$T\Big(S, \{L_i\}\Big) \Leftrightarrow S\Big(T, \{L_i\}\Big), \tag{11.18}$$

for reasons mentioned in section 11.1, we then have the following crucial identity

$$P_i\Big(S, \{L_i\}\Big) = P_i\Big(T, \{L_i\}\Big), \tag{11.19}$$

from which we obtain, albeit differentiating both sides, a set of chain rules which will be computationally very convenient in the following.

Being now equipped from the previous section and the above remark, we will probe the second law of thermodynamics. In doing so, we closely follow [260], and rely on the fact that it may be proven (see, e.g., [259]) that the principle of the maximization of the entropy in an adiabatic process is equivalent to the principle of the minimization of the energy in an *isentropic* process (see, in particular, [264, Chapter 2.8]). In the light of eq. (11.5), the usual two dimensional study of the energy as a function of the entropy and the volume is here extended to a four dimensional study of the total energy $E(S, \{L_i\})$ as a function of the

entropy and the three lengths — albeit at present, for probing the second law, the entropy will be kept fixed.

Thus, we are interested in the curvature of the hyper-surface described by the total energy at constant entropy. And the second law amounts to requiring that the Hessian matrix of the function $E = E(\{L_i\})$ be positive semi-definite, which is to say that we require the matrix

$$\mathcal{E}_{ij} \equiv \frac{L_i L_j}{T^4 V} \frac{\partial^2 E(S, \{L_k\})}{\partial L_i|_{S,\{L_{k\neq i}\}} \, \partial L_j\big|_{S,\{L_{k\neq j}\}}}, \tag{11.20}$$

to have positive semi-definite eigenvalues, each partial derivative being understood to be performed while keeping the entropy and all non-relevant lengths constant. We notice that the above matrix elements are scaled conveniently, which amounts to rescale each of the L_i directions in the curvature study of $E(\{L_i\})$, yet leaving unaffected the positivity requirement on the corresponding Hessian. One may then compute the matrix elements eq. (11.20) (see appendix A.2.3 for more details)

$$\begin{aligned}\mathcal{E}_{ij} = &\left(\tilde{s} + (TLi)\left.\frac{\partial \tilde{s}}{\partial (TLi)}\right|_{T,\{L_{k\neq i}\}}\right)\frac{1}{\tilde{c}_v}\left(\tilde{s} + (TLj)\left.\frac{\partial \tilde{s}}{\partial (TLj)}\right|_{T,\{L_{k\neq j}\}}\right) + \tilde{f}(1-\delta_{ij}) \\ &+(TLi)\left.\frac{\partial \tilde{f}}{\partial (TLi)}\right|_{T,\{L_{k\neq i}\}} + (TLj)\left.\frac{\partial \tilde{f}}{\partial (TLj)}\right|_{T,\{L_{k\neq j}\}} \\ &+(TLi)(TLj)\frac{\partial^2 \tilde{f}}{\partial (TLi)|_{\{L_{k\neq i}\}}\partial (TLj)|_{\{L_{k\neq j}\}}}.\end{aligned} \tag{11.21}$$

Given the particular cases of interest, the relevant expressions for the free energy may be substituted into eq. (11.21), and the eigenvalues may be evaluated numerically. A numerical root finding algorithm can then be applied in order to determine the TLi-range in which the eigenvalues of $\mathcal{E}$ are positive semi-definite, for each of the parallel planes, infinite tube, and fully compactified box cases. This process allows us to put, for now, a lower limit on the region of validity for our present calculations, as is shown in fig. 11.3 for the L_i-symmetric cases.

We claim only a lower limit on the region of validity since, although the second law is violated when the entropy is no longer a concave hypersurface, the problem of computing the entropy when one is only able to derive the free energy becomes a question of ensemble equivalence and the validity of the Legendre or Legendre-Fenchel transform (whichever is applicable). It is known that if the determinant of the Hessian of a hypersurface becomes singular [265, Chapter 7] then the hypersurface contains a change of curvature, but the point at which the Hessian becomes singular is not necessarily the point at which the hypersurface deviates from its convex (or concave) hull [266]. However, determining the breakdown point of the Legendre transform (which requires global convexity or concavity in the variable to be transformed) is not trivial as it requires the determination of the convex hull of the free energy. It is not clear how such a hull may be computed in our case since the free energy diverges at small L_i. A possible solution may be to employ a carefully chosen truncation:

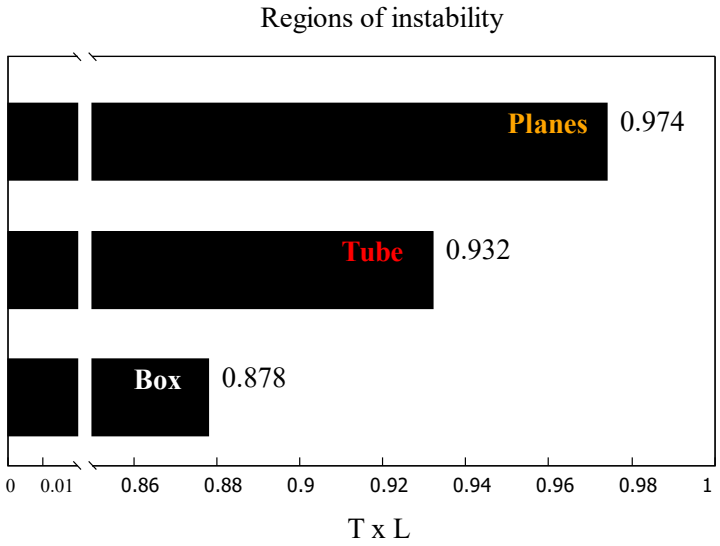

FIGURE 11.3: The regions of instability of the present calculations for the infinite parallel planes, infinite rectangular tube and finite volume box cases.

considering only the plates case, if one restricts oneself to the region in which the determinant of the Hessian matrix of free energy has the proper sign, i.e., truncates the free energy so that it is only defined on a domain in which it has the correct curvature (a saddle in $T - L_1$ space), then the convex hull of the (truncated) free energy is trivial because there is no longer a divergence at small L_1. Therefore, the Legendre-Fenchel transform is equivalent to the Legendre transform and one may compute any thermodynamic function more easily. It is not clear from a large deviation theory point of view that such a truncation is strictly speaking a valid solution to the problem of determining the convex hull. At the very least the region in which the free energy does not respect the second law should not be considered physical.

We refer to [267–269] for somewhat related studies, relevant to the actual QED Casimir effects. In the next section, an interpretation for the "breakdown" of the second-law is offered.

Chapter 12

Thermodynamic properties of a geometrically confined scalar field

In this section, we present a number of thermodynamic quantities, ranging from the free energy to the specific heat capacity at constant lengths, relevant to various geometrically confined systems (infinite parallel plates, infinite tube, and finite volume box). The results are all computed from the canonical ensemble, which is to say for systems in contact with an infinite heat bath held at constant temperature T, for a massless, noninteracting scalar field. Each of the plots has been rescaled by the Stefan-Boltzmann result. Recall that in the Stefan-Boltzmann limit of zero coupling and infinite size in all directions, various thermodynamic expressions we wish to evaluate in the finite size case are $F_{SB} \equiv -\pi^2 T^4 V/90$, $p_{SB} \equiv \pi^2 T^4/90$, $E_{SB} \equiv \pi^2 T^4 V/30$, $S_{SB} \equiv 2\pi^2 T^3 V/45$, $C_{vSB} \equiv 2\pi^2 T^3 V/15$.

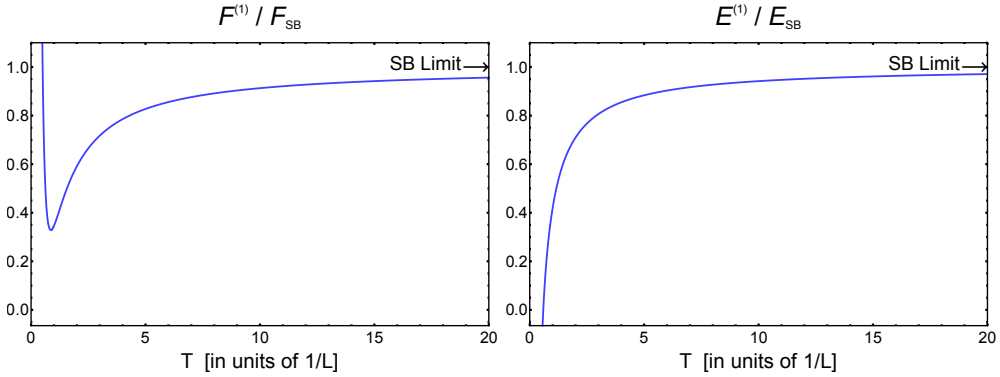

FIGURE 12.1: The free energy (left) and the total energy (right) for a massless, noninteracting scalar field between two infinite parallel plates and rescaled to their Stefan-Boltzmann limits as a function of temperature T in units of $1/L$, where L is the distance between the sides of the system that are of finite length.

In fig. 12.1, we show the free and total internal energies in the case of two infinite parallel plates as a function of the temperature T in units of $1/L$, where L is the distance between plates. Recall that for a plasma of temperature ~ 400 MeV and width of ~ 2 fm, relevant for a high multiplicity pp or pA collision at RHIC or LHC, $T \times L \sim 4$. For a mid-central AA collision resulting in a plasma of temperature $T \sim 400$ MeV and width ~ 10 fm, $T \times L \sim 20$. One can see in the figure that both results tend towards the thermodynamic limit as $T \times L \to$

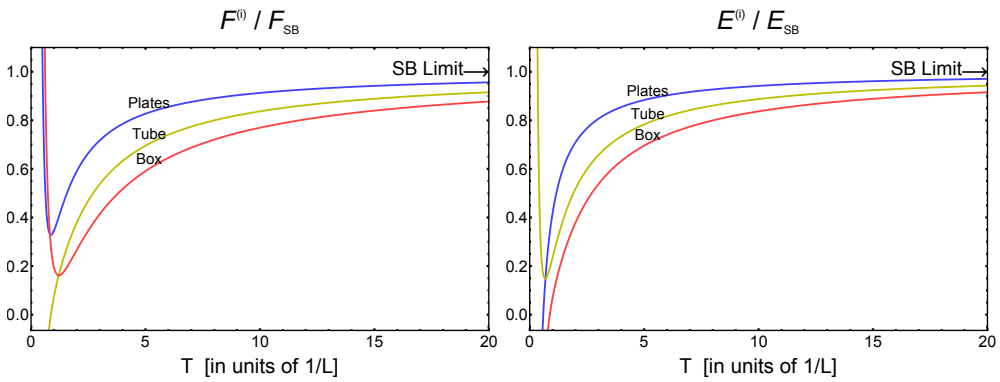

FIGURE 12.2: The free energy (left) and the total energy (right) for a massless, noninteracting scalar field between two infinite parallel plates (blue lines), in an infinite symmetric tube (yellow lines), and in a finite volume symmetric box (red lines) rescaled by the Stefan-Boltzmann limits as a function of temperature T in units of $1/L$, where L is the distance between the sides of the system that are of finite length.

∞. However, both the energy and the free energy are $\gtrsim 5\%$ different from their Stefan-Boltzmann limits even at the relatively large value of $T \times L \sim 20$. The total energy of a system geometrically confined in between two infinite parallel plates separated by a distance L, and in contact with a thermal bath at temperature T, is thus noticeably affected by its finite size.

In fig. 12.2, we display the free and total energies in the three cases of infinite parallel plates (blue lines), infinite tube (yellow lines), and finite volume box (red lines). All results tend towards the Stefan-Boltzmann ones as $T \times L \to \infty$. We see again the large finite size corrections to the Stefan-Boltzmann limits, even for $T \times L \sim 20$, with the size of the corrections increasing with increasing number of compactified directions. Thus the total and free energies of a system geometrically confined is noticeably affected by its finite sized directions. We note that the peculiar behavior of the tube case, that its total energy reaches a $T = 0$ limit which is positive unlike the plates and box cases, is not a surprise. It is indeed due to the dimensionality of the space-time [270].

We now turn towards the different pressures. In fig. 12.3 we plot the perpendicular (left) and parallel (right) pressures as a function of the temperature T in units of length $1/L$ for a massless, noninteracting scalar gas held between two infinite parallel plates that are a perpendicular distance L apart. The plots have a number of interesting properties. First, the pressure in the perpendicular direction (p_1, left panel), i.e. between the plates, is different from the pressure in the parallel direction (p_2 or p_3, right panel), i.e. along the plates. Thus no single scalar pressure can be used to describe the finite sized parallel plates case: there is an intrinsic anisotropy due to the compactification. Furthermore, the compactification of one direction appears to have a greater effect on the pressure in the noncompactified parallel direction than on the pressure in the compactified perpendicular direction: the parallel pressure is nonmonotonic, unlike in the perpendicular case, and approaches the Stefan-Boltzmann limit much slower than the perpendicular pressure.

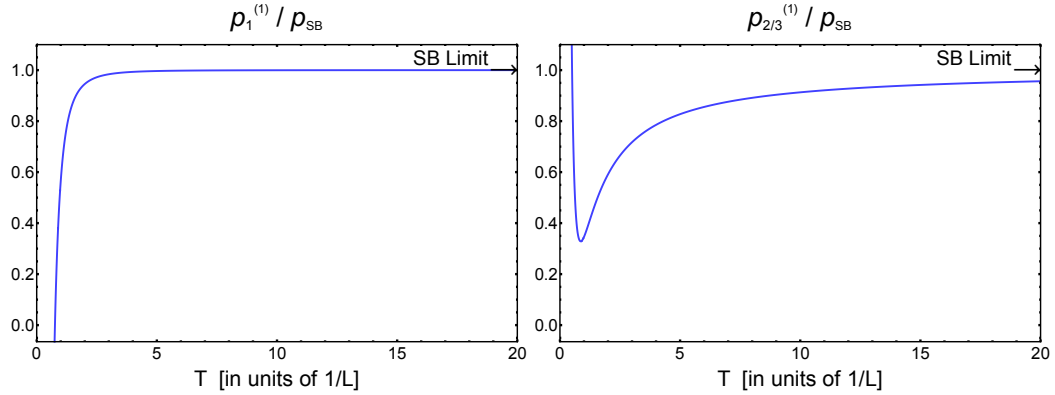

FIGURE 12.3: The pressures, perpendicular (left, p_1) and parallel (right, p_2 or p_3), for a massless, noninteracting scalar field restricted between two infinite parallel plates as a function of temperature T in units of the perpendicular distance L between the two plates. Both quantities are relative to the usual Stefan-Boltzmann pressure.

Note that the pressure for our geometrically confined system dimensionally reduces in the correct way. For our infinite parallel plates case in $4D$ spacetime

$$p_{\parallel}(\beta,\, L) \equiv \frac{\partial(T \ln Z)}{\partial V_{\parallel}} = \frac{1}{2\pi\beta^3} \sum_{\ell=1}^{\infty} \Big[\frac{\pi\beta\ell}{L} \mathrm{Li}_2\Big(e^{-\pi\beta\ell/L}\Big) + \mathrm{Li}_3\Big(e^{-\pi\beta\ell/L}\Big) \Big] + vacuum, \qquad (12.1)$$

where *vacuum* depends only on L. One can see that in the limit $T \times L \ll 1$ eq. 12.1 reproduces the pressure of a massive, noninteracting scalar theory in 3 spacetime dimensions in the Stefan-Boltzmann limit

$$p_{2D}(\beta,\, m) = \frac{1}{2\pi\beta^3} \Big(m\beta\, \mathrm{Li}_2\Big(e^{-m\beta/L}\Big) + \mathrm{Li}_3\Big(e^{-m\beta/L}\Big) \Big), \qquad (12.2)$$

for $m \equiv \pi/L$, where we have dropped the temperature independent, infinite zero point pressure from the last expression. One sees then that the inverse of the compactified length L in $4D$ acts as an effective mass in the $3D$ theory.

We show in fig. 12.4 the pressure in one of the compactified directions for the two infinite parallel plates, the infinite (symmetric) tube and the finite volume (symmetric) box cases, respectively represented by the blue, yellow, and red lines. The pressures are rescaled by their Stefan-Boltzmann limits and are plotted as a function of the temperature T in units of $1/L$, where L is the length of the compactified direction.

Notice that the effect of further compactifications on the pressure is drastic. In the finite box case, for $T \times L \sim 4$, which is relevant for a pp collision resulting in a ~ 400 MeV QGP, the pressure sees a $\sim 40\%$ correction. Even for $T \times L \sim 20$, there are $\sim 10\%$ corrections to the pressure of the finite volume box. Note that while it might appear that the pressures diverge at low T, this apparent divergence is an artifact of plotting the ratio of our finite sized results with the Stefan-Boltzmann limit; recall that the Stefan-Boltzmann case scales as T^4. One may use the un-rescaled expression eq. (10.11) to investigate the asymptotic $T = 0$ behavior, in which case one recovers the usual Casimir pressure in the longitudinal direction in each

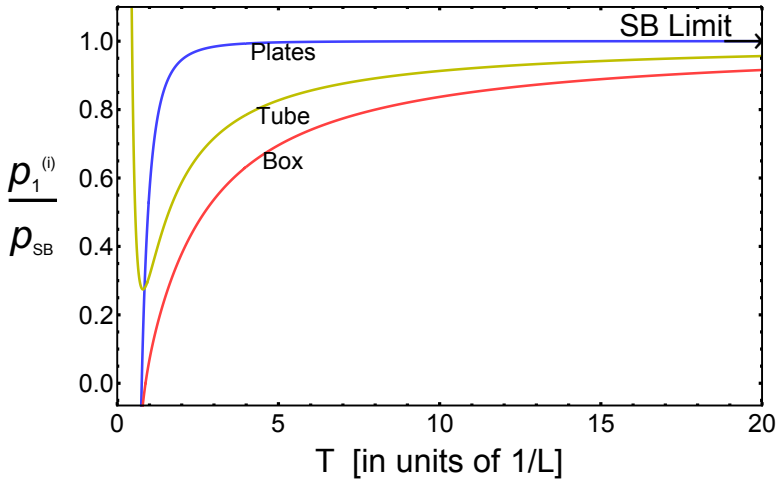

FIGURE 12.4: Longitudinal pressure of a massless, noninteracting scalar field in between two infinite parallel plates (blue line), in an infinite symmetric tube (yellow line), and in a finite volume symmetric box (red line). All results are rescaled to the Stefan-Boltzmann limit. The pressures are plotted as a function of the system temperature T in units of $1/L$, where L measures the length of the compactified direction(s).

compactification case. (This comment also applies to the other pressures, and the free and total energies.)

We plot in fig. 12.5 the entropy (left) and specific heat (right) for the infinite plates case as a function of the temperature T in units of $1/L$, where L measures the length of the finite direction(s) of the systems, and scaled by the Stefan-Boltzmann limit. The inset in the left plot shows that the entropy of our finite sized system indeed goes to zero as the temperature vanishes, as dictated by the Third Law of Thermodynamics, and as opposed to some implementations of Lifschitz's theory for the QED Casimir effect [262]. The inset in the right plot shows that the specific heat for our finite sized system always remains positive.

We plot in fig. 12.6 the entropy (left) and specific heat (right) for the infinite plates (blue), infinite tube (yellow), and finite box (red) cases as a function of the temperature T in units of $1/L$, where L measures the length of the finite direction(s) of the systems, and scaled by the Stefan-Boltzmann limit. Although we do not provide insets in these plots, the entropy for all our cases again goes to 0 as $T \to 0$, in accordance with the Third Law of Thermodynamics and the specific heat remains strictly positive. Notice again that the size of the deviations from the Stefan-Boltzmann limit increases as the number of compactified dimensions increases. In particular the deviation from the Stefan-Boltzmann limit is significant ($\sim 10-15\%$) for the finite box case even out to $T \times L \sim 20$.

We would like to understand a bit better the importance of the type of boundary condition imposed on our systems on the size of the finite size corrections to the Stefan-Boltzmann limit. Intuitively, one might expect that periodic boundary conditions cause the least difference since the system has a finite size but is boundaryless. We show in fig. 12.7 the free energy of a massless, noninteracting scalar field between two infinite parallel plates rescaled to its Stefan-Boltzmann limit as a function of the temperature T in units of $1/L$, where L is

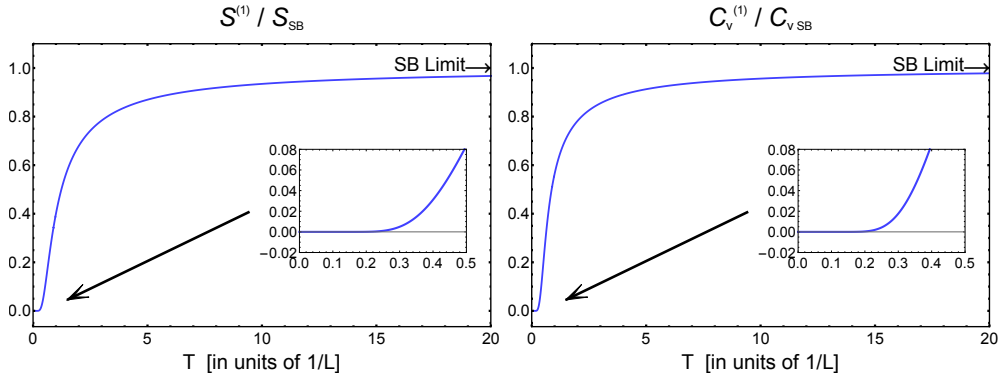

FIGURE 12.5: The total entropy (left) and specific heat at constant lengths (right) for a massless, noninteracting scalar field between two infinite parallel plates separated by a distance L as a function of temperature T measured in units of $1/L$. Both quantities are rescaled to their Stefan-Boltzmann limits. The insets show the small temperature limits of the quantities.

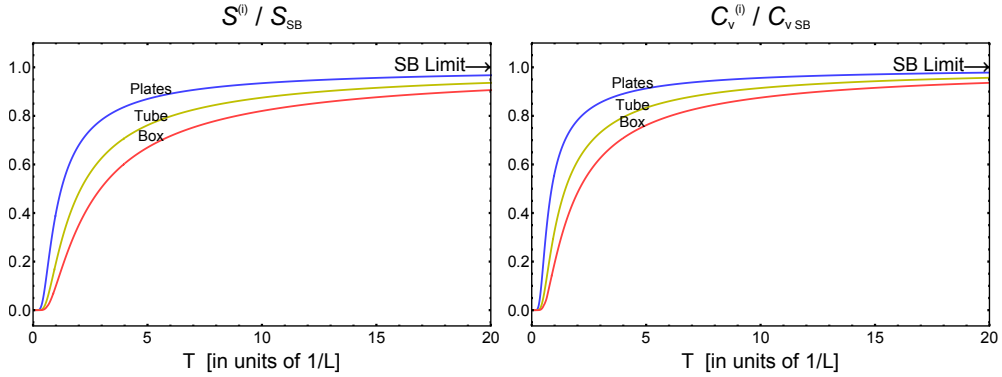

FIGURE 12.6: (Left) The entropy and (right) the specific heat for a massless, noninteracting scalar field for the cases of two infinite parallel plates (blue lines), the infinite symmetric tube (yellow lines), and the finite volume symmetric box (red lines). The quantities are plotted as a function of the temperature T in units of $1/L$, where L is the compactification length for the system, and the quantities are rescaled to their Stefan-Boltzmann limits.

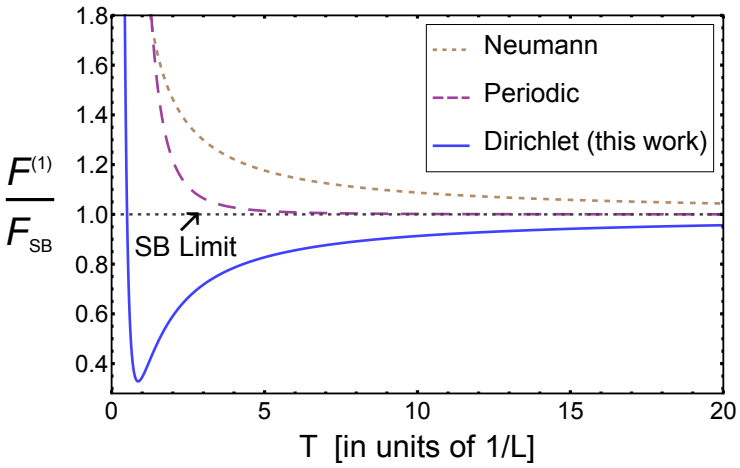

FIGURE 12.7: The free energy of a massless, noninteracting scalar field in between two infinite parallel plates rescaled to its Stefan-Boltzmann limit for Dirichlet (blue), Neumann (dotted brown), and periodic (dashed purple) boundary conditions.

the distance between the plates. The plot shows the results for Dirichlet (solid blue), Neumann (dotted brown), and periodic (dashed purple) boundary conditions, computed using a simple adjustment of the techniques described for the DBC case. One can clearly see from the figure that the system with periodic boundary conditions reaches the Stefan-Boltzmann limit at much smaller $T \times L$ than either the Neumann or Dirichlet cases. One should perhaps then hesitate to conclude that small finite sized corrections computed for a system with periodic BCs [214–222] will remain small for heavy ion phenomenology.

Let us now come back to our geometric confinement boundary conditions. Since our noninteracting scalar field theory is conformal, the trace of the energy momentum tensor should vanish identically. We performed a nontrivial check of our numerics and confirmed that our results do respect $T^{\mu}_{\mu} \equiv \varepsilon - (p_1 + p_2 + p_3) = 0$.

Chapter 13

A novel geometric phase transition

In this section we consider how our results depend on the physical setup of our system. In the previous section we considered our system to be in contact with an infinite thermal heat bath. We now focus in particular on the infinite parallel plates case and consider the possibility of the system existing in isolation: instead of a system at constant temperature T we rather consider a system with constant energy E. Although constant energy calculations pertain to the microcanonical ensemble, all results shown in this section are derived from the partition function calculated in the canonical ensemble. We are justified in this approach as argued in section 11.4: the ratio of the energy fluctuations away from the mean energy divided by the mean energy computed in the canonical ensemble for the Stefan-Boltzmann parallel plates case is zero; hence we will have ensemble equivalence between the canonical and microcanonical ensembles. Thus the canonical ensemble provides exact results for all thermodynamic quantities for a set of parallel plates kept in isolation, i.e. with fixed energy E.

As we explore the different physics associated with a noninteracting scalar field between two infinite parallel plates, it is worth keeping in mind two related thermodynamic concepts. First, a system is thermodynamically stable if, when squeezed and all other parameters are held fixed, the pressure increases. I.e. our parallel plates system separated by a length L is thermodynamically stable so long as

$$\frac{\partial p}{\partial L} < 0 \tag{13.1}$$

for fixed E and plate area V_2, which is to say that the pressure in the system decreases with increasing system size; see, e.g., [213]. Second, a system undergoes a second order phase transition should a susceptibility diverge; see, e.g., [271]. Recall that the susceptibility is the derivative of an extensive parameter with respect to its conjugate intensive parameter. The susceptibility is then nothing more than the multiplicative inverse of the second derivative of the entropy with respect to some parameter. For our case of two parallel plates separated by a distance L, the susceptibility is the length-scaled negative of the compressibility:

$$\chi \equiv \frac{\partial L}{\partial p} = -L\kappa. \tag{13.2}$$

Comparing the condition for stability, eq. (13.1)), to the definition of susceptibility above, one can see that a second order phase transition occurs when the system goes from being thermodynamically stable to unstable[1]. Further, the order parameter associated with the compressibility is the size of the system L.

We can further understand physically what happens at a phase transition by examining the relationship between the entropy and an intensive variable such as the pressure. There are three common, and equivalent, definitions of pressure:

$$p \equiv \frac{1}{\beta}\left.\frac{\partial S}{\partial V}\right|_E \equiv -\left.\frac{\partial E}{\partial V}\right|_S \equiv \frac{1}{\beta}\left.\frac{\partial \ln Z}{\partial V}\right|_\beta . \tag{13.3}$$

The first expression is the quantity that must be equal for two systems in thermodynamic equilibrium separated by a moveable wall. The second expression is the generalized force conjugate to the volume. And the third is the generalized thermodynamic intensive variable conjugate to the extensive volume variable. In the parallel plates case of current interest, the derivatives with respect to volume V become derivatives with respect to separation length L. One can then see that a phase transition occurs precisely when the second derivative of the entropy changes sign; i.e. when the entropy goes from a convex function of L to a concave function of L.

While all three expressions of the pressure in eeq. (13.3) are equivalent, the different expressions are naturally a function of different variables: $p(E,\, L)$, $p(S,\, L)$, and $p(\beta,\, L)$, respectively, where we have already switched over to using the plate separation distance L instead of the volume V for our system. One may freely switch between different definitions of pressure by using relations between the various independent variables. For example, equipped with an expression that relates the energy to the entropy and volume, one can equivalently use the first definition of pressure in the same way as the second definition with $p\Big(E(S,L),L\Big) = p(S,L)$.

In fig. 13.1 we compare the pressure of a massless, noninteracting scalar field between parallel plates of area V_2 as a function of the plate separation length L for fixed temperature T (left) and for fixed energy E (right); i.e. the left plot shows the pressure as a function of L for a system in contact with a heat bath whereas the right plot shows the pressure as a function of L for an isolated system. We computed $p(L)$ from the partition function eq. (10.11) by numerically inverting $E(T,\, V_2,\, L)$ to find $p\Big(T(E,\, V_2,\, L),\, V_2,\, L\Big)$. It is perhaps not so easy to see in the figure, but for the system in contact with a heat bath, the pressure always decreases for decreasing L; i.e. $\partial p/\partial L > 0$ and the system is always unstable: the system always wants to collapse. The isolated system, however, resists collapse as the system size is decreased—i.e. $\partial p/\partial L < 0$ and the system is thermodynamically stable—so long as the system starts off large enough, which is to say the length L is greater than some critical length L_c. As soon as $L \leq L_c$, the system is unstable and will collapse, shrinking until the plates are no longer separated at all. We show explicitly the susceptibilities as a function of plate separation L for

[1] Note that, at this stage of the discussion of the phase transition, we are assuming that we are allowed to employ the truncation discussed in section 11.6 so that the Legendre transform from the free energy to the entropy is valid and that the canonical and microcanonical ensembles are, therefore, equivalent in the region of L_1 where the phase transition occurs.

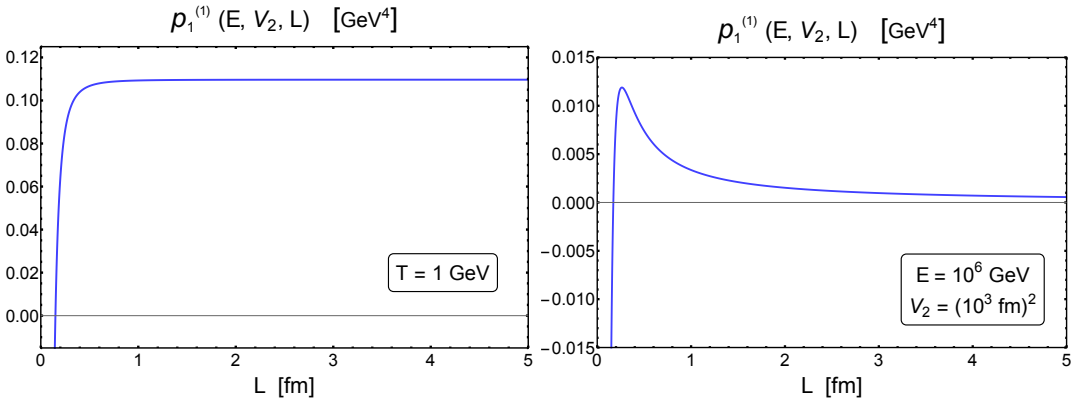

FIGURE 13.1: (Left) Pressure p as a function of L for a massless, noninteracting scalar field between two parallel plates separated by a distance L in contact with a thermal heat bath at a temperature $T = 1$ GeV. (Right) Same but for an isolated system at constant energy $E = 10^6$ GeV and with parallel plates area $V_2 = 10^6$ fm^2.

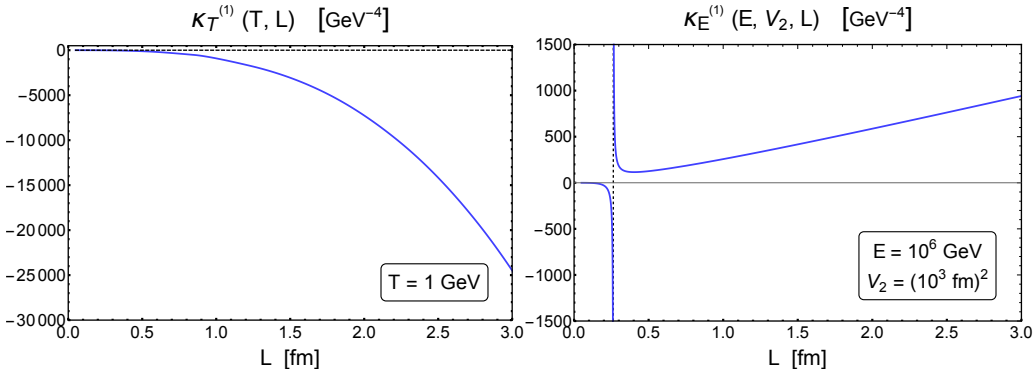

FIGURE 13.2: (Left) Isothermal compressibility $\kappa_T = (1/L)\partial L/\partial p|_T$ as a function of plate separation L for a noninteracting, scalar field between two parallel plates a distance L apart and held at a temperature $T = 1$ GeV. (Right) Isoenergetic compressibility $\kappa_E = (1/L)\partial L/\partial p|_E$ for the same scalar field system with constant energy $E = 10^6$ GeV and with parallel plates area $V_2 = 10^6$ fm^2.

these two systems in fig. 13.2. As claimed, the isothermal compressibility is purely negative while the isoenergetic compressibility clearly exhibits a divergence.

We thus conclude that our massless, noninteracting scalar field theory constrained between two parallel plates exhibits a phase transition at a critical *length* L_c. This novel phase transition length is interesting for two main reasons. First, we believe this is the first example of the explicit derivation of a phase transition induced by changing the size of the system, as opposed to the usual means of inducing a phase transition by changing the temperature of the system[2]. Second, in the derivation shown above, the phase transition is due to changing an extensive variable, as opposed to the usual description of a phase transition due to changing an intensive variable. To be clear: we envision the (somewhat artificial) construct of a pair of (approximately infinitely large) parallel plates of *fixed* separation length L. The space

[2]Although the van der Waal's gas exhibits a phase transition below a critical temperature by changing the volume, we stress that, in our case, no such critical temperature exists and there exists a phase transition at any temperature. Furthermore, our investigation concerns a non-interacting gas while the phase transition in the van der Waal's gas is interpreted as being due to self-interactions.

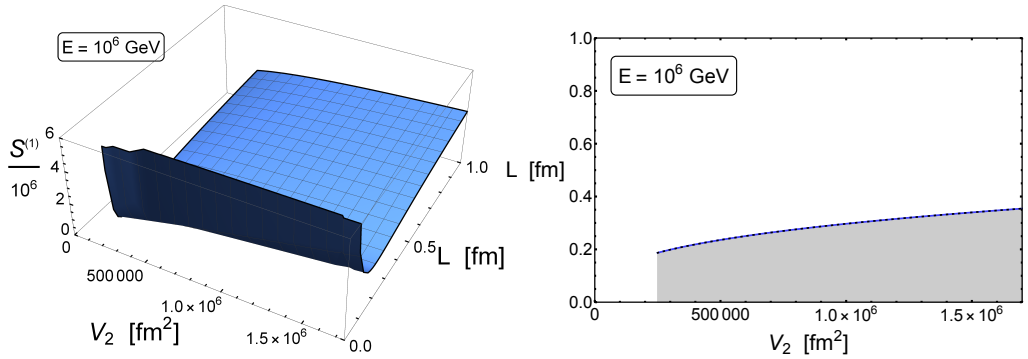

FIGURE 13.3: (Left) The entropy S of a massless, noninteracting scalar field between two parallel plates of area V_2 in fm^2 separated by a distance L in fm for energy $E = 10^6$ GeV. (Right) The region of (V_2, L) space for which one of the eigenvalues of the Hessian of the entropy S is positive is shaded in gray. The edge of the region is given by the equation $L_c(V_2,\ E = 10^6\ \text{GeV},\ T \times L = 1)$.

between the plates is filled with a noninteracting, massless scalar field, and one measures the pressure on the plates. Since the separation length is fixed, the system cannot actually collapse. However, one is tempted to interpret the right plot of fig. 13.1 as follows. Consider a system of two (approximately infinitely large) parallel plates filled with a noninteracting, massless scalar field. One plate is fixed, but the other plate is freely allowed to move and is exposed to a constant external pressure p; at equilibrium, the parallel plates settle down to an average separation distance $\langle L \rangle$ set by p. As one slowly dials up the external pressure p, L decreases but the system continues to find a new, smaller $\langle L \rangle$ at which the plates are in equilibrium with the external pressure p[3]. At a certain large enough critical pressure p_c, the scalar field inside the plates can no longer resist the external pressure, and the system collapses. One would very much like to confirm this extrapolated interpretation from the canonical ensemble; to do so would require going to the higher ensemble in which the system is in contact with a hypothetical thermal pressure bath. It is perhaps not so easy to see from fig. 13.1 or fig. 13.2, but we will show below that the phase transition occurs at a length of order the thermal wavelength, $L_c \sim 1/T$, a fact which does not come as a surprise as it is the only scale in the problem. Since the phase transition seen from the canonical ensemble calculation occurs at a length of order the thermal wavelength, it is possible that fluctuations in the separation distance L from the mean distance $\langle L \rangle$ that one would necessarily observe in a system exposed to a thermal pressure bath spoil the observation of a phase transition. A quantitative derivation of the properties of a massless, noninteracting scalar field between two parallel plates of variable separation distance and exposed to a thermal pressure bath via a higher ensemble is left for future work.

Since we observe this phase transition for a massless, noninteracting scalar field theory in a small enough geometric confinement, a natural question to ask is: is this transition one of Bose-Einstein condensation? One can see an indication of an answer in the negative from fig. 13.3. On the left, we plot the entropy S as a function of the area of the parallel plates, V_2,

[3]To really match in principle the right plot of fig. 13.1 one would have to keep the total energy constant by continuing to remove the energy put into the system by the work of the external pressure squeezing the plates together.

and the separation of the plates, L, for our isolated scalar field theory system with constant total energy E. For small enough L one can explicitly see how the entropy transitions from a convex to a concave function. We further quantify this phase transition by examining the most positive eigenvalue of the Hessian of $S(V_2,\, L)$, i.e. with E fixed. For a concave function, all eigenvalues of the Hessian are negative. The plot on the right of fig. 13.3 shows in gray the region of $(V_2,\, L)$ space for which the most positive eigenvalue of the Hessian is greater than zero, which is to say the region for which the entropy is no longer a convex function of V_2 and L[4]. The critical length that forms the phase transition boundary of this region is a function of the parameters V_2, E, and $T \times L$. In the right hand plot of fig. 13.3, the edge of the region for which the entropy is no longer concave is given by a function $L_c(E,\, V_2,\, T \times L)$ where $T \times L \approx 1$; i.e. the phase transition occurs when $L \approx 1/T$. Therefore this geometrical phase transition can occur for a Bose system at arbitrarily large temperature. We can conclude then that the phase transition is not one of Bose-Einstein condensation.

One may then naturally next ask if the phase transition can be found in a massless, noninteracting Fermi field. We will show below that, yes, the phase transition persists for a massless, noninteracting Fermi field. In order to repeat the above analysis for a Fermi field, we must slightly alter our quantization condition [194, 195]. In order to prevent any Dirac current from leaking through the plates confining our system, we require that, on the boundary[5]

$$\eta^\mu \bar{\psi} \gamma_\mu \psi = 0, \qquad \eta^\mu = (0,\, \vec{\eta})^\mu. \tag{13.4}$$

In order to satisfy eq. (13.4), one must take the momentum modes of our Dirac field to satisfy

$$k_\ell = (\ell + \frac{1}{2})\frac{\pi}{L}, \qquad \ell = 0,\, 1,\, 2, \ldots \tag{13.5}$$

Following the methods of appendix A.1.1 the Fermion partition function for a massless, noninteracting Dirac field constrained between two parallel plates of area V_2 and kept a distance L apart evaluates to

$$\ln Z_F = 2V_2 \sum_{\ell=0}^{\infty} \int \frac{d^2k}{(2\pi)^2} \Big[\beta \sqrt{k^2 + k_\ell^2} + 2\ln(1 + e^{-\beta\sqrt{k^2+k_\ell^2}})\Big] \tag{13.6}$$

$$= \frac{\pi V_2}{L^2}\Big[\frac{7}{2}\frac{\tilde{\beta}}{1440} - \frac{2}{\tilde{\beta}^2}\sum_{\ell=0}^{\infty}(\ell + \frac{1}{2})\tilde{\beta}\mathrm{Li}_2\Big(-e^{-\tilde{\beta}(\ell+\frac{1}{2})}\Big) + \mathrm{Li}_3\Big(-e^{-\tilde{\beta}(\ell+\frac{1}{2})}\Big)\Big], \tag{13.7}$$

where $\tilde{\beta} \equiv \pi/(TL)$. Note that the overall factor of 2 in eq. (13.6) is due to the spin-1/2 nature of the Dirac field. The results of repeating the scalar field theory analysis are shown in figs. 13.4 to 13.6. Qualitatively the picture is the same for the Dirac theory as for the scalar theory; quantitatively, one finds that the critical length separating the concave from convex region of the entropy S as a function of plate area V_2 and separation length L is related to a slightly higher temperature of the gas, $L_c \approx 0.8/T$.

[4] Note that since we are using formulae formally derived in the $V_2 \to \infty$ limit, we restrict our plot to large values of V_2.

[5] We stress that this is not the MIT bag model as we introduce no confining constant.

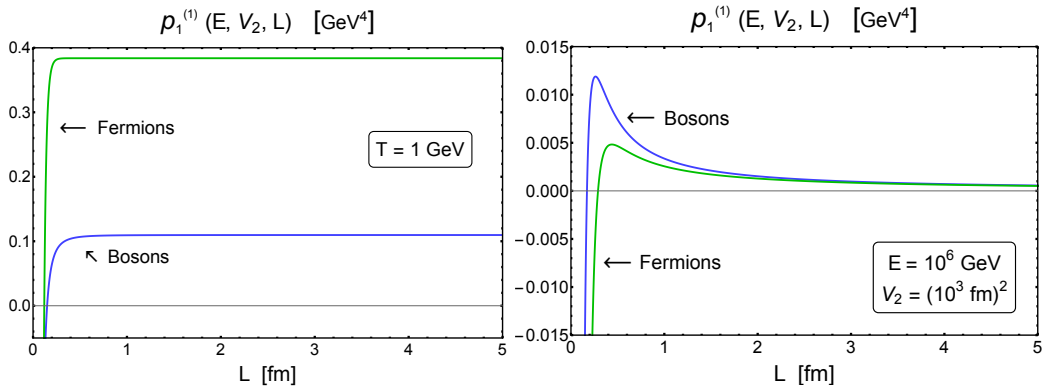

FIGURE 13.4: (Left) Pressure p as a function of L for a massless, noninteracting Dirac field between two parallel plates separated by a distance L in contact with a thermal heat bath at a temperature $T = 1$ GeV. (Right) Same but for an isolated system at constant energy $E = 10^6$ GeV and with parallel plates area $V_2 = 10^6$ fm^2.

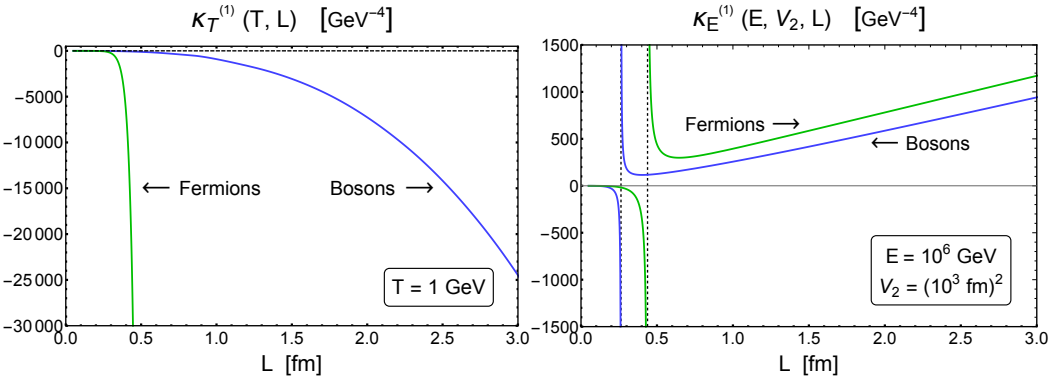

FIGURE 13.5: (Left) Isothermal compressibility $\kappa_T = (1/L)\partial L/\partial p|_T$ as a function of plate separation L for a noninteracting, Dirac field between two parallel plates a distance L apart and held at a temperature $T = 1$ GeV. (Right) Isoenergetic compressibility $\kappa_E = (1/L)\partial L/\partial p|_E$ for the same scalar field system with constant energy $E = 10^6$ GeV and with parallel plates area $V_2 = 10^6$ fm^2.

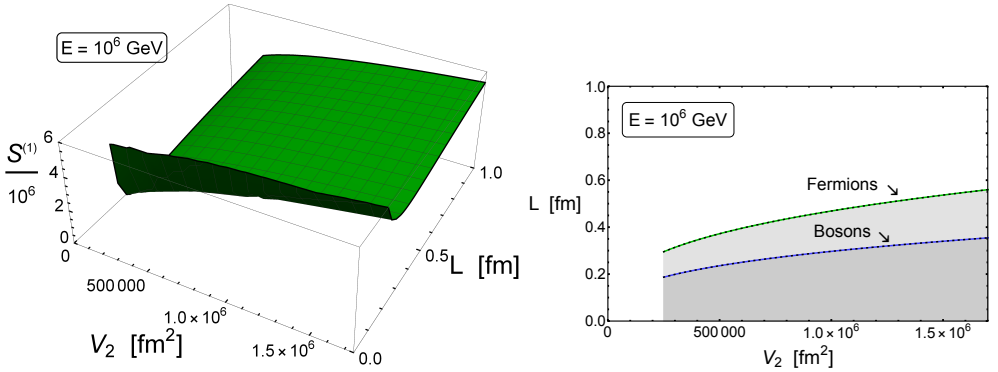

FIGURE 13.6: (Left) The entropy S of a massless, noninteracting Dirac field between two parallel plates of area V_2 in fm^2 separated by a distance L in fm for energy $E = 10^6$ GeV. (Right) The region of (V_2, L) space for which one of the eigenvalues of the Hessian of the entropy S is positive is shaded in gray. The edge of the Fermion region is given by the equation $L_c(V_2,\ E = 10^6\ \text{GeV},\ T \times L = 0.8)$.

One can even go so far as to show that the phase transition exists for massive, nonrelativistic Bosons and Fermions, too, although we leave the details for a future publication.

Chapter 14

Summary and prospects

In this work we implemented the first step of a strategy designed to investigate the thermodynamics of small QGP systems, focusing on the finite size corrections to the usual Stefan-Boltzmann thermodynamic properties computed in thermal field theory and also demonstrating the emergence of a new geometric phase transition. In particular, we set up a framework for probing relevant finite size effects by means of an actual spatial boundary for a geometric confinement, imposing Dirichlet boundary conditions. We argued in section 9.2 that Dirichlet BCs are the most appropriate for capturing the relevant finite size effects for heavy ion collisions and quark-gluon plasma phenomenology because these BCs prevent the weakly coupled quantum fields, supposed to account for the relevant degrees of freedom inside a QGP, from propagating outside of the geometric region defining this QGP system. For the sake of simplicity, we considered $D-1$ spatial dimensions with $c \leq D-1$ dimensions of finite length L_i arranged in standard rectilinear coordinates. We then filled the space inside our geometrically confined region with a massless, noninteracting scalar field. In order to best make contact with lattice QCD results and also for simplicity we computed the thermodynamic quantities in the canonical ensemble, in the process extending standard thermal field theory techniques.

We presented the main results of the detailed analytic calculations in Appendix A.1. The results were computed by two independent methods, resulting in two different infinite sums for each geometrically confined system. The two different sums have very different numerical convergence properties: one converges exponentially fast for $T \times L_i < 1$ while the other converges exponentially fast for $T \times L_i > 1$.

In chapter 11 we discussed some important qualitative consequences of our derivation of the statistical mechanics of our system. In particular, we saw that the First Law of Thermodynamics is generalized by the presence of different pressures: instead of a single scalar pressure as in the case of all spatial dimensions having infinite extent, the pressure in the i^{th} direction may be different from the pressure in the j^{th} direction depending on the various lengths L_k. On the other hand, we found that the limited spatial extent of our system did not affect the Third Law of Thermodynamics. Of critical importance, we computed the size of the fluctuations in energy away from the mean energy dictated by the contact of our system with a thermal heat bath. Even though the systems of parallel plates or a tube have some but

not all direction(s) of finite size, the volume of these systems is infinite. Therefore the relative size of the energy fluctuations compared to the mean energy is 0. As a result, the canonical ensemble can be used to compute the thermodynamic properties for isolated, constant energy parallel plates or infinite tube systems. At the same time, the energy fluctuations in a finite volume box are *not* zero, and there must be corrections in the application of the canonical ensemble to an isolated, finite volume box system.

In chapter 12 we presented a number of quantitative plots of the free energy, entropy, energy, pressure, and heat capacity for a massless, noninteracting scalar field contained inside infinite parallel plates, an infinite rectangular tube, and a finite-sized box. Of particular note was the surprisingly large finite size corrections for the pressure. For a system of the approximate size and temperature of a high multiplicity proton-proton collision at LHC, which has been argued to exhibit hydrodynamic behavior based on thermodynamic quantities computed in the Stefan-Boltzmann limit [272], we found $\sim 20\%$ corrections for an infinite tube and $\sim 40\%$ corrections for a symmetric, finite box. Even for systems of the size of mid-central nucleus-nucleus collisions at LHC the corrections are of order $\sim 10\%$. Since the size of the azimuthal anisotropy measured in such collisions at LHC are of order $\sim 10\%$ [273], these corrections to the equation of state due to the finite size of the system may have important implications for heavy ion phenomenology.

In chapter 13 we discovered that an isolated system of noninteracting particles confined within parallel plates at temperature T undergoes a phase transition at a critical length $L_c \sim 1/T$: for $L > L_c$ the system is stable and resists compression; for $L < L_c$ the system collapses. The phase transition is not one of Bose-Einstein condensation as we showed that a noninteracting Dirac field also experiences such a phase transition. Nor is the transition a relativistic effect as it is also experienced by massive, nonrelativistic Bosons and Fermions. It is tempting to interpret our results as follows: a system of fixed energy can only resist so much external pressure before collapsing. One can see that figs. 13.1 and 13.4 support this interpretation: the system energy density is on the same order as the pressure, with $p \lesssim E/V$, when the system undergoes the phase transition at the critical length. Further clarity on this interpretation requires the use of a higher order ensemble in which the system is put in contact with a thermal pressure bath. Such an investigation would also provide insight into the importance of the fluctuations in the separation distance between the parallel plates about the average, equilibrium length. Should this higher ensemble show that a pressure driven phase transition exists, one could use the higher ensemble to calculate the critical exponent for this second order transition. Other work that has claimed the observation of a first order phase transition in small systems [213] performed the calculation in a finite volume box in the canonical ensemble; it is not clear that the energy fluctuations inherent in using the canonical ensemble invalidates the conclusions reached in that work. In the only other work that we are aware of that examines finite size driven phase transitions [274], the phase transition is due to self interactions of the system; since our system is noninteracting, the phase transition we see is due purely to geometric confinement effects. Future work includes determining whether or not a similar phase transition exists for an isolated system with periodic boundary conditions

in one direction or for a tube system.

It is important for us to point out that geometrically confining a thermal quantum field into a certain region of space with Dirichlet boundary conditions (even with an infinite volume) appears to provide a solution to the infrared Linde problem [220, 275, 276]. The origin of the Linde problem is the existence of the zero mode in systems with, e.g., periodic boundary conditions: a momentum mode with zero energy. Imposing Dirichlet boundary conditions naturally provides an infrared cut-off for the momentum modes $p > p_{\text{min}} \sim 1/L$ dictated by the system size L. We explicitly showed in this work that the Matsubara zero mode disappears from the leading order thermal field theory calculations. It would be interesting to quantitatively check that in fact Dirichlet boundary conditions cure the zero mode Linde problem at higher orders in perturbation theory, too, and see that the perturbative series becomes analytic in the coupling.

Chapter 15

Postlude

"It is always possible to do better."

- Adv. Thulisile Madonsela,
Former public protector of the Republic of South Africa

The aim of the present thesis was to determine the extent to which a reasonably sound theoretical answer could be given to the question: *Can we systematically and rigorously either rule out or realize the possibility that the energy loss in small systems is simply too small to measure?*

As a starting point, a brute-force small system correction to a standard pQCD energy loss model was investigated numerically in order to understand the way in which the usual large system pQCD energy loss results may be affected when considering small systems. The main result of that investigation was that, not only are all of the major pQCD energy loss formalisms inapplicable to small systems, but it is also clear that the early time and short separation distance dynamics of the medium play a crucial role in the determination of the energy loss in small systems. Therefore, a serious investigation into small system corrections to the properties of the medium is sorely needed.

As a first step to remedying this deficiency, a thorough thermodynamical investigation into the nature of a geometrically confined quantum field theory was presented, and substantial corrections to the usual Stefan-Boltzmann results were found. Furthermore, a geometrical phase transition was discovered at the characteristic scale (the inverse of the temperature) of the field. Although the bulk of the present investigation relates to a single, massless, scalar field, the results strongly suggest that a quantum field is subjected to large corrections when confined to a spatial region that is similar in size to its characteristic scale. A future investigation might compute the small system corrections to the Debye screening length and apply such a – possibly L-dependent – result to an energy loss model.

On the one hand, this work shows that the investigation of small systems is a technically compelling endeavor: From a radiative pQCD energy loss perspective there is, in particular, much to be learned still about the formation time of the radiated gluon and the importance of the

large formation time assumption. Thermally we have shown that the basic thermodynamic quantities associated with a spatially confined quantum field are significantly altered, but that such a treatment still provides a natural tensor-like structure to the pressure, and might solve the infra-red Linde problem.

On the other hand we have shown that it is, as yet, impossible to presume to know much about the energy loss in small systems; we have shown that radiative pQCD energy loss, although successful in central *AA*-collisions, is heavily reliant on the early time and short separation distance behavior of the medium, while all indications, albeit from a toy model, are that the medium is significantly modified when spatially confined.

However, we can, and we must, do better. Although the modification of jets in central *AA* collisions has long been considered a probe of the properties of the medium, it is perhaps time to start asking how the medium itself is modified in small systems. The study of small systems appears to be wide open and fascinating. A particularly promising area of investigation is jet sub-structure and the medium response to the presence of a jet [277] - perhaps the theory community has here a real opportunity to investigate the question of whether or not a particular colliding system produces a QGP. Closely related to the medium response to the presence of a jet is the response of the spectator nucleons in a peripheral *AA* collision to the presence of the QGP. It appears as though the QGP formed in small colliding systems, if indeed there is a QGP, must be fundamentally very different to the QGP formed in *AA* collisions.

Nevertheless, in attempting to formulate a standard model of QGP in small systems, one may start by refining the techniques presented in this thesis. From a pQCD perspective, it is clear that the inclusion of effects from the early times of the evolution of the QGP is essential. To this end, one might consider developing other scattering center distributions whose forms are derived from knowledge of the early times by, for instance, incorporating medium sizes and thermalization times, as well as perhaps including effects developed from an understanding of the pre-equilibrium dynamics of the medium [186, 187]. Analytically there remain a number of model assumptions that still need to be relaxed, in particular the soft radiation and the collinear radiation assumptions. Some progress along these lines has already been made [175, 278, 279] Relaxing the large formation time assumption in DGLV might go a long way toward realizing the relaxation of the collinear assumption. From the thermal field theoretic side the calculation of the Debye screening length in finite systems remains an important next step, but much work needs to be done to ensure that a consistent understanding of ensemble equivalence and potential phase transitions is developed.

Small colliding systems have placed the heavy-ion community in the extraordinarily privileged position of having an entirely unexpected and exhilarating problem to solve, may it keep us busy for decades to come.

Appendix A

Appendix to Part III

A.1 Details of calculations

In this section, we detail two different methods of computing the free energy density for a single neutral noninteracting massless scalar field in c geometrically confined dimensions by deriving the logarithm of the partition function. It is important to note that the usual method for computing such a logarithm cannot be applied in a way that is necessarily straightforward since the compactification of any number of spatial dimensions leads to summations that are formally divergent.

For both methods we employ dimensional regularization [280] within the modified minimal subtraction ($\overline{\text{MS}}$) scheme [281] in order to regulate the divergences, but we also complement this regularization procedure through the use of zeta type of regularization whenever necessary. In the present massless case of interest, the usual (power like) divergences, if any, are set to zero by Dim. Reg. so that there are no divergences that would need to be cured by means of renormalizing the vacuum [282].

Inappendix A.1.1 we follow the usual method as described by [253, 255]. Inappendix A.1.2 we present an alternative calculation. Naturally, the two methods yield analytically equivalent results which then of course agree numerically—even though their different convergence properties, when the summations are truncated at some finite orders, make them conveniently suitable in different regimes.

It is important to note that we will make significant use of Epstein zeta functions and their various analytic representations. The derivation of these representations often exploits the Poisson summation formula,

$$\sum_{s=-\infty}^{\infty}\left(e^{-x\alpha s^2}\right)=\sqrt{\frac{\pi}{x\alpha}}\times\sum_{s=-\infty}^{\infty}\left(e^{-\frac{\pi^2}{x\alpha}s^2}\right). \tag{A.1}$$

We will not go into the detail of these derivations, but rather point the interested reader to the extensive literature [256, 283–290] that is the result of three decades of intensive work on these special functions.

A.1.1 Usual computation

In this section, we compute the canonical representations for the free energy density in different scenarios, following and adapting the general methods of [253, 255]. For pedagogical reasons, we present the case of $c = 1$ in detail, but the result will then be easy to extend to arbitrary $c \leq D-1$. Our starting point is then either eq. (10.8) or eq. (10.9), leading to

$$\ln \mathcal{Z}^{(1)} = -\frac{1}{2} \sum_{n\in\mathbb{Z}} \sum_{\ell_1\in\mathbb{N}} \sum_{\boldsymbol{n}_k\in\mathbb{Z}^{D-2}} \ln\left[\beta^2\left(\omega_n^2 + \omega_{\ell_1}^2 + \boldsymbol{\omega}_k^2 + m^2\right)\right]. \tag{A.2}$$

We then consider the following two identities

$$\ln\left\{(2\pi n)^2 + \beta^2\chi^2\right\} = \int_1^{(\beta\chi)^2} \frac{d\theta^2}{\theta^2 + (2\pi n)^2} + \ln\left\{1 + (2\pi n)^2\right\}, \tag{A.3}$$

$$\sum_{n=-\infty}^{+\infty} \frac{1}{(\theta/2\pi)^2 + n^2} = \frac{2\pi^2}{\theta}\left(1 + \frac{2}{\mathrm{e}^\theta - 1}\right), \tag{A.4}$$

and after substituting eq. (A.3) into eq. (A.2), defining for brevity $\omega^2 \equiv \boldsymbol{\omega}_k^2 + m^2$, dropping an infinite T- and L_i-independent term, and employing eq. (A.4), we obtain

$$\ln \mathcal{Z}^{(1)} = -\sum_{\ell_1\in\mathbb{N}} \sum_{\boldsymbol{n}_k\in\mathbb{Z}^{D-2}} \left[\int_1^{\beta\sqrt{\omega_{\ell_1}^2+\omega^2}} d\theta \left(\frac{1}{2} + \frac{1}{\mathrm{e}^\theta - 1}\right)\right] \tag{A.5}$$

$$= -\sum_{\ell_1\in\mathbb{N}} \sum_{\boldsymbol{n}_k\in\mathbb{Z}^{D-2}} \left[\frac{\beta}{2}\sqrt{\omega_{\ell_1}^2 + \omega^2} + \ln\left\{1 - \mathrm{e}^{-\beta\sqrt{\omega_{\ell_1}^2+\omega^2}}\right\}\right], \tag{A.6}$$

where we again dropped infinite T- and L_i-independent terms.

Assessing the case $c = 1$, it is time to release the momentary (periodic) compactifications of the $D-2$ other spatial dimensions, sending each of the R compactification lengths to its appropriate value (presently L_2 or L_3) each being asymptotically large, and get

$$\ln \mathcal{Z}^{(1)} = -L_2 L_3 \left(\frac{\bar{\Lambda}^2 e^{\gamma_E}}{4\pi}\right)^{2-\frac{D}{2}} \sum_{\ell_1\in\mathbb{N}} \int \frac{d^{D-2}\boldsymbol{k}}{(2\pi)^{D-2}} \left[\frac{\beta}{2}\sqrt{\omega_{\ell_1}^2 + \omega^2} + \ln\left\{1 - \mathrm{e}^{-\beta\sqrt{\omega_{\ell_1}^2+\omega^2}}\right\}\right], \tag{A.7}$$

where $\omega^2 \to \boldsymbol{k}^2 + m^2$. Since we will shortly be taking $D \equiv 4 - 2\epsilon$ (ϵ will be set to zero at the end), we introduced an arbitrary regularization scale ($\Lambda^2 \equiv \bar{\Lambda}^2 e^{\gamma_E}/4\pi$) in order to keep the proper dimensionality when $D \neq 4$, since we will employ Dim. Reg. within the $\overline{\text{MS}}$ scheme.

We now focus on the computation of the second term of eq. (A.7). To do so, recall that the volume of an N-dimensional unit sphere is given by $\Omega_N = 2\pi^{N/2}/\Gamma(N/2)$, and consider the fully general integral

$$J(a, N) \equiv \int \frac{d^N p}{(2\pi)^N} \ln\left\{1 - \mathrm{e}^{-\beta\sqrt{p^2+a^2}}\right\}. \tag{A.8}$$

Following [255], we make the substitutions $p \to T\,x$ and $a = T\,b$ in the above integral, Taylor expand the logarithm, and rewrite the integration measure, obtaining

$$J\left(a,N\right) = -\frac{\Omega_N}{\left(2\pi/T\right)^N}\sum_{s=1}^{\infty}\left[\frac{1}{s}\int_0^{\infty} dx\; x^{N-1}\;\mathrm{e}^{-s\sqrt{x^2+b^2}}\right]. \tag{A.9}$$

Then, the substitution $z = \sqrt{x^2+b^2}$ leads to an integral representation of the modified Bessel function of the second kind, namely K, and we get, for general a and N

$$J\left(a,N\right) = -\frac{2\pi^{N/2}}{\left(2\pi/T\right)^N\Gamma\left(N/2\right)}\sum_{s=1}^{\infty}\frac{1}{s}\int_b^{\infty} dz\; z\left(z^2-b^2\right)^{\frac{N}{2}-1}\;\mathrm{e}^{-sz} \tag{A.10}$$

$$= -\frac{2\;T^N}{\left(2\pi\right)^{(N+1)/2}}\sum_{s=1}^{\infty}\left[\left(\frac{b}{s}\right)^{\frac{N+1}{2}} K_{\frac{N+1}{2}}\left(bs\right)\right]. \tag{A.11}$$

Therefore, in order to compute the second term of eq. (A.7), we need the following result

$$J\left(\sqrt{\omega_{\ell_1}^2+m^2}, D-2\right) = -\frac{2\;T^{D-2}}{\left(2\pi\right)^{\frac{D-1}{2}}}\sum_{s=1}^{\infty}\left[\left(\frac{\sqrt{\omega_{\ell_1}^2+m^2}}{sT}\right)^{\frac{D-1}{2}} K_{\frac{D-1}{2}}\left(\frac{s}{T}\sqrt{\omega_{\ell_1}^2+m^2}\right)\right]. \tag{A.12}$$

We further notice that the above result is indeed finite, as the second term of eq. (A.7) contains neither Ultra-Violet (UV) nor Infra-Red (IR) divergences.

We focus now on the computation of the first term of eq. (A.7), which obviously contains a UV divergence. In order to regularize this divergence, we will have to employ both Dim. Reg. and Epstein-Zeta regularization. However, we will be able to derive a general formula for the free energy density if we only partially perform Dim. Reg. until such a time as one needs to compute the free energy density for a particular value of c. Which is to say that we will start by transforming the $D-1-c$ - dimensional momentum integral as is the usual first step in Dim. Reg. within the $\overline{\mathrm{MS}}$ scheme. We will then apply Epstein-Zeta regularization to the remaining c - dimensional summations. The final result, eq. (A.19), may then be used to compute the free energy density for a given value of c by writing $D = 4-1-c-2\epsilon$, expanding around $\epsilon = 0$ and then taking $\epsilon \to 0$. This process ensures that all the regularization processes are not applied far outside the convergence regions of the integrals in question. It should also be noted that no counter terms are required.

To now continue our example of the $c = 1$ case, we therefore begin with the transformation

$$\int \frac{d^{D-2}\boldsymbol{k}}{\left(2\pi\right)^{D-2}}\;\sqrt{\omega_{\ell_1}^2+\boldsymbol{k}^2+m^2} = \frac{\Gamma\left(-\frac{D-1}{2}\right)}{\left(4\pi\right)^{\frac{D-2}{2}}\Gamma\left(-\frac{1}{2}\right)}\left[\left(\frac{\pi\ell_1}{L_1}\right)^2+m^2\right]^{\frac{D-1}{2}}. \tag{A.13}$$

We notice an important point related to the above calculation: the integral does not feature any IR divergences in the massless limit as long as L_1 is finite, because ℓ_1 never vanishes.

Combining eq. (A.7) with eqs. (A.12) and (A.13), we may write the free energy density, $f^{(c=1)}(T, L_1)$, of a system with one geometrically confined dimension as

$$f^{(1)} = \frac{\Gamma\left(-\frac{D-1}{2}\right)}{2(4\pi)^{\frac{D-2}{2}} L_1 \Gamma\left(-\frac{1}{2}\right)} \left(\frac{\bar{\Lambda}^2 e^{\gamma_E}}{4\pi}\right)^{2-\frac{D}{2}} \sum_{\ell_1 \in \mathbb{N}} \left[\frac{\pi \ell_1}{L_1}\right]^{D-1} - \frac{2\, T^{D-1}}{(2\pi)^{\frac{D-1}{2}} L_1} \left(\frac{\bar{\Lambda}^2 e^{\gamma_E}}{4\pi}\right)^{2-\frac{D}{2}} \sum_{s=1}^{\infty} \sum_{\ell_1 \in \mathbb{N}} \left[\left(\frac{\pi \ell_1}{s T L_1}\right)^{\frac{D-1}{2}} K_{\frac{D-1}{2}}\left(\frac{\pi}{T L_1}\, s \ell_1\right)\right], \tag{A.14}$$

where, of course, we took the massless limit. It is then straightforward to extend the above procedure to an arbitrary number c of compactified dimensions, and obtain the result

$$f^{(c)} = \frac{\Gamma\left(-\frac{D-c}{2}\right)}{2(4\pi)^{\frac{D-1}{2}} \prod_{i=1}^{c}(L_i) \Gamma\left(-\frac{1}{2}\right)} \left(\frac{\bar{\Lambda}^2 e^{\gamma_E}}{4\pi}\right)^{2-\frac{D}{2}} \sum_{\boldsymbol{\ell} \in \mathbb{N}^c} \left[\sum_{i=1}^{c} \left(\frac{\pi \ell_i}{L_i}\right)^2\right]^{\frac{D-c}{2}} - \frac{2\, T^{D-c} \left(\frac{\bar{\Lambda}^2 e^{\gamma_E}}{4\pi}\right)^{2-\frac{D}{2}}}{(2\pi)^{\frac{D-1}{2}} \prod_{i=1}^{c}(L_i)} \sum_{s=1}^{\infty} \sum_{\boldsymbol{\ell} \in \mathbb{N}^c} \left[\left(\frac{\sum_{i=1}^{c} \left(\frac{\pi \ell_i}{L_i}\right)^2}{(sT)^2}\right)^{\frac{D-1}{4}} K_{\frac{D-c}{2}}\left(\frac{s}{T} \sqrt{\sum_{i=1}^{c} \left(\frac{\pi \ell_i}{L_i}\right)^2}\right)\right], \tag{A.15}$$

for which we notice that Dim. Reg. took care of the non logarithmic UV divergence, and that the above result will not need to be renormalized[1].

Computing the summand in the first term of eq. (A.15) will then require some Epstein-Zeta regularization. Note the present Epstein-Zeta function of interest is defined [286] as

$$E_N^{m^2}(s; a_1, \ldots, a_N) \equiv \sum_{(n_1, \ldots, n_N) \in \mathbb{N}^N} \left(a_1 n_1^2 + \cdots + a_N n_N^2 + m^2\right)^{-s} \quad \forall a_1, \ldots, a_N, m^2 > 0. \tag{A.16}$$

We reproduce now the result for the analytic continuation of the above function (see [286] for more details), in which the following recursion relation is useful

$$\begin{aligned} E_N^{m^2}(s; a_1, \ldots, a_N) = & -\frac{1}{2} E_{N-1}^{m^2}(s; a_1, \ldots, a_{N-1}) \\ & + \frac{1}{2} \sqrt{\frac{\pi}{a_N}} \frac{\Gamma(s - \frac{1}{2})}{\Gamma(s)}\, E_{N-1}^{m^2}(s - 1/2; a_1, \ldots, a_{N-1}) \\ & + \frac{2\pi^s}{\Gamma(s)} a_N^{-\frac{1}{2}\left(s+\frac{1}{2}\right)} \sum_{(n_1, \ldots, n_N) \in \mathbb{N}^N} n_N^{s-\frac{1}{2}} \left(a_1 n_1^2 + \cdots + a_{N-1} n_{N-1}^2 + m^2\right)^{\frac{1}{2}\left(\frac{1}{2}-s\right)} \times \\ & \times K_{s-\frac{1}{2}}\left(\frac{2\pi n_N}{\sqrt{a_N}} \sqrt{a_1 n_1^2 + \cdots + a_{N-1} n_{N-1}^2 + m^2}\right), \end{aligned} \tag{A.17}$$

with

[1] Note that for certain values of $D - c$ the gamma function in the numerator of eq. (A.15) will have a pole. For precisely those values of $D - c$ the Epstein zeta function will multiply these infinities by trivial zeros thus rendering the divergences harmless.

$$E_1^{m^2}(s;a) = -\frac{1}{2m^{2s}} + \left(\frac{\pi}{a}\right)^{\frac{1}{2}} \frac{1}{2m^{2s-1}\Gamma(s)} \left(\Gamma\left(s-\frac{1}{2}\right) + 4\sum_{\ell\in\mathbb{N}} \left[\frac{a^{\frac{1}{4}-\frac{s}{2}}}{(\pi\ell m)^{\frac{1}{2}-s}} K_{s-\frac{1}{2}}\left(2\pi\ell m\sqrt{a}\right)\right]\right), \tag{A.18}$$

which reduces to $E_1^0(s;a) = a^{-s}\zeta(2s)$ in the limit $m \to 0$, providing $\mathrm{Re}\,(s) < 1/2$. We may now use the eqs. (A.17) and (A.18) in order to rewrite eq. (A.15) as

$$\begin{aligned} f^{(c)} = {} & \frac{\Gamma\left(-\frac{D-c}{2}\right)\left(\frac{\bar{\Lambda}^2 e^{\gamma_E}}{4\pi}\right)^{2-\frac{D}{2}}}{2(4\pi)^{\frac{D-1}{2}}\prod_{i=1}^{c}(L_i)\Gamma\left(-\frac{1}{2}\right)} E_c^0\left(-\frac{D-c}{2};\left(\frac{\pi}{L_1}\right)^2,\ldots,\left(\frac{\pi}{L_c}\right)^2\right) \\ & - \frac{2\,T^{D-c}\left(\frac{\bar{\Lambda}^2 e^{\gamma_E}}{4\pi}\right)^{2-\frac{D}{2}}}{(2\pi)^{\frac{D-1}{2}}\prod_{i=1}^{c}(L_i)} \sum_{s=1}^{\infty}\sum_{\ell\in\mathbb{N}^c}\left[\left(\frac{\sum_{i=1}^{c}\left(\frac{\pi\ell_i}{L_i}\right)^2}{(sT)^2}\right)^{\frac{D-1}{4}} K_{\frac{D-c}{2}}\left(\frac{s}{T}\sqrt{\sum_{i=1}^{c}\left(\frac{\pi\ell_i}{L_i}\right)^2}\right)\right], \end{aligned} \tag{A.19}$$

which is our canonical result for the free energy density with c geometrically compactified dimensions. Notice that the first line in eq. (A.19) may now be explicitly computed using eqs. (A.17) and (A.18), for any number of compactified dimensions, and we refer the reader to section 10.2 for the corresponding final, and furthermore refined, results.

A.1.2 Alternative computation

In this section, we compute the alternative representations for the free energy density in different scenarios. We generally follow the methods of [253, 255] but take great care with the regularization procedure; given the spatial compactification(s), we avoid the formal manipulation of divergences. Moreover, we notice that certain massive results will be given as byproducts, even though these are of no interest for the present work.

In fact, straightforwardly taking the asymptotically large R limits in eq. (10.9) could appear problematic for some values of c. Indeed, the subsequent integral and the remaining infinite sums may not have a common strip of convergence. To show that this would not be a problem, we could make use of the monotone convergence (or Beppo–Levi) theorem. Given the asymptotically large R limits and since the infinite summation kernel of eq. (10.9) would then still be positive definite and monotonically increasing[2], one could take the infinite series as a set of partial summations under a limit and exchange the order between the limit and the integral. This could allow for an analytic continuation without spoiling the convergence of the expression, thereby asserting the existence of the dimensionally regularized free energy density for all c. However, we could, instead, proceed with a convenient trick, making use of the following identity

[2]The β^2 normalization of the logarithm argument could be changed without modifying the final result, so to keep this statement true for all values of T and L_i.

$$\ln\left(A\right) \equiv -\frac{\partial}{\partial\alpha}\left(\frac{1}{A^{\alpha}}\right)\bigg|_{\alpha\to 0}, \tag{A.20}$$

where A is positive definite and α is real. $1/A^{\alpha}$ can serve the purpose of defining a master expression that can be analytically continued as a function of the dimension D, before applying eq. (A.20) to find the log. Doing so and momentarily assuming a convenient range for α, allows us to work with convergent expressions. Using this identity, and sending all R to their asymptotically large values, we define the following master sum-integral[3]

$$I_{\alpha}^{(c)} \equiv -\frac{T^{1+2\alpha}}{2\prod_{i=1}^{c}\left(L_i\right)}\left(\frac{\bar{\Lambda}^2 e^{\gamma_E}}{4\pi}\right)^{2-\frac{D}{2}}\sum_{n\in\mathbb{Z}}\sum_{\boldsymbol{\ell}\in\mathbb{N}^c}\int\frac{\mathrm{d}^{\mathrm{D}-1-\mathrm{c}}\boldsymbol{k}}{(2\pi)^{D-1-c}}\left[\frac{1}{\left(\omega_n^2+\sum_{i=1}^{c}\omega_{\ell_i}^2+\boldsymbol{k}^2+m^2\right)^{\alpha}}\right], \tag{A.21}$$

related to the free energy density in D dimensions, after analytic continuation in terms of the complex D variable, via the following identity

$$f^{(c)} = \frac{\partial}{\partial\alpha}\left[I_{\alpha}^{(c)}\right]\bigg|_{\alpha\to 0}. \tag{A.22}$$

We will then first focus on the evaluation of eq. (A.21). Prior to setting the number of compactified spatial dimensions c to some value in order to do so, and thus to compute the free energy density, let us perform the continuous momentum integration. By doing so, we will be able to analytically continue the expression as a function of the dimensional parameter D, and evaluate the infinite summations outside of their original radii of convergence when needed. For now, we shall assume that there exists some strip (to be specified below) for the complex variable D, in which eq. (A.21) is convergent. We then proceed to rescale the continuous momentum $\boldsymbol{k}$, in order to factorize all the frequencies and the mass. We then obtain the following expression

$$\begin{aligned} I_{\alpha}^{(c)} = -\frac{T^{1+2\alpha}\left(\frac{\bar{\Lambda}^2 e^{\gamma_E}}{4\pi}\right)^{2-\frac{D}{2}}}{2\left(4\pi\right)^{2-\frac{D}{2}}\prod_{i=1}^{c}\left(L_i\right)}\int\frac{\mathrm{d}^{\mathrm{D}-1-\mathrm{c}}\boldsymbol{k}}{(2\pi)^{D-1-c}}\left[\left(1+\boldsymbol{k}^2\right)^{-\alpha}\right]\times \\ \times\sum_{n\in\mathbb{Z}}\sum_{\boldsymbol{\ell}\in\mathbb{N}^c}\left(\omega_n^2+\sum_{i=1}^{c}\omega_{\ell_i}^2+m^2\right)^{\frac{D-1-c}{2}-\alpha}. \end{aligned} \tag{A.23}$$

In order to assure the existence of the strip we take $\alpha > 0$. Then the integral above is clearly convergent in the D-strip such that $\mathrm{Re}\left(D\right)-1-c \in (0,2\alpha)$. The set of infinite summations, being some Epstein zeta type of function, naturally converges in a D-strip such that $2\alpha+1+c-\mathrm{Re}\left(D\right) > c$. Consequently, all we need to assume for now is that α and D satisfy the following conditions: $2\alpha > \mathrm{Re}\left(D\right)-1 \geq \mathrm{Re}\left(D\right)-1-c > 0$, the middle one

[3] We recall that we use Dim. Reg. within the $\overline{\mathrm{MS}}$ scheme, and refer to the beginning ofappendix A.1.1 for more details on this scheme and the induced modifications on the dimensionality of the expressions.

being automatically satisfied. We shall then work under this assumption, until we are able to perform an analytic continuation in the dimensional parameter D. Then, the constraint on α will be released, and we will be able to compute the free energy density according to eq. (A.22), in all the possible spatial compactification cases.

Next, we use standard techniques [253, 255] to perform the continuous momentum integration in eq. (A.23), and we get

$$I_{\alpha}^{(c)} = -\frac{T^{1+2\alpha}\left(\frac{\bar{\Lambda}^2 e^{\gamma_E}}{4\pi}\right)^{2-\frac{D}{2}}\Gamma\left(\alpha+\frac{1+c}{2}-\frac{D}{2}\right)}{2^{4-c}\,\pi^{\frac{3-c}{2}}\prod_{i=1}^{c}\left(L_i\right)\Gamma\left(\alpha\right)}\times \\ \times\sum_{n\in\mathbb{Z}}\sum_{\boldsymbol{\ell}\in\mathbb{N}^c}\left(\omega_n^2+\sum_{i=1}^{c}\omega_{\ell_i}^2+m^2\right)^{\frac{D-1-c}{2}-\alpha}, \tag{A.24}$$

being left with the evaluation of the following $(1+c)$-dimensional Epstein zeta function

$$Z_{1+c}\left(\alpha+\frac{1+c-D}{2}\right)\equiv\sum_{n\in\mathbb{Z}}\sum_{\boldsymbol{\ell}\in\mathbb{N}^c}\left(\omega_n^2+\sum_{i=1}^{c}\omega_{\ell_i}^2+m^2\right)^{\frac{D-1-c}{2}-\alpha}, \tag{A.25}$$

for which we need to set c to some particular value prior to any evaluation.

A.1.2.0.1 Two infinite parallel plates

In this subsection, we shall analytically continue eq. (A.25) in order to analytically continue eq. (A.24). Taking $c=1$

$$Z_2\Big(1+\alpha-D/2\Big)=\sum_{n\in\mathbb{Z}}\sum_{\ell_1\in\mathbb{N}}\left(\omega_n^2+\omega_{\ell_1}^2+m^2\right)^{\frac{D}{2}-\alpha-1}. \tag{A.26}$$

We then split the Matsubara sum into a zero and a nonzero mode contribution, following

$$G_{1+1}\equiv\sum_{n\in\mathbb{Z}}\sum_{\ell_1\in\mathbb{N}}g\left(n^2,\ell_1^2\right)=\sum_{\ell_1=1}^{+\infty}g\left(0,\ell_1^2\right)+2\sum_{n,\ell_1=1}^{+\infty}g\left(n^2,\ell_1^2\right), \tag{A.27}$$

and make use of the two-dimensional Epstein zeta function representation [285]

$$\sum_{n,\ell=1}^{+\infty}\left[\left(a\ell^2+bn^2\right)^{-s}\right]=-\frac{b^{-s}}{2}\,\zeta\left(2s\right)+\frac{\sqrt{\pi}}{2}\,\frac{b^{1/2-s}}{\sqrt{a}}\,\frac{\Gamma\left(s-1/2\right)}{\Gamma\left(s\right)}\,\zeta\left(2s-1\right) \\ +\frac{2\pi^s}{\Gamma\left(s\right)}\,\frac{(b/a)^{1/4}}{(ab)^{s/2}}\sum_{n,\ell=1}^{+\infty}\left[\left(\frac{\ell}{n}\right)^{s-1/2}K_{s-1/2}\left(2\pi\sqrt{\frac{b}{a}}\,n\ell\right)\right], \tag{A.28}$$

for the second term, the first one being the usual Riemann zeta function. Analytic continuation of the above formula readily follows from the straightforward continuation of the Euler

gamma function, the Riemann zeta and modified Bessel functions, or simply using the functional equation for the corresponding Epstein zeta function [285].

As it turns out, given a certain choice for a and b, the limit of vanishing T or asymptotically high L_1 appears explicitly. Note also the change in the argument of the Bessel function, upon an exchange between a and b. This gives the possibility to slightly enhance the convergence of the remaining two-fold sum, as depending on the choice for a and b, a factor of $\sqrt{b/a}$ or $\sqrt{a/b}$ (giving either a $2TL_1$ or its inverse) appears in the argument of the Bessel function. And given that the larger the argument the better the convergence, we choose the former possibility in order to easily reach the thermodynamic, Stefan-Boltzmann limit. Therefore, the asymptotically high L_1 limit (that is the usual Stefan-Boltzmann finite temperature result) will appear explicitly in the analytically continued result. Using then eq. (A.28) with $a \equiv (\pi/L_1)^2$ and $b \equiv (2\pi T)^2$, we further analytically continue eq. (A.26) and can finally extend it together with eq. (A.24) for $c = 1$, as functions of D from the original D-strip to the whole complex plane. Gathering all together, we get the following result

$$
\begin{aligned}
I_{\alpha}^{(1)} = & -\frac{T^{1+2\alpha}\left(\bar{\Lambda}^2 e^{\gamma_E}\right)^{2-\frac{D}{2}}}{8\pi L_1\,\Gamma(\alpha)} \times \Bigg\{ \left(\frac{\pi}{L_1}\right)^{D-2\alpha-2} \zeta\Big(2+2\alpha-D\Big)\,\Gamma\left(1+\alpha-\frac{D}{2}\right) \\
& + \frac{2\sqrt{\pi}\,TL_1}{(2\pi T)^{2+2\alpha-D}}\ \zeta\Big(1+2\alpha-D\Big)\ \Gamma\left(\frac{1}{2}+\alpha-\frac{D}{2}\right) \\
& - (2\pi T)^{D-2\alpha-2}\ \zeta\Big(2+2\alpha-D\Big)\,\Gamma\left(1+\alpha-\frac{D}{2}\right) \\
& + \frac{4\sqrt{2}\,L_1\,(T/L_1)^{\frac{D-1}{2}-\alpha}}{(2\pi)^{1+\alpha-\frac{D}{2}}} \sum_{n,\ell_1=1}^{+\infty} \left[\left(\frac{n}{\ell_1}\right)^{\frac{D-1}{2}-\alpha} K_{\frac{D-1}{2}-\alpha}\left(4\pi T L_1 n\ell_1\right)\right] \Bigg\},
\end{aligned}
\tag{A.29}
$$

for the corresponding eq. (A.24) with $c = 1$ and $m = 0$, valid on the whole D-complex plane. This means that we can actually probe the above result for any value of α. We then apply eq. (A.22), and since there is no pole around $D = 4$ (i.e., no logarithmic UV divergence), we readily set the dimension to four and get the renormalized[4] result

$$
f^{(1)} = -\frac{\pi^2 T^4}{90} + \frac{T^3\zeta(3)}{4\pi L_1} - \frac{T\zeta(3)}{16\pi L_1^3} - \frac{\sqrt{2}\,T^{5/2}}{L_1^{3/2}} \sum_{n,\ell_1=1}^{+\infty} \left[\left(\frac{n}{\ell_1}\right)^{\frac{3}{2}} K_{\frac{3}{2}}\left(4\pi T L_1 n\ell_1\right)\right],
\tag{A.30}
$$

for the corresponding free energy density. We notice indeed that the first term is the usual Stefan-Boltzmann finite temperature result, relevant to a massless scalar field in a noncompactified space. In addition, we see that the above result reduces to the Stefan-Boltzmann one when sending L_1 to infinity. Note however, that the zero temperature result relevant to the usual Casimir effect, and equal to $-\pi^2/1440L_1^4$ [285], appears only explicitly when using the same analytical representation for the two-dimensional Epstein zeta function, but done

[4] No counter term was needed, yet Dim. Reg. set the non logarithmic type of divergence to zero which makes the result formally renormalized.

with $a = (2\pi T)^2$ and $b = (\pi/L_1)^2$ instead of the present choice. Our result contains a two-fold infinite summation which is of course convergent. And in fact, one can also get a closed form when performing one (or the other) summation, with once again two different looking yet equivalent representations, depending on which summation is explicitly done. We choose to explicitly perform the summation over the ℓ_1 variable, for convenience when further enhancing the convergence as we are going to explain below.[5] Doing so, we end up with the following one-fold representation

$$f^{(1)} = -\frac{\pi^2 T^4}{90} - \frac{T^2}{2L_1^2}\sum_{n=1}^{+\infty}\left[n\,\mathrm{Li}_2\left(e^{-4\pi T L_1 n}\right)\right] + \frac{T^3\zeta(3)}{4\pi L_1} - \frac{T\zeta(3)}{16\pi L_1^3} - \frac{T}{8\pi L_1^3}\sum_{n=1}^{+\infty}\mathrm{Li}_3\left(e^{-4\pi T L_1 n}\right), \tag{A.31}$$

involving, again, two polylogarithm functions. With the above representation, one would need to change the remaining infinite summations by the corresponding integrals, in order to probe the asymptotic $T = 0$ limit where the n variable becomes then continuous. Note that this representation, when truncated to some finite order, is relatively well behaved in terms of convergence. However, the situation can easily be further improved. Indeed, making use of a contour integral representation for the polylogarithm functions, one can replace the summations above with another set of summations with much better convergence properties. This new one-fold representation happens to be exponentially enhanced, as can be easily checked. Relabeling the dummy variables, our final result for the free energy density of one neutral massless noninteracting scalar field is

$$\begin{aligned} f^{(1)} = &-\frac{\pi^2 T^4}{90} + \frac{\zeta(3)T^3}{4\pi L_1} - \frac{T^2}{8L_1^2}\sum_{\ell=1}^{+\infty}\left[\frac{\mathrm{csch}^2\left(2\pi T L_1 \ell\right)}{\ell^2}\right] \\ &- \frac{\zeta(3)T}{16\pi L_1^3} - \frac{T}{16\pi L_1^3}\sum_{\ell=1}^{+\infty}\left[\frac{\coth\left(2\pi T L_1 \ell\right) - 1}{\ell^3}\right]. \end{aligned} \tag{A.32}$$

As a matter of fact, this new representation allows for both the $T = 0$ and $L_1 = \infty$ limits to be carried out, which is relevant to the corresponding quantum field when coupled to a heat bath at temperature T, and geometrically confined in between two infinite parallel plates separated by a distance L_1. We notice that the term proportional to TL_1^{-3} actually cancels the s^{-3} term in the second sum, but it is preferable to keep the result as such. The above second sum indeed converges more rapidly.

A.1.2.0.2 Infinite rectangular tube

We shall now analytically continue eq. (A.25) with $c = 2$, that is

[5] Notice that both the Matsubara and the spatial summations have been done. Even though we keep the same dummy variables n and ℓ_1, they do not correspond anymore to the original modes which have been summed over.

$$Z_3\left(\frac{3}{2}+\alpha-\frac{D}{2}\right)=\sum_{n\in\mathbb{Z}}\sum_{\ell_1\in\mathbb{N}}\sum_{\ell_2\in\mathbb{N}}\left(\omega_n^2+\omega_{\ell_1}^2+\omega_{\ell_2}^2+m^2\right)^{\frac{D}{2}-\alpha-\frac{3}{2}}, \tag{A.33}$$

which will allow us to investigate the free energy density of a neutral noninteracting scalar field coupled to a heat bath at temperature T, and geometrically confined inside an infinite tube of rectangular section with two sides of respective finite lengths L_1 and L_2. For computational convenience, let us keep the mass nonzero for a little longer.

We then notice that we can use the following identity

$$\begin{aligned}G_{1+2}&\equiv\sum_{n\in\mathbb{Z}}\sum_{\ell_1\in\mathbb{N}}\sum_{\ell_2\in\mathbb{N}}g\left(n^2,\ell_1^2,\ell_2^2;m\right)\\&=\frac{1}{4}\sum_{n\in\mathbb{Z}}\sum_{\ell_1\in\mathbb{Z}}\sum_{\ell_2\in\mathbb{Z}}g\left(n^2,\ell_1^2,\ell_2^2;m\right)-\frac{1}{4}\sum_{n\in\mathbb{Z}}\sum_{\ell_1\in\mathbb{Z}}g\left(n^2,\ell_1^2,0;m\right)\\&-\frac{1}{4}\sum_{n\in\mathbb{Z}}\sum_{\ell_2\in\mathbb{Z}}g\left(n^2,0,\ell_2^2;m\right)+\frac{1}{4}\sum_{n\in\mathbb{Z}}g\left(n^2,0,0;m\right),\end{aligned} \tag{A.34}$$

in order to rewrite the multifold summation, in eq. (A.33), in a more convenient way. For the sake of analytically continuing the corresponding Epstein zeta function, let us make use of the following representation [256]

$$\begin{aligned}E_{1+c}^{m^2}&=\sum_{(n,\boldsymbol{\ell})\in\mathbb{Z}^{1+c}}\left(a_0^2n^2+a_1^2\ell_1^2+...+a_c^2\ell_c^2+m^2\right)^{-s}\\&=\frac{\pi^{\frac{1+c}{2}}\Gamma\left(s-\frac{1+c}{2}\right)\left(m^2\right)^{\frac{1+c}{2}-s}}{a_0a_1...a_c\Gamma\left(s\right)}\\&+\frac{2\pi^s\left(m^2\right)^{\frac{1+c}{4}-\frac{s}{2}}}{a_0a_1...a_c\Gamma\left(s\right)}\sum_{(n,\boldsymbol{\ell})\in\mathbb{Z}^{1+c}\setminus\{\mathbf{0}\}}\left[\frac{K_{\frac{1+c}{2}-s}\left(2\pi m\sqrt{\frac{n^2}{a_0^2}+\frac{\ell_1^2}{a_1^2}+...+\frac{\ell_c^2}{a_c^2}}\right)}{\left(\frac{n^2}{a_0^2}+\frac{\ell_1^2}{a_1^2}+...+\frac{\ell_c^2}{a_c^2}\right)^{\frac{1+c}{4}-\frac{s}{2}}}\right],\end{aligned} \tag{A.35}$$

noticing the difference of definition for the a_i coefficients, with respect to eq. (A.17). Thus, with the help of this above representation, together with the identity eq. (A.34), we can obtain an analytic and symmetric representation for the corresponding master sum-integral $I_\alpha^{(2)}$, and further apply eq. (A.22) for obtaining the free energy density. Finally, given that $D=4-2\epsilon$, we expand the resulting expression around $\epsilon=0$. After a few more steps, which we will avoid here for the sake of brevity, we finally obtain

$$\begin{aligned}f^{(2)}&=-\frac{m^4}{64\pi^2\,\epsilon}+\frac{m^2}{32\pi L_1L_2\,\epsilon}+\frac{m^4}{128\pi^2}\left[4\,\ln\left(\frac{m}{\bar{\Lambda}}\right)-3\right]-\frac{m^2}{32\pi L_1L_2}\left[2\,\ln\left(\frac{m}{\bar{\Lambda}}\right)-1\right]\\&+\frac{m^3}{24\pi}\left(\frac{L_1+L_2}{L_1L_2}\right)-\frac{mT}{4\pi L_1L_2}\sum_{n=1}^{+\infty}\left[\frac{1}{n}\,K_1\left(\frac{m}{T}n\right)\right]\end{aligned}$$

$$
\begin{aligned}
&+\frac{T^3}{8\pi L_2}\sum_{(n,\ell_1)\in\mathbb{Z}^2\setminus\{\mathbf{0}\}}\left[\frac{e^{-\frac{m}{T}\sqrt{n^2+(2TL_1)^2\ell_1^2}}\left(1+\frac{m}{T}\sqrt{n^2+(2TL_1)^2\ell_1^2}\right)}{\left(n^2+(2TL_1)^2\ell_1^2\right)^{3/2}}\right]\\
&+\frac{T^3}{8\pi L_1}\sum_{(n,\ell_2)\in\mathbb{Z}^2\setminus\{\mathbf{0}\}}\left[\frac{e^{-\frac{m}{T}\sqrt{n^2+(2TL_2)^2\ell_2^2}}\left(1+\frac{m}{T}\sqrt{n^2+(2TL_2)^2\ell_2^2}\right)}{\left(n^2+(2TL_2)^2\ell_2^2\right)^{3/2}}\right]\\
&-\frac{m^2T^2}{4\pi^2}\sum_{(n,\ell_1,\ell_2)\in\mathbb{Z}^3\setminus\{\mathbf{0}\}}\left[\frac{K_2\left(\frac{m}{T}\sqrt{n^2+(2TL_1)^2\ell_1^2+(2TL_2)^2\ell_2^2}\right)}{\left(n^2+(2TL_1)^2\ell_1^2+(2TL_2)^2\ell_2^2\right)}\right]+O\left(\epsilon^1\right).
\end{aligned}
\tag{A.36}
$$

Let us now simply comment on the massless limit, given the unusual UV structure of the above expression whose renormalization techniques, if necessary, can be found at [193, 291] by means of background field methods. However, we notice that under the limit $m\to 0$, the above result becomes convergent. Applying this limit, and performing the summations whenever it is possible to get a closed form, we obtain the following massless finite result

$$
\begin{aligned}
\lim_{m\to 0}\left(f^{(2)}\right)=&-\frac{\pi T^2}{24L_1L_2}-\frac{T^4}{2\pi^2}\sum_{(n,\ell_1,\ell_2)\in\mathbb{Z}^3\setminus\{\mathbf{0}\}}\left(n^2+(2TL_1)^2\ell_1^2+(2TL_2)^2\ell_2^2\right)^{-2}\\
&+\frac{T^3}{8\pi L_2}\sum_{(n,\ell_1)\in\mathbb{Z}^2\setminus\{\mathbf{0}\}}\left(n^2+(2TL_1)^2\ell_1^2\right)^{-3/2}\\
&+\frac{T^3}{8\pi L_1}\sum_{(n,\ell_2)\in\mathbb{Z}^2\setminus\{\mathbf{0}\}}\left(n^2+(2TL_2)^2\ell_2^2\right)^{-3/2}.
\end{aligned}
\tag{A.37}
$$

In addition, the first set of summations can be conveniently rewritten in a symmetric fashion with

$$
\begin{aligned}
S_3\equiv&-\frac{T^4}{2\pi^2}\sum_{(n,\ell_1,\ell_2)\in\mathbb{Z}^3\setminus\{\mathbf{0}\}}\left(n^2+(2TL_1)^2\ell_1^2+(2TL_2)^2\ell_2^2\right)^{-2}\\
=&-\frac{T^4}{2\pi^2}\times\frac{2}{2}\times\sum_{\ell_1=1}^{+\infty}\sum_{(n,\ell_2)\in\mathbb{Z}^2}\left(n^2+(2TL_1)^2\ell_1^2+(2TL_2)^2\ell_2^2\right)^{-2}\\
&-\frac{T^4}{2\pi^2}\times\frac{2}{2}\times\sum_{\ell_2=1}^{+\infty}\sum_{(n,\ell_1)\in\mathbb{Z}^2}\left(n^2+(2TL_1)^2\ell_1^2+(2TL_2)^2\ell_2^2\ Big\right)^{-2}\\
&-\frac{T^4}{2\pi^2}\times\frac{1}{2}\times\sum_{(n,\ell_2)\in\mathbb{Z}^2\setminus\{\mathbf{0}\}}\left(n^2+(2TL_2)^2\ell_2^2\right)^{-2}\\
&-\frac{T^4}{2\pi^2}\times\frac{1}{2}\times\sum_{(n,\ell_1)\in\mathbb{Z}^2\setminus\{\mathbf{0}\}}\left(n^2+(2TL_1)^2\ell_1^2\right)^{-2}.
\end{aligned}
\tag{A.38}
$$

While the above expressions are finite, as we just mentioned, their convergence is rather

slow, but can be enhanced using some Poisson resummation formulas such as in eq. (A.1). Thus, let us first use eq. (A.28) in order to improve the convergence properties of the two-fold summations, once properly re-expressed using eq. (A.34). Then, we can proceed in implementing a specific resummation to the remaining three-fold summations, following

$$\begin{aligned}
S_{3;(i,j)} &\equiv -\frac{T^4}{2\pi^2}\sum_{\ell_i=1}^{+\infty}\sum_{(n,\ell_j)\in\mathbb{Z}^2}\left(n^2+(2TL_i)^2\ell_i^2+(2TL_j)^2\ell_j^2\right)^{-2}\\
&= -\frac{T^4}{2\pi^2}\int_0^{+\infty}\mathrm{d}t\,\left[t\sum_{\ell_i=1}^{+\infty}\left(e^{-t(2TL_i)^2\ell_i^2}\right)\sum_{n=-\infty}^{+\infty}\left(e^{-tn^2}\right)\sum_{\ell_j=-\infty}^{+\infty}\left(e^{-t(2TL_j)^2\ell_j^2}\right)\right]\\
&= -\frac{T^3}{4\pi L_j}\sum_{\ell_i=1}^{+\infty}\sum_{(n,\ell_j)\in\mathbb{Z}^2\setminus\{\mathbf{0}\}}\int_0^{+\infty}\mathrm{d}t\,e^{-t(2TL_i)^2\ell_i^2-\frac{\pi^2}{t}\left(n^2+\frac{\ell_j^2}{(2TL_j)^2}\right)}\\
&\quad -\frac{T^3}{4\pi L_j}\sum_{\ell_i=1}^{+\infty}\int_0^{+\infty}\mathrm{d}t\,e^{-t(2TL_i)^2\ell_i^2}\\
&= -\frac{T}{8L_iL_j^2}\sum_{\ell_i=1}^{+\infty}\sum_{(n,\ell_j)\in\mathbb{Z}^2\setminus\{\mathbf{0}\}}\left[\frac{\sqrt{\ell_j^2+(2TL_j)^2n^2}}{\ell_i}K_1\left(\frac{2\pi L_i}{L_j}\,\ell_i\,\sqrt{\ell_j^2+(2TL_j)^2n^2}\right)\right]\\
&\quad -\frac{\pi T}{96L_jL_i^2}\,,
\end{aligned}\tag{A.39}$$

where from the second to the third line, we used eq. (A.1) for the n- and ℓ_j-summations, and singled out the $\ell_j = n = 0$ term. From the third to the last line, we used the integral representation of the modified Bessel function of the second kind.

Bringing all the results together, performing some of the summations to get closed forms when it is possible, and relabeling some of the variables, we finally arrive to the following

$$\begin{aligned}
f^{(2)} &= -\frac{\pi^2T^4}{90}+\frac{\zeta(3)\,T^3(L_1+L_2)}{4\pi L_1L_2}-\frac{\pi T^2}{24L_1L_2}+\frac{\pi T(L_1+L_2)}{96L_1^2L_2^2}-\frac{\zeta(3)\,T(L_1^3+L_2^3)}{32\pi L_1^3L_2^3}\\
&\quad -\frac{T^2}{4L_1^2}\sum_{\ell=1}^{+\infty}\left[\ell\,\mathrm{Li}_2\left(e^{-4\pi TL_1\ell}\right)\right]-\frac{T^2}{4L_2^2}\sum_{\ell=1}^{+\infty}\left[\ell\,\mathrm{Li}_2\left(e^{-4\pi TL_2\ell}\right)\right]\\
&\quad -\frac{T}{16\pi L_1^3}\sum_{\ell=1}^{+\infty}\mathrm{Li}_3\left(e^{-4\pi TL_1\ell}\right)-\frac{T}{16\pi L_2^3}\sum_{\ell=1}^{+\infty}\mathrm{Li}_3\left(e^{-4\pi TL_2\ell}\right)\\
&\quad +\frac{T^2}{L_1L_2}\sum_{n,\ell=1}^{+\infty}\left[\frac{n}{\ell}\,K_1\left(4\pi TL_1n\ell\right)+\frac{n}{\ell}\,K_1\left(4\pi TL_2n\ell\right)\right]\\
&\quad -\frac{T}{8L_1L_2^2}\sum_{\ell_1=1}^{+\infty}\sum_{(n,\ell_2)\in\mathbb{Z}^2\setminus\{\mathbf{0}\}}\left[\frac{\sqrt{\ell_2^2+(2TL_2)^2n^2}}{\ell_1}\,K_1\left(\frac{2\pi L_1}{L_2}\,\ell_1\,\sqrt{\ell_2^2+(2TL_2)^2n^2}\right)\right]
\end{aligned}\tag{A.40}$$

$$-\frac{T}{8L_2L_1^2}\sum_{\ell_2=1}^{+\infty}\sum_{(n,\ell_1)\in\mathbb{Z}^2\setminus\{\mathbf{0}\}}\left[\frac{\sqrt{\ell_1^2+(2TL_1)^2n^2}}{\ell_2}\,K_1\left(\frac{2\pi L_2}{L_1}\,\ell_2\,\sqrt{\ell_1^2+(2TL_1)^2n^2}\right)\right],$$

which is the symmetrized and renormalized result for the free energy density of a noninteracting massless neutral scalar field coupled to a heat bath at temperature T, and geometrically confined inside an infinite tube of rectangular section with two sides of respective lengths L_1 and L_2.

A.1.2.0.3 Finite volume box Let us finally take care of the last case, analytically continuing eq. (A.25) with $c=3$, that is

$$Z_4\left(2+\alpha-\frac{D}{2}\right)=\sum_{n\in\mathbb{Z}}\sum_{\ell_1\in\mathbb{N}}\sum_{\ell_2\in\mathbb{N}}\sum_{\ell_3\in\mathbb{N}}\left(\omega_n^2+\omega_{\ell_1}^2+\omega_{\ell_2}^2+\omega_{\ell_3}^2+m^2\right)^{\frac{D}{2}-\alpha-2}, \tag{A.41}$$

in order to investigate the free energy density of a neutral noninteracting scalar field coupled to a heat bath at temperature T, and geometrically confined inside a finite volume box with sides of respective finite lengths L_1, L_2, and L_3.

As previously, notice again that we can use a convenient identity, which in this case reads

$$\begin{aligned}
G_{1+3}\equiv\sum_{n\in\mathbb{Z}}\sum_{\ell_1\in\mathbb{N}}\sum_{\ell_2\in\mathbb{N}}\sum_{\ell_3\in\mathbb{N}}g\left(n^2,\ell_1^2,\ell_2^2,\ell_3^2;m\right)&=\frac{1}{8}\sum_{n\in\mathbb{Z}}\sum_{\ell_1\in\mathbb{Z}}\sum_{\ell_2\in\mathbb{Z}}\sum_{\ell_3\in\mathbb{Z}}g\left(n^2,\ell_1^2,\ell_2^2,\ell_3^2;m\right)\\
&-\frac{1}{8}\sum_{n\in\mathbb{Z}}\sum_{\ell_1\in\mathbb{Z}}\sum_{\ell_2\in\mathbb{Z}}g\left(n^2,\ell_1^2,\ell_2^2,0;m\right)-\frac{1}{8}\sum_{n\in\mathbb{Z}}\sum_{\ell_1\in\mathbb{Z}}\sum_{\ell_3\in\mathbb{Z}}g\left(n^2,\ell_1^2,0,\ell_3^2;m\right)\\
&-\frac{1}{8}\sum_{n\in\mathbb{Z}}\sum_{\ell_2\in\mathbb{Z}}\sum_{\ell_3\in\mathbb{Z}}g\left(n^2,0,\ell_2^2,\ell_3^2;m\right)+\frac{1}{8}\sum_{n\in\mathbb{Z}}\sum_{\ell_1\in\mathbb{Z}}g\left(n^2,\ell_1^2,0,0;m\right)\\
&+\frac{1}{8}\sum_{n\in\mathbb{Z}}\sum_{\ell_2\in\mathbb{Z}}g\left(n^2,0,\ell_2^2,0;m\right)+\frac{1}{8}\sum_{n\in\mathbb{Z}}\sum_{\ell_3\in\mathbb{Z}}g\left(n^2,0,0,\ell_3^2;m\right)\\
&-\frac{1}{8}\sum_{n\in\mathbb{Z}}g\left(n^2,0,0,0;m\right),
\end{aligned} \tag{A.42}$$

in order to rewrite the multifold summation in eq. (A.41), and make use of an appropriate representation for computing the free energy density with the help of eq. (A.35). Doing so allows us to obtain an analytic and symmetric representation for corresponding master sum-integral $I_\alpha^{(3)}$, which we do not display here for the sake of brevity. Further applying eq. (A.22), in order to get the free energy density, we Laurent expand the resulting expression around $\epsilon=0$. Again, skipping some minor technical details, we finally obtain

$$f^{(3)}=-\frac{m^4}{64\pi^2\,\epsilon}+\frac{m^2}{32\pi\,\epsilon}\left(\frac{L_1+L_2+L_3}{L_1L_2L_3}\right)+\frac{m^4}{128\pi^2}\left[4\,\ln\left(\frac{m}{\bar{\Lambda}}\right)-3\right]$$

$$
\begin{aligned}
&-\frac{m}{16L_1L_2L_3}-\frac{m^2}{32\pi}\left(\frac{L_1+L_2+L_3}{L_1L_2L_3}\right)\left[2\,\ln\left(\frac{m}{\bar{\Lambda}}\right)-1\right]+\frac{m^3}{24\pi}\left(\frac{L_1L_2+L_1L_3+L_2L_3}{L_1L_2L_3}\right)\\
&-\frac{T}{8L_1L_2L_3}\log\left(1-e^{-\frac{m}{T}}\right)-\frac{mT}{8\pi L_1L_2}\sum_{\substack{(n,\ell_3)\\ \in\mathbb{Z}^2\setminus\{\mathbf{0}\}}}\left[\frac{K_1\left(\frac{m}{T}\sqrt{n^2+(2TL_3)^2\ell_3^2}\right)}{\sqrt{n^2+(2TL_3)^2\ell_3^2}}\right]\\
&-\frac{mT}{8\pi L_1L_3}\sum_{\substack{(n,\ell_2)\\ \in\mathbb{Z}^2\setminus\{\mathbf{0}\}}}\left[\frac{K_1\left(\frac{m}{T}\sqrt{n^2+(2TL_2)^2\ell_2^2}\right)}{\sqrt{n^2+(2TL_2)^2\ell_2^2}}\right]\\
&-\frac{mT}{8\pi L_2L_3}\sum_{\substack{(n,\ell_1)\\ \in\mathbb{Z}^2\setminus\{\mathbf{0}\}}}\left[\frac{K_1\left(\frac{m}{T}\sqrt{n^2+(2TL_1)^2\ell_1^2}\right)}{\sqrt{n^2+(2TL_1)^2\ell_1^2}}\right]\\
&+\frac{T^3}{8\pi L_1}\sum_{\substack{(n,\ell_2,\ell_3)\\ \in\mathbb{Z}^3\setminus\{\mathbf{0}\}}}\left[\frac{e^{-\frac{m}{T}\sqrt{n^2+(2TL_2)^2\ell_2^2+(2TL_3)^2\ell_3^2}}\left(1+\frac{m}{T}\sqrt{n^2+(2TL_2)^2\ell_2^2+(2TL_3)^2\ell_3^2}\right)}{\left(n^2+(2TL_2)^2\ell_2^2+(2TL_3)^2\ell_3^2\right)^{3/2}}\right]\\
&+\frac{T^3}{8\pi L_2}\sum_{\substack{(n,\ell_1,\ell_3)\\ \in\mathbb{Z}^3\setminus\{\mathbf{0}\}}}\left[\frac{e^{-\frac{m}{T}\sqrt{n^2+(2TL_1)^2\ell_1^2+(2TL_3)^2\ell_3^2}}\left(1+\frac{m}{T}\sqrt{n^2+(2TL_1)^2\ell_1^2+(2TL_3)^2\ell_3^2}\right)}{\left(n^2+(2TL_1)^2\ell_1^2+(2TL_3)^2\ell_3^2\right)^{3/2}}\right]\\
&+\frac{T^3}{8\pi L_3}\sum_{\substack{(n,\ell_1,\ell_2)\\ \in\mathbb{Z}^3\setminus\{\mathbf{0}\}}}\left[\frac{e^{-\frac{m}{T}\sqrt{n^2+(2TL_1)^2\ell_1^2+(2TL_2)^2\ell_2^2}}\left(1+\frac{m}{T}\sqrt{n^2+(2TL_1)^2\ell_1^2+(2TL_2)^2\ell_2^2}\right)}{\left(n^2+(2TL_1)^2\ell_1^2+(2TL_2)^2\ell_2^2\right)^{3/2}}\right]\\
&-\frac{m^2T^2}{4\pi^2}\sum_{\substack{(n,\ell_1,\ell_2,\ell_3)\\ \in\mathbb{Z}^4\setminus\{\mathbf{0}\}}}\left[\frac{K_2\left(\frac{m}{T}\sqrt{n^2+(2TL_1)^2\ell_1^2+(2TL_2)^2\ell_2^2+(2TL_3)^2\ell_3^2}\right)}{\left(n^2+(2TL_1)^2\ell_1^2+(2TL_2)^2\ell_2^2+(2TL_3)^2\ell_3^2\right)}\right]+O\left(\epsilon^1\right).
\end{aligned}
\tag{A.43}
$$

Unlike in the case of the tube geometry, we cannot here simply come back to an earlier version of the massive result such as eq. (A.43). Indeed, even though there is no infrared (or even UV) divergence, and the application of the massless limit upon eq. (A.43) would leave an expression which is overall finite, each of the summations therein produces, in fact, a divergence. And only the sum of all of these divergences actually vanishes. The reason is that when $m = 0$, each of the sums in eq. (A.43) can be represented by a certain zeta function, and we hit the corresponding pole in the $\epsilon \to 0$ limit. Therefore, we will implement the limit $m \to 0$, keeping ϵ nonzero for the sake of regularizing intermediate stage divergences. Doing so, we find

$$
\lim_{m\to 0}\left(f^{(3)}\right)=\left(\frac{e^{\gamma_E\epsilon}(\bar{\Lambda}/T)^{2\epsilon}}{2^{3+2\epsilon}\pi^{1/2}}\right)\left(\frac{T}{L_1L_2L_3}\right)\Gamma\left(\frac{1}{2}-\epsilon\right)\zeta\left(1-2\epsilon\right)
$$

$$
\begin{aligned}
&-\left(\frac{e^{\gamma_E\epsilon}(\bar{\Lambda}/T)^{2\epsilon}}{2^{3+2\epsilon}\pi}\right)\left(\frac{T^2}{L_1L_2}\right)\Gamma\big(1-\epsilon\big)\sum_{\substack{(n,\ell_3)\\ \in\mathbb{Z}^2\setminus\{\mathbf{0}\}}}\Big(n^2+(2TL_3)^2\ell_3^2\Big)^{\epsilon-1}\\
&-\left(\frac{e^{\gamma_E\epsilon}(\bar{\Lambda}/T)^{2\epsilon}}{2^{3+2\epsilon}\pi}\right)\left(\frac{T^2}{L_1L_3}\right)\Gamma\big(1-\epsilon\big)\sum_{\substack{(n,\ell_2)\\ \in\mathbb{Z}^2\setminus\{\mathbf{0}\}}}\Big(n^2+(2TL_2)^2\ell_2^2\Big)^{\epsilon-1}\\
&-\left(\frac{e^{\gamma_E\epsilon}(\bar{\Lambda}/T)^{2\epsilon}}{2^{3+2\epsilon}\pi}\right)\left(\frac{T^2}{L_2L_3}\right)\Gamma\big(1-\epsilon\big)\sum_{\substack{(n,\ell_1)\\ \in\mathbb{Z}^2\setminus\{\mathbf{0}\}}}\Big(n^2+(2TL_1)^2\ell_1^2\Big)^{\epsilon-1}\\
&+\left(\frac{e^{\gamma_E\epsilon}(\bar{\Lambda}/T)^{2\epsilon}}{2^{2+2\epsilon}\pi^{3/2}}\right)\left(\frac{T^3}{L_1}\right)\Gamma\left(\frac{3}{2}-\epsilon\right)\sum_{\substack{(n,\ell_2,\ell_3)\\ \in\mathbb{Z}^3\setminus\{\mathbf{0}\}}}\Big(n^2+(2TL_2)^2\ell_2^2+(2TL_3)^2\ell_3^2\Big)^{\epsilon-3/2}\\
&+\left(\frac{e^{\gamma_E\epsilon}(\bar{\Lambda}/T)^{2\epsilon}}{2^{2+2\epsilon}\pi^{3/2}}\right)\left(\frac{T^3}{L_2}\right)\Gamma\left(\frac{3}{2}-\epsilon\right)\sum_{\substack{(n,\ell_1,\ell_3)\\ \in\mathbb{Z}^3\setminus\{\mathbf{0}\}}}\Big(n^2+(2TL_1)^2\ell_1^2+(2TL_3)^2\ell_3^2\Big)^{\epsilon-3/2}\\
&+\left(\frac{e^{\gamma_E\epsilon}(\bar{\Lambda}/T)^{2\epsilon}}{2^{2+2\epsilon}\pi^{3/2}}\right)\left(\frac{T^3}{L_3}\right)\Gamma\left(\frac{3}{2}-\epsilon\right)\sum_{\substack{(n,\ell_1,\ell_2)\\ \in\mathbb{Z}^3\setminus\{\mathbf{0}\}}}\Big(n^2+(2TL_1)^2\ell_1^2+(2TL_2)^2\ell_2^2\Big)^{\epsilon-3/2}\\
&-\left(\frac{e^{\gamma_E\epsilon}(\bar{\Lambda}/T)^{2\epsilon}}{2^{1+2\epsilon}\pi^2}\right)\Big(T^4\Big)\Gamma\big(2-\epsilon\big)\times\\
&\qquad\times\sum_{\substack{(n,\ell_1,\ell_2,\ell_3)\\ \in\mathbb{Z}^4\setminus\{\mathbf{0}\}}}\Big(n^2+(2TL_1)^2\ell_1^2+(2TL_2)^2\ell_2^2+(2TL_3)^2\ell_3^2\Big)^{\epsilon-2}
\end{aligned}
\tag{A.44}
$$

where the structure of the intermediate divergences, which we mentioned previously, is now obvious. Notice further that as the sum of all the poles in ϵ identically vanishes, the finite part which is by construction $\bar{\Lambda}$-dependent will also vanish, leaving the overall result not only finite but also thankfully renormalization scale independent.

Following the massless result of the infinite rectangular tube case, we can again use the Poisson resummation formula eq. (A.1), together with expressions such as eq. (A.28) and eq. (A.34) in order to compute the above two-fold summations while singling out the intermediate stage divergences. In addition, we can use eq. (A.38) in order to deal with the three-fold summations, including those which will appear in the decomposition of the four-fold summation. In the end, we are only left with the computation of the last term in the above expression, and to do so we define

$$
S_4 \equiv \sum_{(n,\ell_1,\ell_2,\ell_3)\in\mathbb{Z}^4\setminus\{\mathbf{0}\}}\Big(n^2+(2TL_1)^2\ell_1^2+(2TL_2)^2\ell_2^2+(2TL_3)^2\ell_3^2\Big)^{\epsilon-2}, \tag{A.45}
$$

in order to give more details on this last technical step. The above expression can be decomposed and symmetrized following

$$
\begin{aligned}
S_4 = & \frac{2}{3}\sum_{\ell_1=1}^{+\infty} \sum_{(n,\ell_2,\ell_3)\in\mathbb{Z}^3} \left(n^2+(2TL_1)^2\ell_1^2+(2TL_2)^2\ell_2^2+(2TL_3)^2\ell_3^2\right)^{\epsilon-2} \\
& + \frac{2}{3}\sum_{\ell_2=1}^{+\infty} \sum_{(n,\ell_1,\ell_3)\in\mathbb{Z}^3} \left(n^2+(2TL_1)^2\ell_1^2+(2TL_2)^2\ell_2^2+(2TL_3)^2\ell_3^2\right)^{\epsilon-2} \\
& + \frac{2}{3}\sum_{\ell_3=1}^{+\infty} \sum_{(n,\ell_1,\ell_2)\in\mathbb{Z}^3} \left(n^2+(2TL_1)^2\ell_1^2+(2TL_2)^2\ell_2^2+(2TL_3)^2\ell_3^2\right)^{\epsilon-2} \\
& + \frac{1}{3} \sum_{(n,\ell_2,\ell_3)\in\mathbb{Z}^3\setminus\{\mathbf{0}\}} \left(n^2+(2TL_2)^2\ell_2^2+(2TL_3)^2\ell_3^2\right)^{\epsilon-2} \\
& + \frac{1}{3} \sum_{(n,\ell_1,\ell_3)\in\mathbb{Z}^3\setminus\{\mathbf{0}\}} \left(n^2+(2TL_1)^2\ell_1^2+(2TL_3)^2\ell_3^2\right)^{\epsilon-2} \\
& + \frac{1}{3} \sum_{(n,\ell_1,\ell_2)\in\mathbb{Z}^3\setminus\{\mathbf{0}\}} \left(n^2+(2TL_1)^2\ell_1^2+(2TL_2)^2\ell_2^2\right)^{\epsilon-2}. \qquad \text{(A.46)}
\end{aligned}
$$

And while the last three terms can be handled via the procedure which we used for the three-fold summations in the previous subsection, the first three terms need to be computed separately. We then define another set of summations, namely S_{1+3}, which denotes the first of the above terms. Analytically continuing this set of sums, using for example eq. (A.35), leads to the following result

$$
\begin{aligned}
S_{1+3} = & \left(\frac{\pi^{3/2}(TL_1)^{2\epsilon-1}\Gamma\left(\frac{1}{2}-\epsilon\right)\zeta\left(1-2\epsilon\right)}{3\times 4^{1-\epsilon}\, T^2L_2L_3\,\Gamma\left(2-\epsilon\right)}\right) + \left(\frac{\pi^{2-\epsilon}(TL_1)^{\epsilon-\frac{1}{2}}}{2^{\frac{1}{2}-\epsilon}\times 3\, T^2L_2L_3\,\Gamma\left(2-\epsilon\right)}\right)\times \\
& \times \sum_{\ell_1=1}^{+\infty} \sum_{(n,\ell_2,\ell_3)\in\mathbb{Z}^3\setminus\{\mathbf{0}\}} \left[\frac{\left(n^2+\frac{\ell_2^2}{(2TL_2)^2}+\frac{\ell_3^2}{(2TL_3)^2}\right)^{\frac{1}{4}-\frac{\epsilon}{2}}}{\ell_1^{\frac{1}{2}-\epsilon}}\times\right. \\
& \left.\times K_{\frac{1}{2}-\epsilon}\left(4\pi TL_1\ell_1\sqrt{n^2+\frac{\ell_2^2}{(2TL_2)^2}+\frac{\ell_3^2}{(2TL_3)^2}}\right)\right]. \qquad \text{(A.47)}
\end{aligned}
$$

Finally bringing all the results together, and expanding around $\epsilon = 0$, we see that all the ϵ- intermediate stage divergences indeed cancel. In addition, the renormalization scale dependence disappears as a consequence of the fact that there is no overall logarithmic UV divergence in the present case. We further perform some of the summations, in order to get closed forms whenever it is possible. Then, relabeling some of the variables, we finally obtain

$$
f^{(3)} = -\frac{\pi^2T^4}{90} + \frac{T\,\log\left(8T^3L_1L_2L_3\right)}{24L_1L_2L_3} + \frac{\zeta\left(3\right)T^3(L_1L_2+L_1L_3+L_2L_3)}{4\pi L_1L_2L_3}
$$

$$
\begin{aligned}
&- \frac{\pi T^2 (L_1+L_2+L_3)}{24 L_1 L_2 L_3} - \frac{\zeta(3)\, T (L_1^3 L_2^3 + L_1^3 L_3^3 + L_2^3 L_3^3)}{48\pi L_1^3 L_2^3 L_3^3} \\
&+ \frac{\pi T (L_1^2 L_2 + L_1 L_2^2 + L_1^2 L_3 + L_1 L_3^2 + L_2^2 L_3 + L_2 L_3^2)}{144 L_1^2 L_2^2 L_3^2} \\
&+ \frac{T}{4 L_1 L_2 L_3} \sum_{\ell=1}^{+\infty} \left[\log\left(1 - e^{-4\pi T L_1 \ell}\right) + \log\left(1 - e^{-4\pi T L_2 \ell}\right) + \log\left(1 - e^{-4\pi T L_3 \ell}\right) \right] \\
&- \frac{T^2}{6 L_1^2} \sum_{\ell=1}^{+\infty} \left[\ell\, \mathrm{Li}_2\left(e^{-4\pi T L_1 \ell}\right) \right] - \frac{T}{24\pi L_1^3} \sum_{\ell=1}^{+\infty} \mathrm{Li}_3\left(e^{-4\pi T L_1 \ell}\right) \\
&- \frac{T^2}{6 L_2^2} \sum_{\ell=1}^{+\infty} \left[\ell\, \mathrm{Li}_2\left(e^{-4\pi T L_2 \ell}\right) \right] - \frac{T}{24\pi L_2^3} \sum_{\ell=1}^{+\infty} \mathrm{Li}_3\left(e^{-4\pi T L_2 \ell}\right) \\
&- \frac{T^2}{6 L_3^2} \sum_{\ell=1}^{+\infty} \left[\ell\, \mathrm{Li}_2\left(e^{-4\pi T L_3 \ell}\right) \right] - \frac{T}{24\pi L_3^3} \sum_{\ell=1}^{+\infty} \mathrm{Li}_3\left(e^{-4\pi T L_3 \ell}\right) \\
&+ \frac{T^2}{2 L_1 L_2 L_3} \sum_{n,\ell=1}^{+\infty} \left[\frac{(L_2+L_3)\,\ell}{n} K_1\left(4\pi T L_1 n \ell\right) + \frac{(L_1+L_3)\,\ell}{n} K_1\left(4\pi T L_2 n \ell\right) \right. \\
&\qquad \left. + \frac{(L_1+L_2)\,\ell}{n} K_1\left(4\pi T L_3 n \ell\right) \right] \\
&- \frac{T}{16 L_1 L_2 L_3} \sum_{(n,\ell)\in\mathbb{Z}^2\setminus\{\mathbf{0}\}} \left[\log\left(1 - e^{-\frac{2\pi L_2}{L_1}\sqrt{\ell^2 + (2T L_1)^2 n^2}}\right) + \log\left(1 - e^{-\frac{2\pi L_3}{L_1}\sqrt{\ell^2 + (2T L_1)^2 n^2}}\right) \right. \\
&\qquad + \log\left(1 - e^{-\frac{2\pi L_1}{L_2}\sqrt{\ell^2 + (2T L_2)^2 n^2}}\right) + \log\left(1 - e^{-\frac{2\pi L_3}{L_2}\sqrt{\ell^2 + (2T L_2)^2 n^2}}\right) \\
&\qquad \left. + \log\left(1 - e^{-\frac{2\pi L_1}{L_3}\sqrt{\ell^2 + (2T L_3)^2 n^2}}\right) + \log\left(1 - e^{-\frac{2\pi L_2}{L_3}\sqrt{\ell^2 + (2T L_3)^2 n^2}}\right) \right] \\
&- \frac{T}{24 L_1^2 L_2^2 L_3^2} \sum_{\ell_1=1}^{+\infty} \sum_{(n,\ell_2)\in\mathbb{Z}^2\setminus\{\mathbf{0}\}} \left[L_2 L_3^2\, \frac{\sqrt{\ell_2^2 + (2T L_1)^2 n^2}}{\ell_1} K_1\left(\frac{2\pi L_2}{L_1}\, \ell_1\, \sqrt{\ell_2^2 + (2T L_1)^2 n^2}\right) \right. \\
&\qquad + L_3 L_2^2\, \frac{\sqrt{\ell_2^2 + (2T L_1)^2 n^2}}{\ell_1} K_1\left(\frac{2\pi L_3}{L_1}\, \ell_1\, \sqrt{\ell_2^2 + (2T L_1)^2 n^2}\right) \\
&\qquad + L_1 L_3^2\, \frac{\sqrt{\ell_2^2 + (2T L_2)^2 n^2}}{\ell_1} K_1\left(\frac{2\pi L_1}{L_2}\, \ell_1\, \sqrt{\ell_2^2 + (2T L_2)^2 n^2}\right) \\
&\qquad + L_3 L_1^2\, \frac{\sqrt{\ell_2^2 + (2T L_2)^2 n^2}}{\ell_1} K_1\left(\frac{2\pi L_3}{L_2}\, \ell_1\, \sqrt{\ell_2^2 + (2T L_2)^2 n^2}\right) \\
&\qquad + L_1 L_2^2\, \frac{\sqrt{\ell_2^2 + (2T L_3)^2 n^2}}{\ell_1} K_1\left(\frac{2\pi L_1}{L_3}\, \ell_1\, \sqrt{\ell_2^2 + (2T L_3)^2 n^2}\right) \\
&\qquad \left. + L_2 L_1^2\, \frac{\sqrt{\ell_2^2 + (2T L_3)^2 n^2}}{\ell_1} K_1\left(\frac{2\pi L_2}{L_3}\, \ell_1\, \sqrt{\ell_2^2 + (2T L_3)^2 n^2}\right) \right]
\end{aligned}
$$

$$+\frac{T}{24L_1L_2L_3}\sum_{(n,\ell_1,\ell_2)\in\mathbb{Z}^3\setminus\{\mathbf{0}\}}\Bigg[\log\left(1-e^{-4\pi TL_1\sqrt{n^2+\frac{\ell_1^2}{(2TL_2)^2}+\frac{\ell_2^2}{(2TL_3)^2}}}\right)$$
$$+\log\left(1-e^{-4\pi TL_2\sqrt{n^2+\frac{\ell_1^2}{(2TL_1)^2}+\frac{\ell_2^2}{(2TL_3)^2}}}\right)$$
$$+\log\left(1-e^{-4\pi TL_3\sqrt{n^2+\frac{\ell_1^2}{(2TL_1)^2}+\frac{\ell_2^2}{(2TL_2)^2}}}\right)\Bigg], \tag{A.48}$$

which is the symmetrized and renormalized free energy density of a noninteracting massless neutral scalar field coupled to a heat bath at temperature T, and geometrically confined inside a box with sides of respective finite lengths L_1, L_2, and L_3. We refer to eq. (10.16) for a conveniently much more compact form of this result.

A.2 Various proofs

A.2.1 Fourier decomposition

In this section, we first describe the derivation of the form and normalization of the Fourier decomposition of a massless scalar field (adding a mass does not modify the argument), along the direction of a compactified dimension with DBCs. To this end, we apply the method of separation of variables to the scalar field, and consider only, for the sake of argument, the part relevant to one of the DBCs which must also obey the Klein-Gordon equation

$$\left(\omega_\ell^2+\frac{\partial^2}{\partial\xi^2}\right)\phi_\ell(\xi)=0, \tag{A.49}$$

where we recall that $\omega_\ell\equiv\pi\ell/L$. Compactifying this direction onto a finite length $[0,L]$, and imposing DBCs, implies that

$$\phi_\ell(0)=\phi_\ell(L)=0. \tag{A.50}$$

We then remember that the general solution to a differential equation such as eq. (A.49) is

$$\phi_\ell(\xi)=A\sin\left(\omega_\ell\xi\right)+B\cos\left(\omega_\ell\xi\right). \tag{A.51}$$

Thus, by applying the boundary conditions eq. (A.50) to the above, we obtain

$$B\overset{!}{=}0,\quad \omega_\ell\overset{!}{=}\frac{\pi\ell}{L}, \tag{A.52}$$

We may then obtain a convenient prefactor by normalizing the field to unity

$$\int_0^L d\xi \;\; \phi_\ell(\xi)\phi_\ell(\xi) = \int_0^L d\xi \;\; A^2 \sin^2\left(\frac{\pi\ell}{L}\xi\right) \stackrel{!}{=} 1, \tag{A.53}$$

$$\Rightarrow A \stackrel{!}{=} \sqrt{\frac{2}{L}}\,. \tag{A.54}$$

Therefore, we obtain the Fourier decomposition along a compactified dimension with DBCs

$$\phi_\ell\,(\xi) = \sqrt{\frac{2}{L}}\;\sin\left(\frac{\pi\ell}{L}\xi\right). \tag{A.55}$$

We now give some useful identities: It should be noted, indeed, that in order to go from eq. (10.4) to eq. (10.5), the following integral identities, defining the usual Kronecker delta function, are needed

$$\int_0^{1/T} \mathrm{d}\tau e^{i(\omega_{n_1}+\omega_{n_2})\tau} \equiv \delta_{n_1+n_2}/T, \quad \int_R \mathrm{d}^{D-1-c}\boldsymbol{x}\, e^{i(\omega_{k_1}+\omega_{k_2})\,\boldsymbol{x}} \equiv R^{D-1-c}\delta_{\boldsymbol{n}_{k_1}+\boldsymbol{n}_{k_2}}, \tag{A.56}$$

$$\int_0^{L_i} \mathrm{d}z_i \;\; \sin\left(\omega_{\ell_{i_1}} z_i\right)\sin\left(\omega_{\ell_{i_2}} z_i\right) \equiv L_i\delta_{\ell_{i_1}-\ell_{i_2}}/2, \tag{A.57}$$

the last equation holding only for all ℓ_i strictly positive integers, which is presently the case.

A.2.2 Length derivatives

We present a short derivation of an important result, i.e. the length derivatives of the internal and free energies, which allows us to compute the pressures directly from the free energy. Consider eq. (11.1) which we differentiate following

$$dF(T,\,\{L_i\}) + S\,dT = dE(S,\,\{L_i\}) - T dS\,. \tag{A.58}$$

On both sides of the above equation, fixing all variables but one length L_j (preferably the same on both sides) gives us the following important equation

$$\left.\frac{\partial F(T,\,\{L_i\})}{\partial L_j}\right|_{T,\{L_{k\neq j}\}} dL_j = \left.\frac{\partial E(S,\,\{L_i\})}{\partial L_j}\right|_{S,\{L_{k\neq j}\}} dL_j. \tag{A.59}$$

The above result indicates that both partial differential expressions are equal, namely that

$$\left.\frac{\partial F(T,\,\{L_i\})}{\partial L_j}\right|_{T,\{L_{k\neq j}\}} = \left.\frac{\partial E(S,\,\{L_i\})}{\partial L_j}\right|_{S,\{L_{k\neq j}\}}, \tag{A.60}$$

allowing to probe the pressure P_j from either of the two functions $E(S,\,\{L_i\})$ or $F(T,\,\{L_i\})$

$$P_j = -\frac{L_j}{V}\left.\frac{\partial E(S,\{L_i\})}{\partial L_j}\right|_{S,\{L_{k\neq j}\}} = -\frac{L_j}{V}\left.\frac{\partial F(T,\{L_i\})}{\partial L_j}\right|_{T,\{L_{k\neq j}\}}. \tag{A.61}$$

A.2.3 Hessian of the energy

In order to compute the matrix elements in eq. (11.20), that is

$$\mathcal{E}_{ij} \equiv \frac{L_i L_j}{T^4 V}\frac{\partial^2 E(S,\{L_k\})}{\partial L_i|_{S,\{L_{k\neq i}\}}\,\partial L_j\big|_{S,\{L_{k\neq j}\}}}, \tag{A.62}$$

consider first that from eq. (11.7) we obtain

$$\begin{aligned} S \equiv -\left.\frac{\partial F}{\partial T}\right|_{\{L_k\}} &= -\left.\frac{\partial}{\partial T}\left\{T^4 V \tilde{f}\right\}\right|_{\{L_k\}} = -T^3 V(4\tilde{f} + T\partial_T \tilde{f}) \\ &= -T^3 V\left(4\tilde{f} + \sum_{L_i\in\Omega}\left[(TLi)\left.\frac{\partial \tilde{f}}{\partial(TLi)}\right|_{\{L_k\}}\right]\right), \end{aligned} \tag{A.63}$$

and therefore that

$$\tilde{s} \equiv \frac{S}{T^3 V} = -4\tilde{f} - \sum_{L_i\in\Omega}\left[(TLi)\left.\frac{\partial \tilde{f}}{\partial(TLi)}\right|_{\{L_{k\neq i}\}}\right], \tag{A.64}$$

and

$$\begin{aligned} (TLi)\left.\frac{\partial \tilde{s}}{\partial(TLi)}\right|_{\{L_{k\neq i}\}} &= -5\,(TLi)\left.\frac{\partial \tilde{f}}{\partial(TLi)}\right|_{T,\{L_{k\neq i}\}} \\ &\quad - \sum_{L_j\in\Omega}\left[(TLj)(TLi)\frac{\partial^2 \tilde{f}}{\partial\,(TLj)\big|_{\{L_k\}}\,\partial\,(TLi)\big|_{T,\{L_{k\neq i}\}}}\right]. \end{aligned} \tag{A.65}$$

Furthermore, given eq. (11.6), we also have

$$P_i \equiv -\frac{L_i}{V}\left.\frac{\partial F}{\partial L_i}\right|_{T,\{L_{k\neq i}\}} = -\frac{L_i}{V}\left.\frac{\partial}{\partial L_i}\left\{T^4 V\tilde{f}\right\}\right|_{T,\{L_{k\neq i}\}} = -T^4\left(\tilde{f} + (TLi)\left.\frac{\partial \tilde{f}}{\partial(TLi)}\right|_{T,\{L_{k\neq i}\}}\right), \tag{A.66}$$

so that

$$\tilde{p}_i \equiv \frac{P_i}{T^4} = -\tilde{f} - (TLi)\left.\frac{\partial \tilde{f}}{\partial(TLi)}\right|_{\{T,L_{k\neq i}\}}, \tag{A.67}$$

and

$$
\begin{aligned}
T\left.\frac{\partial\tilde{p}_i}{\partial T}\right|_{\{L_k\}} &= \sum_{L_j\in\Omega}\left[(TLj)\left.\frac{\partial\tilde{p}_i}{\partial(TLj)}\right|_{\{L_{j\neq i}\}}\right] \\
&= -\sum_{L_j\in\Omega}\left[(TLj)\left.\frac{\partial\tilde{f}}{\partial(TLj)}\right|_{\{L_k\}} - \frac{\partial^2\tilde{f}}{\partial\,(TLj)\big|_{\{L_k\}}\,\partial\,(TLi)\big|_{T,\{L_{k\neq i}\}}}\right] \\
&\quad -(TLi)\left.\frac{\partial\tilde{f}}{\partial(TLi)}\right|_{\{L_k\}}. \qquad \text{(A.68)}
\end{aligned}
$$

we may now write eq. (11.20) as

$$
\begin{aligned}
\mathcal{E}_{ij} &\equiv \frac{L_iL_j}{T^4V}\frac{\partial^2E(S,\{L_k\})}{\partial L_i|_{S,\{L_{k\neq i}\}}\,\partial L_j\big|_{S,\{L_{k\neq i}\}}} \\
&\overset{eq.\ (A.60)}{=} \frac{L_iL_j}{T^4V}\frac{\partial}{\partial L_j}\left\{\left.\frac{\partial F}{\partial L_i}\right|_{T,\{L_{k\neq i}\}}\right\}\Bigg|_{S,\{L_{k\neq j}\}} \\
&\overset{eq.\ (11.6)}{=} -\frac{L_iL_j}{T^4V}\frac{\partial}{\partial L_j}\left\{\frac{V}{L_i}P_i\right\}\Bigg|_{S,\{L_{k\neq j}\}} \\
&= -\frac{L_iL_j}{T^4V}\left(\frac{V}{L_i}\left.\frac{\partial P_i}{\partial L_j}\right|_{S,\{L_{k\neq j}\}} - \frac{VP_i}{L_i^2}\delta_{ij} + \frac{P_i}{L_i}\frac{V}{L_j}\right). \qquad \text{(A.69)}
\end{aligned}
$$

Further notice that, due to eq. (11.19), and the subsequent set of chain rules, we have

$$
\left.\frac{\partial P_i}{\partial L_j}\right|_{S,\{L_{k\neq j}\}} = \left.\frac{\partial P_i}{\partial T}\right|_{\{L_k\}}\left.\frac{\partial T}{\partial L_j}\right|_{S,\{L_{k\neq j}\}} + \left.\frac{\partial P_i}{\partial L_j}\right|_{T,\{L_{k\neq j}\}}, \qquad \text{(A.70)}
$$

each term of which we may evaluate individually

$$
\begin{aligned}
\left.\frac{\partial P_i}{\partial T}\right|_{\{L_k\}} &= \frac{\partial}{\partial T}\left\{-T^4\left(\tilde{f}+(TLi)\left.\frac{\partial\tilde{f}}{\partial(TLi)}\right|_{T,\{L_{k\neq i}\}}\right)\right\}\Bigg|_{\{L_k\}} \\
&= T^3\Bigg(-4\tilde{f}-4(TLi)\left.\frac{\partial\tilde{f}}{\partial(TLi)}\right|_{T,\{L_{k\neq i}\}} - T\left.\frac{\partial\tilde{f}}{\partial T}\right|_{\{L_k\}} - (TLi)\left.\frac{\partial\tilde{f}}{\partial(TLi)}\right|_{T,\{L_{k\neq i}\}} \\
&\quad - T\,TLi\frac{\partial^2\tilde{f}}{\partial T|_{\{L_k\}}\partial(TLi)|_{T,\{L_{k\neq i}\}}}\Bigg) \\
&= -T^3\Bigg(4\tilde{f}+5\,(TLi)\left.\frac{\partial\tilde{f}}{\partial(TLi)}\right|_{T,\{L_{k\neq i}\}} + \sum_{L_k\in\Omega}\left[(TLk)\left.\frac{\partial\tilde{f}}{\partial(TLk)}\right|_{\{L_j\}}\right. \\
&\quad \left. + (TLi)(TLk)\frac{\partial^2\tilde{f}}{\partial(TLk)|_{\{L_k\}}\partial(TLi)|_{T,\{L_{k\neq i}\}}}Bigg\right]\Bigg) \\
&\overset{eq.\ (A.65)}{\overset{eq.\ (A.65)}{=}} -T^3\left(\tilde{s}+(TLi)\left.\frac{\partial\tilde{s}}{\partial(TLi)}\right|_{T,\{L_{k\neq i}\}}\right) \qquad \text{(A.71)}
\end{aligned}
$$

$$\overset{\substack{eq.\ (A.67)\\ eq.\ (A.68)}}{=} -T^3\left(4\tilde{p}_i + \sum_{j\in\Omega}\left[TLj\ \frac{\partial\tilde{p}_i}{\partial TLj}\bigg|_{\{L_k\}}\right]\right), \tag{A.72}$$

$$\begin{aligned}\frac{\partial T}{\partial L_j}\bigg|_{S,\{L_{k\neq j}\}} &= -\frac{T}{L_j}\left(L_j\ \frac{\partial S}{\partial L_j}\bigg|_{T,\{L_{k\neq j}\}}\right)\left(T\ \frac{\partial S}{\partial T}\bigg|_{\{L_k\}}\right)^{-1} \qquad \text{(Jacobian identitiy)}\\ &= -\frac{T}{L_j}\frac{1}{\tilde{c}_v}\left(\tilde{s} + (TLj)\ \frac{\partial\tilde{s}}{\partial(TLj)}\bigg|_{T,\{L_{k\neq j}\}}\right), \end{aligned}\tag{A.73}$$

$$\begin{aligned}\frac{\partial P_i}{\partial L_j}\bigg|_{T,\{\{L_{\neq j}\}} &= -\frac{T^4}{L_j}\left((TLj)\ \frac{\partial\tilde{f}}{\partial(TLj)}\bigg|_{T,\{\{L_{\neq j}\}} + (TLi)(TLj)\ \frac{\partial^2\tilde{f}}{\partial(TLi)|_{\{L_{k\neq i}\}}\partial(TLj)|_{\{L_{k\neq j}\}}}\right.\\ &\quad \left. +\delta_{ij}(TLi)\ \frac{\partial\tilde{f}}{\partial(TLi)}\bigg|_{T,\{L_{\neq j}\}}\right). \end{aligned}\tag{A.74}$$

Finally, combining all these expressions gives us

$$\begin{aligned}\mathcal{E}_{ij} = &\left(\tilde{s} + (TLi)\ \frac{\partial\tilde{s}}{\partial(TLi)}\bigg|_{T,\{L_{k\neq i}\}}\right) + \tilde{f}(1-\delta_{ij})\frac{1}{\tilde{c}_v}\left(\tilde{s} + (TLj)\ \frac{\partial\tilde{s}}{\partial(TLj)}\bigg|_{T,\{L_{k\neq j}\}}\right)\\ &+ (TLi)\ \frac{\partial\tilde{f}}{\partial(TLi)}\bigg|_{T,\{L_{k\neq i}\}} + (TLj)\ \frac{\partial\tilde{f}}{\partial(TLj)}\bigg|_{T,\{L_{k\neq j}\}}\\ &+ (TLi)(TLj)\frac{\partial^2\tilde{f}}{\partial(TLi)|_{\{L_{k\neq i}\}}\partial(TLj)|_{\{L_{k\neq j}\}}}. \end{aligned}\tag{A.75}$$

Bibliography

[1] E. Rutherford. "The scattering of alpha and beta particles by matter and the structure of the atom". In: *Phil. Mag. Ser.6* 21 (1911), pp. 669–688. DOI: 10.1080/14786440508637080.

[2] Freeman Dyson. "Seeing the Unseen". In: *The New York Review of Books* 25.3 (Feb. 2005).

[3] Jaroslav Adam et al. "Direct photon production in Pb-Pb collisions at $\sqrt{s_{\mathrm{NN}}} = 2.76$ TeV". In: *Phys. Lett.* B754 (2016), pp. 235–248. DOI: 10.1016/j.physletb.2016.01.020. arXiv: 1509.07324 [nucl-ex].

[4] Dominik J. Schwarz. "The first second of the universe". In: *Annalen Phys.* 12 (2003), pp. 220–270. DOI: 10.1002/andp.200310010. arXiv: astro-ph/0303574 [astro-ph].

[5] N. Cabibbo and G. Parisi. "Exponential Hadronic Spectrum and Quark Liberation". In: *Phys. Lett.* 59B (1975), pp. 67–69. DOI: 10.1016/0370-2693(75)90158-6.

[6] John C. Collins and M. J. Perry. "Superdense Matter: Neutrons Or Asymptotically Free Quarks?" In: *Phys. Rev. Lett.* 34 (1975), p. 1353. DOI: 10.1103/PhysRevLett.34.1353.

[7] R. Hagedorn. "Statistical thermodynamics of strong interactions at high-energies". In: *Nuovo Cim. Suppl.* 3 (1965), pp. 147–186.

[8] Miklos Gyulassy. "The QGP discovered at RHIC". In: *Structure and dynamics of elementary matter. Proceedings, NATO Advanced Study Institute, Camyuva-Kemer, Turkey, September 22-October 2, 2003*. 2004, pp. 159–182. arXiv: nucl-th/0403032 [nucl-th].

[9] Gordon Baym et al. "From hadrons to quarks in neutron stars: a review". In: *Rept. Prog. Phys.* 81.5 (2018), p. 056902. DOI: 10.1088/1361-6633/aaae14. arXiv: 1707.04966 [astro-ph.HE].

[10] Yuval Ne'eman and Y. Kirsh. *THE PARTICLE HUNTERS*. 1986. URL: http://www.cambridge.org/uk/catalogue/catalogue.asp?isbn=0521301947.

[11] David Griffiths. *Introduction to elementary particles*. 2008. ISBN: 9783527406012.

[12] Francois Gelis et al. "The Color Glass Condensate". In: *Ann. Rev. Nucl. Part. Sci.* 60 (2010), pp. 463–489. DOI: 10.1146/annurev.nucl.010909.083629. arXiv: 1002.0333 [hep-ph].

[13] John Adams et al. "Experimental and theoretical challenges in the search for the quark gluon plasma: The STAR Collaboration's critical assessment of the evidence

from RHIC collisions". In: *Nucl. Phys.* A757 (2005), pp. 102–183. DOI: 10.1016/j.nuclphysa.2005.03.085. arXiv: nucl-ex/0501009 [nucl-ex].

[14] Heikki Mäntysaari et al. "Proton structure fluctuations: from HERA to the LHC". In: *PoS* DIS2017 (2018), p. 060. DOI: 10.22323/1.297.0060. arXiv: 1706.05937 [nucl-th].

[15] Carlos A. Salgado and Johannes P. Wessels. "Proton–Lead Collisions at the CERN LHC". In: *Ann. Rev. Nucl. Part. Sci.* 66 (2016), pp. 449–473. DOI: 10.1146/annurev-nucl-102014-022110.

[16] T. Ludlam. "Experimental results from the early measurements at RHIC: Hunting for the quark-gluon plasma". In: *Nucl. Phys.* A750 (2005), pp. 9–29. DOI: 10.1016/j.nuclphysa.2004.11.005.

[17] M. Gyulassy. "Theory of high-energy A+A at RHIC." In: *Lect. Notes Phys.* 583 (2002), pp. 37–79. DOI: 10.1007/3-540-45792-5_2. arXiv: nucl-th/0106072 [nucl-th].

[18] Jean-Yves Ollitrault. "Anisotropy as a signature of transverse collective flow". In: *Phys. Rev.* D46 (1992), pp. 229–245. DOI: 10.1103/PhysRevD.46.229.

[19] Charles Gale et al. "Event-by-event anisotropic flow in heavy-ion collisions from combined Yang-Mills and viscous fluid dynamics". In: *Phys. Rev. Lett.* 110.1 (2013), p. 012302. DOI: 10.1103/PhysRevLett.110.012302. arXiv: 1209.6330 [nucl-th].

[20] Zhe Xu and Carsten Greiner. "Shear viscosity in a gluon gas". In: *Phys. Rev. Lett.* 100 (2008), p. 172301. DOI: 10.1103/PhysRevLett.100.172301. arXiv: 0710.5719 [nucl-th].

[21] Zi-Wei Lin et al. "A Multi-phase transport model for relativistic heavy ion collisions". In: *Phys. Rev.* C72 (2005), p. 064901. DOI: 10.1103/PhysRevC.72.064901. arXiv: nucl-th/0411110 [nucl-th].

[22] Aleksi Kurkela, Urs Achim Wiedemann, and Bin Wu. "Kinetic transport is needed to reliably extract shear viscosity from pA and AA data". In: (2018). arXiv: 1805.04081 [hep-ph].

[23] Adam Bzdak and Guo-Liang Ma. "Elliptic and triangular flow in p+Pb and peripheral Pb+Pb collisions from parton scatterings". In: *Phys. Rev. Lett.* 113.25 (2014), p. 252301. DOI: 10.1103/PhysRevLett.113.252301. arXiv: 1406.2804 [hep-ph].

[24] J. D. Orjuela Koop et al. "Azimuthal anisotropy relative to the participant plane from a multiphase transport model in central p + Au , d + Au , and ^{3}He + Au collisions at $\sqrt{s_{NN}} = 200$ GeV". In: *Phys. Rev.* C92.5 (2015), p. 054903. DOI: 10.1103/PhysRevC.92.054903. arXiv: 1501.06880 [nucl-ex].

[25] Hanlin Li et al. "Origin of the mass splitting of azimuthal anisotropies in a multiphase transport model". In: *Phys. Rev.* C96.1 (2017), p. 014901. DOI: 10.1103/PhysRevC.96.014901. arXiv: 1604.07387 [nucl-th].

[26] Werner Scheid, Hans Muller, and Walter Greiner. "Nuclear Shock Waves in Heavy-Ion Collisions". In: *Phys. Rev. Lett.* 32 (1974), pp. 741–745. DOI: 10.1103/PhysRevLett.32.741.

[27] S. Voloshin and Y. Zhang. "Flow study in relativistic nuclear collisions by Fourier expansion of Azimuthal particle distributions". In: *Z. Phys.* C70 (1996), pp. 665–672. DOI: 10.1007/s002880050141. arXiv: hep-ph/9407282 [hep-ph].

[28] K. H. Ackermann et al. "Elliptic flow in Au + Au collisions at (S(NN))**(1/2) = 130 GeV". In: *Phys. Rev. Lett.* 86 (2001), pp. 402–407. DOI: 10.1103/PhysRevLett.86.402. arXiv: nucl-ex/0009011 [nucl-ex].

[29] K. Adcox et al. "Flow measurements via two particle azimuthal correlations in Au+Au collisions at s(NN)**(1/2) = 130-GeV". In: *Phys. Rev. Lett.* 89 (2002), p. 212301. DOI: 10.1103/PhysRevLett.89.212301. arXiv: nucl-ex/0204005 [nucl-ex].

[30] B. B. Back et al. "Pseudorapidity and centrality dependence of the collective flow of charged particles in Au+Au collisions at s(NN)**(1/2) = 130-GeV". In: *Phys. Rev. Lett.* 89 (2002), p. 222301. DOI: 10.1103/PhysRevLett.89.222301. arXiv: nucl-ex/0205021 [nucl-ex].

[31] Georges Aad et al. "Measurement of event-plane correlations in $\sqrt{s_{NN}} = 2.76$ TeV lead-lead collisions with the ATLAS detector". In: *Phys. Rev.* C90.2 (2014), p. 024905. DOI: 10.1103/PhysRevC.90.024905. arXiv: 1403.0489 [hep-ex].

[32] Georges Aad et al. "Measurement of the distributions of event-by-event flow harmonics in lead-lead collisions at = 2.76 TeV with the ATLAS detector at the LHC". In: *JHEP* 11 (2013), p. 183. DOI: 10.1007/JHEP11(2013)183. arXiv: 1305.2942 [hep-ex].

[33] Vardan Khachatryan et al. "Long-range two-particle correlations of strange hadrons with charged particles in pPb and PbPb collisions at LHC energies". In: *Phys. Lett.* B742 (2015), pp. 200–224. DOI: 10.1016/j.physletb.2015.01.034. arXiv: 1409.3392 [nucl-ex].

[34] K. Aamodt et al. "Harmonic decomposition of two-particle angular correlations in Pb-Pb collisions at $\sqrt{s_{NN}} = 2.76$ TeV". In: *Phys. Lett.* B708 (2012), pp. 249–264. DOI: 10.1016/j.physletb.2012.01.060. arXiv: 1109.2501 [nucl-ex].

[35] Serguei Chatrchyan et al. "Long-range and short-range dihadron angular correlations in central PbPb collisions at a nucleon-nucleon center of mass energy of 2.76 TeV". In: *JHEP* 07 (2011), p. 076. DOI: 10.1007/JHEP07(2011)076. arXiv: 1105.2438 [nucl-ex].

[36] Serguei Chatrchyan et al. "Centrality dependence of dihadron correlations and azimuthal anisotropy harmonics in PbPb collisions at $\sqrt{s_{NN}} = 2.76$ TeV". In: *Eur. Phys. J.* C72 (2012), p. 2012. DOI: 10.1140/epjc/s10052-012-2012-3. arXiv: 1201.3158 [nucl-ex].

[37] Georges Aad et al. "Measurement of the azimuthal anisotropy for charged particle production in $\sqrt{s_{NN}} = 2.76$ TeV lead-lead collisions with the ATLAS detector". In:

Phys. Rev. C86 (2012), p. 014907. DOI: 10.1103/PhysRevC.86.014907. arXiv: 1203.3087 [hep-ex].

[38] Betty Bezverkhny Abelev et al. "Elliptic flow of identified hadrons in Pb-Pb collisions at $\sqrt{s_{\mathrm{NN}}}$ = 2.76 TeV". In: *JHEP* 06 (2015), p. 190. DOI: 10.1007/JHEP06(2015)190. arXiv: 1405.4632 [nucl-ex].

[39] Betty Abelev et al. "Anisotropic flow of charged hadrons, pions and (anti-)protons measured at high transverse momentum in Pb-Pb collisions at $\sqrt{s_{NN}}$=2.76 TeV". In: *Phys. Lett.* B719 (2013), pp. 18–28. DOI: 10.1016/j.physletb.2012.12.066. arXiv: 1205.5761 [nucl-ex].

[40] Jaroslav Adam et al. "Higher harmonic flow coefficients of identified hadrons in Pb-Pb collisions at $\sqrt{s_{NN}}$ = 2.76 TeV". In: *JHEP* 09 (2016), p. 164. DOI: 10.1007/JHEP09(2016)164. arXiv: 1606.06057 [nucl-ex].

[41] John Adams et al. "Particle type dependence of azimuthal anisotropy and nuclear modification of particle production in Au + Au collisions at s(NN)**(1/2) = 200-GeV". In: *Phys. Rev. Lett.* 92 (2004), p. 052302. DOI: 10.1103/PhysRevLett.92.052302. arXiv: nucl-ex/0306007 [nucl-ex].

[42] Betty Bezverkhny Abelev et al. "Long-range angular correlations of ß, K and p in p-Pb collisions at $\sqrt{s_{\mathrm{NN}}}$ = 5.02 TeV". In: *Phys. Lett.* B726 (2013), pp. 164–177. DOI: 10.1016/j.physletb.2013.08.024. arXiv: 1307.3237 [nucl-ex].

[43] S. Acharya et al. "Anisotropic flow in Xe-Xe collisions at $\sqrt{s_{NN}}$ = **5.44** TeV". In: *Phys. Lett.* B784 (2018), pp. 82–95. DOI: 10.1016/j.physletb.2018.06.059. arXiv: 1805.01832 [nucl-ex].

[44] P. Huovinen et al. "Radial and elliptic flow at RHIC: Further predictions". In: *Phys. Lett.* B503 (2001), pp. 58–64. DOI: 10.1016/S0370-2693(01)00219-2. arXiv: hep-ph/0101136 [hep-ph].

[45] Georges Aad et al. "Measurement with the ATLAS detector of multi-particle azimuthal correlations in p+Pb collisions at $\sqrt{s_{NN}}$ =5.02 TeV". In: *Phys. Lett.* B725 (2013), pp. 60–78. DOI: 10.1016/j.physletb.2013.06.057. arXiv: 1303.2084 [hep-ex].

[46] Serguei Chatrchyan et al. "Multiplicity and transverse momentum dependence of two- and four-particle correlations in pPb and PbPb collisions". In: *Phys. Lett.* B724 (2013), pp. 213–240. DOI: 10.1016/j.physletb.2013.06.028. arXiv: 1305.0609 [nucl-ex].

[47] Vardan Khachatryan et al. "Evidence for collectivity in pp collisions at the LHC". In: *Phys. Lett.* B765 (2017), pp. 193–220. DOI: 10.1016/j.physletb.2016.12.009. arXiv: 1606.06198 [nucl-ex].

[48] Vardan Khachatryan et al. "Observation of Long-Range Near-Side Angular Correlations in Proton-Proton Collisions at the LHC". In: *JHEP* 09 (2010), p. 091. DOI: 10.1007/JHEP09(2010)091. arXiv: 1009.4122 [hep-ex].

[49] Georges Aad et al. "Observation of Long-Range Elliptic Azimuthal Anisotropies in $\sqrt{s}$ =13 and 2.76 TeV pp Collisions with the ATLAS Detector". In: *Phys. Rev. Lett.*

116.17 (2016), p. 172301. DOI: 10.1103/PhysRevLett.116.172301. arXiv: 1509.04776 [hep-ex].

[50] CMS Collaboration. *Observation of long-range near-side two-particle correlations in pp collisions at $\sqrt{s}$ = 13 TeV*. Tech. rep. CMS-PAS-FSQ-15-002. 2015.

[51] Vardan Khachatryan et al. "Evidence for Collective Multiparticle Correlations in p-Pb Collisions". In: *Phys. Rev. Lett.* 115.1 (2015), p. 012301. DOI: 10.1103/PhysRevLett.115.012301. arXiv: 1502.05382 [nucl-ex].

[52] Betty Bezverkhny Abelev et al. "Multiparticle azimuthal correlations in p -Pb and Pb-Pb collisions at the CERN Large Hadron Collider". In: *Phys. Rev.* C90.5 (2014), p. 054901. DOI: 10.1103/PhysRevC.90.054901. arXiv: 1406.2474 [nucl-ex].

[53] A. Adare et al. "Measurement of long-range angular correlation and quadrupole anisotropy of pions and (anti)protons in central d+Au collisions at $\sqrt{s_{NN}}$=200 GeV". In: *Phys. Rev. Lett.* 114.19 (2015), p. 192301. DOI: 10.1103/PhysRevLett.114.192301. arXiv: 1404.7461 [nucl-ex].

[54] A. Adare et al. "Measurements of elliptic and triangular flow in high-multiplicity ^{3}He+Au collisions at $\sqrt{s_{NN}} = 200$ GeV". In: *Phys. Rev. Lett.* 115.14 (2015), p. 142301. DOI: 10.1103/PhysRevLett.115.142301. arXiv: 1507.06273 [nucl-ex].

[55] Serguei Chatrchyan et al. "Observation of long-range near-side angular correlations in proton-lead collisions at the LHC". In: *Phys. Lett.* B718 (2013), pp. 795–814. DOI: 10.1016/j.physletb.2012.11.025. arXiv: 1210.5482 [nucl-ex].

[56] Panagiota Foka and Małgorzata Anna Janik. "An overview of experimental results from ultra-relativistic heavy-ion collisions at the CERN LHC: Bulk properties and dynamical evolution". In: *Rev. Phys.* 1 (2016), pp. 154–171. DOI: 10.1016/j.revip.2016.11.002. arXiv: 1702.07233 [hep-ex].

[57] Heikki Mäntysaari and Björn Schenke. "Evidence of strong proton shape fluctuations from incoherent diffraction". In: *Phys. Rev. Lett.* 117.5 (2016), p. 052301. DOI: 10.1103/PhysRevLett.117.052301. arXiv: 1603.04349 [hep-ph].

[58] Betty Abelev et al. "Long-range angular correlations on the near and away side in p-Pb collisions at $\sqrt{s_{NN}} = 5.02$ TeV". In: *Phys. Lett.* B719 (2013), pp. 29–41. DOI: 10.1016/j.physletb.2013.01.012. arXiv: 1212.2001 [nucl-ex].

[59] Georges Aad et al. "Observation of Associated Near-Side and Away-Side Long-Range Correlations in $\sqrt{s_{NN}}$=5.02 TeV Proton-Lead Collisions with the ATLAS Detector". In: *Phys. Rev. Lett.* 110.18 (2013), p. 182302. DOI: 10.1103/PhysRevLett.110.182302. arXiv: 1212.5198 [hep-ex].

[60] P. Koch, Berndt Muller, and Johann Rafelski. "Strangeness in Relativistic Heavy Ion Collisions". In: *Phys. Rept.* 142 (1986), pp. 167–262. DOI: 10.1016/0370-1573(86)90096-7.

[61] J. Bartke et al. "Neutral strange particle production in sulphur sulphur and proton sulphur collisions at 200-GeV/nucleon". In: *Z. Phys.* C48 (1990), pp. 191–200. DOI: 10.1007/BF01554465.

[62] Johann Rafelski and Michael Danos. "The Importance of the Reaction Volume in Hadronic Collisions". In: *Phys. Lett.* 97B (1980), pp. 279–282. DOI: 10.1016/0370-2693(80)90601-2.

[63] R. Hagedorn and K. Redlich. "Statistical Thermodynamics in Relativistic Particle and Ion Physics: Canonical or Grand Canonical?" In: *Z. Phys.* C27 (1985), p. 541. DOI: 10.1007/BF01436508.

[64] Natasha Sharma, Jean Cleymans, and Boris Hippolyte. "Thermodynamic limit in high-multiplicity pp collisions at $\sqrt{s}$ = 7 TeV". In: (2018). arXiv: 1803.05409 [hep-ph].

[65] E. Andersen et al. "Strangeness enhancement at mid-rapidity in Pb Pb collisions at 158-A-GeV/c". In: *Phys. Lett.* B449 (1999), pp. 401–406. DOI: 10.1016/S0370-2693(99)00140-9.

[66] T. Virgili et al. "Recent results from NA57 on strangeness production in p-A and Pb-Pb collisions at 40-A-GeV/c and 158-A-GeV/c". In: *QCD and high energy hadronic interactions. Proceedings, 39th Rencontres de Moriond, La Thuile, Italy, March 28-April 2, 2004*. 2004, pp. 337–342. arXiv: hep-ex/0405052 [hep-ex].

[67] Anthony R. Timmins. "Strange Particle Production at RHIC". In: *Eur. Phys. J.* C62 (2009), pp. 249–254. DOI: 10.1140/epjc/s10052-009-0979-1. arXiv: 0810.0017 [nucl-ex].

[68] H. Appelshauser et al. "Recent results on central Pb + Pb collisions from experiment NA49". In: *Nucl. Phys.* A638 (1998), pp. 91–102. DOI: 10.1016/S0375-9474(98)00402-3.

[69] F. Antinori. "The heavy ion physics programme at the CERN OMEGA spectrometer". In: *The CERN OMEGA spectrometer: 25 years of physics. Proceedings, Symposium, Geneva, Switzerland, March 19, 1997*. 1997, pp. 43–49.

[70] Peter Koch, Berndt Müller, and Johann Rafelski. "From strangeness enhancement to quark–gluon plasma discovery". In: *Int. J. Mod. Phys.* A32.31 (2017), p. 1730024. DOI: 10.1142/S0217751X17300241. arXiv: 1708.08115 [nucl-th].

[71] Jaroslav Adam et al. "Enhanced production of multi-strange hadrons in high-multiplicity proton-proton collisions". In: *Nature Phys.* 13 (2017), pp. 535–539. DOI: 10.1038/nphys4111. arXiv: 1606.07424 [nucl-ex].

[72] Jaroslav Adam et al. "Production of $K^*(892)^0$ and $\phi(1020)$ in p–Pb collisions at $\sqrt{s_{NN}}$ = 5.02 TeV". In: *Eur. Phys. J.* C76.5 (2016), p. 245. DOI: 10.1140/epjc/s10052-016-4088-7. arXiv: 1601.07868 [nucl-ex].

[73] Jaroslav Adam et al. "Multi-strange baryon production in p-Pb collisions at $\sqrt{s_{\mathrm{NN}}}$ = 5.02 TeV". In: *Phys. Lett.* B758 (2016), pp. 389–401. DOI: 10.1016/j.physletb.2016.05.027. arXiv: 1512.07227 [nucl-ex].

[74] Vardan Khachatryan et al. "Multiplicity and rapidity dependence of strange hadron production in pp, pPb, and PbPb collisions at the LHC". In: *Phys. Lett.* B768 (2017), pp. 103–129. DOI: 10.1016/j.physletb.2017.01.075. arXiv: 1605.06699 [nucl-ex].

[75] Betty Bezverkhny Abelev et al. "Multiplicity Dependence of Pion, Kaon, Proton and Lambda Production in p-Pb Collisions at $\sqrt{s_{NN}}$ = 5.02 TeV". In: *Phys. Lett.* B728 (2014), pp. 25–38. DOI: 10.1016/j.physletb.2013.11.020. arXiv: 1307.6796 [nucl-ex].

[76] CMS Collaboration. *Multiplicity and rapidity dependence of strange hadrons spectra in pp, pPb, and PbPb collisions at LHC energies*. CMS-PAS-HIN-15-006. 2015.

[77] Kevin Dusling, Wei Li, and Björn Schenke. "Novel collective phenomena in high-energy proton–proton and proton–nucleus collisions". In: *Int. J. Mod. Phys.* E25.01 (2016), p. 1630002. DOI: 10.1142/S0218301316300022. arXiv: 1509.07939 [nucl-ex].

[78] Constantin Loizides. "Experimental overview on small collision systems at the LHC". In: *Nucl. Phys.* A956 (2016), pp. 200–207. DOI: 10.1016/j.nuclphysa.2016.04.022. arXiv: 1602.09138 [nucl-ex].

[79] J. D. Bjorken. "Energy Loss of Energetic Partons in Quark - Gluon Plasma: Possible Extinction of High p(t) Jets in Hadron - Hadron Collisions". In: (1982).

[80] Urs Achim Wiedemann. "Jet Quenching in Heavy Ion Collisions". In: (2010). [Landolt-Bornstein23,521(2010)], pp. 521–562. DOI: 10.1007/978-3-642-01539-7_17. arXiv: 0908.2306 [hep-ph].

[81] Xin-Nian Wang and Miklos Gyulassy. "Gluon shadowing and jet quenching in A + A collisions at s**(1/2) = 200-GeV". In: *Phys. Rev. Lett.* 68 (1992), pp. 1480–1483. DOI: 10.1103/PhysRevLett.68.1480.

[82] Miklos Gyulassy and Xin-nian Wang. "Multiple collisions and induced gluon Bremsstrahlung in QCD". In: *Nucl. Phys.* B420 (1994), pp. 583–614. DOI: 10.1016/0550-3213(94)90079-5. arXiv: nucl-th/9306003 [nucl-th].

[83] Xin-Nian Wang, Miklos Gyulassy, and Michael Plumer. "The LPM effect in QCD and radiative energy loss in a quark gluon plasma". In: *Phys. Rev.* D51 (1995), pp. 3436–3446. DOI: 10.1103/PhysRevD.51.3436. arXiv: hep-ph/9408344 [hep-ph].

[84] M. Gyulassy, P. Levai, and I. Vitev. "NonAbelian energy loss at finite opacity". In: *Phys. Rev. Lett.* 85 (2000), pp. 5535–5538. DOI: 10.1103/PhysRevLett.85.5535. arXiv: nucl-th/0005032 [nucl-th].

[85] M. Gyulassy, P. Levai, and I. Vitev. "Reaction operator approach to nonAbelian energy loss". In: *Nucl. Phys.* B594 (2001), pp. 371–419. DOI: 10.1016/S0550-3213(00)00652-0. arXiv: nucl-th/0006010 [nucl-th].

[86] M. Gyulassy, P. Levai, and I. Vitev. "Jet tomography of Au+Au reactions including multigluon fluctuations". In: *Phys. Lett.* B538 (2002), pp. 282–288. DOI: 10.1016/S0370-2693(02)01990-1. arXiv: nucl-th/0112071 [nucl-th].

[87] Magdalena Djordjevic and Miklos Gyulassy. "Heavy quark radiative energy loss in QCD matter". In: *Nucl. Phys.* A733 (2004), pp. 265–298. DOI: 10.1016/j.nuclphysa.2003.12.020. arXiv: nucl-th/0310076 [nucl-th].

[88] Magdalena Djordjevic, Miklos Gyulassy, and Simon Wicks. "The Charm and beauty of RHIC and LHC". In: *Phys. Rev. Lett.* 94 (2005), p. 112301. DOI: 10.1103/PhysRevLett.94.112301. arXiv: hep-ph/0410372 [hep-ph].

[89] R. Baier et al. "Induced gluon radiation in a QCD medium". In: *Phys. Lett.* B345 (1995), pp. 277–286. DOI: 10.1016/0370-2693(94)01617-L. arXiv: hep-ph/9411409 [hep-ph].

[90] R. Baier et al. "Radiative energy loss of high-energy quarks and gluons in a finite volume quark - gluon plasma". In: *Nucl. Phys.* B483 (1997), pp. 291–320. DOI: 10.1016/S0550-3213(96)00553-6. arXiv: hep-ph/9607355 [hep-ph].

[91] R. Baier et al. "Radiative energy loss and p(T) broadening of high-energy partons in nuclei". In: *Nucl. Phys.* B484 (1997), pp. 265–282. DOI: 10.1016/S0550-3213(96)00581-0. arXiv: hep-ph/9608322 [hep-ph].

[92] R. Baier et al. "Radiative energy loss of high-energy partons traversing an expanding QCD plasma". In: *Phys. Rev.* C58 (1998), pp. 1706–1713. DOI: 10.1103/PhysRevC.58.1706. arXiv: hep-ph/9803473 [hep-ph].

[93] R. Baier et al. "Quenching of hadron spectra in media". In: *JHEP* 09 (2001), p. 033. DOI: 10.1088/1126-6708/2001/09/033. arXiv: hep-ph/0106347 [hep-ph].

[94] B. G. Zakharov. "Fully quantum treatment of the Landau-Pomeranchuk-Migdal effect in QED and QCD". In: *JETP Lett.* 63 (1996), pp. 952–957. DOI: 10.1134/1.567126. arXiv: hep-ph/9607440 [hep-ph].

[95] B. G. Zakharov. "Radiative energy loss of high-energy quarks in finite size nuclear matter and quark - gluon plasma". In: *JETP Lett.* 65 (1997), pp. 615–620. DOI: 10.1134/1.567389. arXiv: hep-ph/9704255 [hep-ph].

[96] B. G. Zakharov. "Light cone path integral approach to the Landau-Pomeranchuk-Migdal effect". In: *Phys. Atom. Nucl.* 61 (1998). [Yad. Fiz.61,924(1998)], pp. 838–854. arXiv: hep-ph/9807540 [hep-ph].

[97] Urs Achim Wiedemann. "Jet quenching versus jet enhancement: A Quantitative study of the BDMPS-Z gluon radiation spectrum". In: *Nucl. Phys.* A690 (2001), pp. 731–751. DOI: 10.1016/S0375-9474(01)00362-1. arXiv: hep-ph/0008241 [hep-ph].

[98] Urs Achim Wiedemann. "Transverse dynamics of hard partons in nuclear media and the QCD dipole". In: *Nucl. Phys.* B582 (2000), pp. 409–450. DOI: 10.1016/S0550-3213(00)00286-8. arXiv: hep-ph/0003021 [hep-ph].

[99] Urs Achim Wiedemann. "Gluon radiation off hard quarks in a nuclear environment: Opacity expansion". In: *Nucl. Phys.* B588 (2000), pp. 303–344. DOI: 10.1016/S0550-3213(00)00457-0. arXiv: hep-ph/0005129 [hep-ph].

[100] Carlos A. Salgado and Urs Achim Wiedemann. "Calculating quenching weights". In: *Phys. Rev.* D68 (2003), p. 014008. DOI: 10.1103/PhysRevD.68.014008. arXiv: hep-ph/0302184 [hep-ph].

[101] Nestor Armesto, Carlos A. Salgado, and Urs Achim Wiedemann. "Medium induced gluon radiation off massive quarks fills the dead cone". In: *Phys. Rev.* D69 (2004),

p. 114003. DOI: 10.1103/PhysRevD.69.114003. arXiv: hep-ph/0312106 [hep-ph].

[102] Peter Brockway Arnold, Guy D. Moore, and Laurence G. Yaffe. "Photon emission from ultrarelativistic plasmas". In: *JHEP* 11 (2001), p. 057. DOI: 10.1088/1126-6708/2001/11/057. arXiv: hep-ph/0109064 [hep-ph].

[103] Peter Brockway Arnold, Guy D. Moore, and Laurence G. Yaffe. "Photon emission from quark gluon plasma: Complete leading order results". In: *JHEP* 12 (2001), p. 009. DOI: 10.1088/1126-6708/2001/12/009. arXiv: hep-ph/0111107 [hep-ph].

[104] Peter Brockway Arnold, Guy D. Moore, and Laurence G. Yaffe. "Photon and gluon emission in relativistic plasmas". In: *JHEP* 06 (2002), p. 030. DOI: 10.1088/1126-6708/2002/06/030. arXiv: hep-ph/0204343 [hep-ph].

[105] Xiao-feng Guo and Xin-Nian Wang. "Multiple scattering, parton energy loss and modified fragmentation functions in deeply inelastic e A scattering". In: *Phys. Rev. Lett.* 85 (2000), pp. 3591–3594. DOI: 10.1103/PhysRevLett.85.3591. arXiv: hep-ph/0005044 [hep-ph].

[106] A. Majumder and Berndt Muller. "Higher twist jet broadening and classical propagation". In: *Phys. Rev.* C77 (2008), p. 054903. DOI: 10.1103/PhysRevC.77.054903. arXiv: 0705.1147 [nucl-th].

[107] Abhijit Majumder. "Hard collinear gluon radiation and multiple scattering in a medium". In: *Phys. Rev.* D85 (2012), p. 014023. DOI: 10.1103/PhysRevD.85.014023. arXiv: 0912.2987 [nucl-th].

[108] Xin-Nian Wang and Xiao-feng Guo. "Multiple parton scattering in nuclei: Parton energy loss". In: *Nucl. Phys.* A696 (2001), pp. 788–832. DOI: 10.1016/S0375-9474(01)01130-7. arXiv: hep-ph/0102230 [hep-ph].

[109] T. Matsui and H. Satz. "J/ψ Suppression by Quark-Gluon Plasma Formation". In: *Phys. Lett.* B178 (1986), pp. 416–422. DOI: 10.1016/0370-2693(86)91404-8.

[110] Xin-Nian Wang. "Effect of jet quenching on high p_T hadron spectra in high-energy nuclear collisions". In: *Phys. Rev.* C58 (1998), p. 2321. DOI: 10.1103/PhysRevC.58.2321. arXiv: hep-ph/9804357 [hep-ph].

[111] Ivan Vitev and Miklos Gyulassy. "High p_T tomography of d + Au and Au+Au at SPS, RHIC, and LHC". In: *Phys. Rev. Lett.* 89 (2002), p. 252301. DOI: 10.1103/PhysRevLett.89.252301. arXiv: hep-ph/0209161 [hep-ph].

[112] I. Arsene et al. "Transverse momentum spectra in Au+Au and d+Au collisions at s**(1/2) = 200-GeV and the pseudorapidity dependence of high p(T) suppression". In: *Phys. Rev. Lett.* 91 (2003), p. 072305. DOI: 10.1103/PhysRevLett.91.072305. arXiv: nucl-ex/0307003 [nucl-ex].

[113] Serguei Chatrchyan et al. "Study of high-pT charged particle suppression in PbPb compared to pp collisions at $\sqrt{s_{NN}} = 2.76$ TeV". In: *Eur. Phys. J.* C72 (2012), p. 1945. DOI: 10.1140/epjc/s10052-012-1945-x. arXiv: 1202.2554 [nucl-ex].

[114] Tadaaki Isobe. "Measurements of high-p(T) neutral mesons in s(NN)**(1/2) = 200-GeV Au + Au and Cu + Cu Collisions at RHIC-PHENIX". In: *AIP Conf. Proc.* 842 (2006). [,56(2006)], pp. 56–58. DOI: 10.1063/1.2220186. arXiv: nucl-ex/0604016 [nucl-ex].

[115] Peter Braun-Munzinger and Benjamin Dönigus. "Loosely-bound objects produced in nuclear collisions at the LHC". In: (2018). arXiv: 1809.04681 [nucl-ex].

[116] Jaroslav Adam et al. "Centrality dependence of particle production in p-Pb collisions at $\sqrt{s_{\mathrm{NN}}}$= 5.02 TeV". In: *Phys. Rev.* C91.6 (2015), p. 064905. DOI: 10.1103/PhysRevC.91.064905. arXiv: 1412.6828 [nucl-ex].

[117] Nestor Armesto, Doga Can Gülhan, and Jose Guilherme Milhano. "Kinematic bias on centrality selection of jet events in pPb collisions at the LHC". In: *Phys. Lett.* B747 (2015), pp. 441–445. DOI: 10.1016/j.physletb.2015.06.032. arXiv: 1502.02986 [hep-ph].

[118] Shreyasi Acharya et al. "Analysis of the apparent nuclear modification in peripheral Pb-Pb collisions at 5.02 TeV". In: (2018). arXiv: 1805.05212 [nucl-ex].

[119] C. Adler et al. "Centrality dependence of high p_T hadron suppression in Au+Au collisions at $\sqrt{s_{NN}}$ = 130-GeV". In: *Phys. Rev. Lett.* 89 (2002), p. 202301. DOI: 10.1103/PhysRevLett.89.202301. arXiv: nucl-ex/0206011 [nucl-ex].

[120] CMS Collaboration. *Charged-particle nuclear modification factors in XeXe collisions at* $\sqrt{s_{\mathrm{NN}}} = 5.44$ TeV. CMS-PAS-HIN-18-004. 2018.

[121] Shreyasi Acharya et al. "Transverse momentum spectra and nuclear modification factors of charged particles in pp, p-Pb and Pb-Pb collisions at the LHC". In: (2018). arXiv: 1802.09145 [nucl-ex].

[122] I. Arsene et al. "Quark gluon plasma and color glass condensate at RHIC? The Perspective from the BRAHMS experiment". In: *Nucl. Phys.* A757 (2005), pp. 1–27. DOI: 10.1016/j.nuclphysa.2005.02.130. arXiv: nucl-ex/0410020 [nucl-ex].

[123] B. B. Back et al. "The PHOBOS perspective on discoveries at RHIC". In: *Nucl. Phys.* A757 (2005), pp. 28–101. DOI: 10.1016/j.nuclphysa.2005.03.084. arXiv: nucl-ex/0410022 [nucl-ex].

[124] Georges Aad et al. "Measurement of charged-particle spectra in Pb+Pb collisions at $\sqrt{s_{\mathrm{NN}}} = 2.76$ TeV with the ATLAS detector at the LHC". In: *JHEP* 09 (2015), p. 050. DOI: 10.1007/JHEP09(2015)050. arXiv: 1504.04337 [hep-ex].

[125] A. Adare et al. "Azimuthal anisotropy of π^0 and η mesons in Au + Au collisions at $\sqrt{s_{NN}} = 200$ GeV". In: *Phys. Rev.* C88.6 (2013), p. 064910. DOI: 10.1103/PhysRevC.88.064910. arXiv: 1309.4437 [nucl-ex].

[126] Betty Bezverkhny Abelev et al. "Neutral pion production at midrapidity in pp and Pb-Pb collisions at $\sqrt{s_{NN}} = 2.76$ TeV". In: *Eur. Phys. J.* C74.10 (2014), p. 3108. DOI: 10.1140/epjc/s10052-014-3108-8. arXiv: 1405.3794 [nucl-ex].

[127] Betty Abelev et al. "Centrality Dependence of Charged Particle Production at Large Transverse Momentum in Pb–Pb Collisions at $\sqrt{s_{\mathrm{NN}}} = 2.76$ TeV". In: *Phys. Lett.* B720 (2013), pp. 52–62. DOI: 10.1016/j.physletb.2013.01.051. arXiv: 1208.2711 [hep-ex].

[128] B. I. Abelev et al. "Transverse momentum and centrality dependence of high-p_T non-photonic electron suppression in Au+Au collisions at $\sqrt{s_{NN}} = 200$ GeV". In: *Phys. Rev. Lett.* 98 (2007). [Erratum: Phys. Rev. Lett.106,159902(2011)], p. 192301. DOI: 10.1103/PhysRevLett.106.159902, 10.1103/PhysRevLett.98.192301. arXiv: nucl-ex/0607012 [nucl-ex].

[129] Shingo Sakai. "Measurement of R_{AA} and v_2 of electrons from heavy-flavour decays in Pb-Pb collisions at $\sqrt{s_{NN}}$ = 2.76 TeV with ALICE". In: *Nucl. Phys.* A904-905 (2013), pp. 661c–664c. DOI: 10.1016/j.nuclphysa.2013.02.102.

[130] A. Adare et al. "Single electron yields from semileptonic charm and bottom hadron decays in Au+Au collisions at $\sqrt{s_{NN}} = 200$ GeV". In: *Phys. Rev.* C93.3 (2016), p. 034904. DOI: 10.1103/PhysRevC.93.034904. arXiv: 1509.04662 [nucl-ex].

[131] Jaroslav Adam et al. "Transverse momentum dependence of D-meson production in Pb-Pb collisions at $\sqrt{s_{NN}} = 2.76$ TeV". In: *JHEP* 03 (2016), p. 081. DOI: 10.1007/JHEP03(2016)081. arXiv: 1509.06888 [nucl-ex].

[132] Serguei Chatrchyan et al. "Suppression of non-prompt J/ψ, prompt J/ψ, and Y(1S) in PbPb collisions at $\sqrt{s_{NN}} = 2.76$ TeV". In: *JHEP* 05 (2012), p. 063. DOI: 10.1007/JHEP05(2012)063. arXiv: 1201.5069 [nucl-ex].

[133] Albert M Sirunyan et al. "Measurement of prompt and nonprompt charmonium suppression in PbPb collisions at 5.02 TeV". In: *Eur. Phys. J.* C78.6 (2018), p. 509. DOI: 10.1140/epjc/s10052-018-5950-6. arXiv: 1712.08959 [nucl-ex].

[134] Serguei Chatrchyan et al. "Observation of sequential Upsilon suppression in PbPb collisions". In: *Phys. Rev. Lett.* 109 (2012). [Erratum: Phys. Rev. Lett.120,no.19, 199903(2018)], p. 222301. DOI: 10.1103/PhysRevLett.109.222301, 10.1103/PhysRevLett.120.199903. arXiv: 1208.2826 [nucl-ex].

[135] Jaroslav Adam et al. "Inclusive, prompt and non-prompt J/ψ production at mid-rapidity in Pb-Pb collisions at $\sqrt{s_{NN}}$ = 2.76 TeV". In: *JHEP* 07 (2015), p. 051. DOI: 10.1007/JHEP07(2015)051. arXiv: 1504.07151 [nucl-ex].

[136] Betty Abelev et al. "J/ψ suppression at forward rapidity in Pb-Pb collisions at $\sqrt{s_{NN}} = 2.76$ TeV". In: *Phys. Rev. Lett.* 109 (2012), p. 072301. DOI: 10.1103/PhysRevLett.109.072301. arXiv: 1202.1383 [hep-ex].

[137] L. Adamczyk et al. "J/ψ production at low p_T in Au+Au and Cu+Cu collisions at $\sqrt{s_{NN}} = 200$ GeV with the STAR detector ". In: *Phys. Rev.* C90.2 (2014), p. 024906. DOI: 10.1103/PhysRevC.90.024906. arXiv: 1310.3563 [nucl-ex].

[138] A. Adare et al. "J/psi Production in s(NN)**(1/2) = 200-GeV Cu+Cu Collisions". In: *Phys. Rev. Lett.* 101 (2008), p. 122301. DOI: 10.1103/PhysRevLett.101.122301. arXiv: 0801.0220 [nucl-ex].

[139] A. Adare et al. "J/ψ Production vs Centrality, Transverse Momentum, and Rapidity in Au+Au Collisions at $\sqrt{s_{NN}} = 200$ GeV". In: *Phys. Rev. Lett.* 98 (2007), p. 232301. DOI: 10.1103/PhysRevLett.98.232301. arXiv: nucl-ex/0611020 [nucl-ex].

[140] Nestor Armesto et al. "How sensitive are high-p(T) electron spectra at RHIC to heavy quark energy loss?" In: *Phys. Lett.* B637 (2006), pp. 362–366. DOI: 10.1016/j.physletb.2005.12.073. arXiv: hep-ph/0511257 [hep-ph].

[141] W. A. Horowitz. "Heavy Quark Production and Energy Loss". In: *Nucl. Phys.* A904-905 (2013), pp. 186c–193c. DOI: 10.1016/j.nuclphysa.2013.01.061. arXiv: 1210.8330 [nucl-th].

[142] Karen M. Burke et al. "Extracting the jet transport coefficient from jet quenching in high-energy heavy-ion collisions". In: *Phys. Rev.* C90.1 (2014), p. 014909. DOI: 10.1103/PhysRevC.90.014909. arXiv: 1312.5003 [nucl-th].

[143] Magdalena Djordjevic, Marko Djordjevic, and Bojana Blagojevic. "RHIC and LHC jet suppression in non-central collisions". In: *Phys. Lett.* B737 (2014), pp. 298–302. DOI: 10.1016/j.physletb.2014.08.063. arXiv: 1405.4250 [nucl-th].

[144] J. Badier et al. "Experimental J/psi Hadronic Production from 150-GeV/c to 280-GeV/c". In: *Z. Phys.* C20 (1983), p. 101. DOI: 10.1007/BF01573213.

[145] R Aaij et al. "Study of J/ψ production and cold nuclear matter effects in pPb collisions at $\sqrt{s_{NN}} = 5$ TeV". In: *JHEP* 02 (2014), p. 072. DOI: 10.1007/JHEP02(2014)072. arXiv: 1308.6729 [nucl-ex].

[146] R. Aaij et al. "Prompt and nonprompt J/ψ production and nuclear modification in pPb collisions at $\sqrt{s_{\rm NN}} = 8.16$ TeV". In: *Phys. Lett.* B774 (2017), pp. 159–178. DOI: 10.1016/j.physletb.2017.09.058. arXiv: 1706.07122 [hep-ex].

[147] Serguei Chatrchyan et al. "Event activity dependence of Y(nS) production in $\sqrt{s_{NN}}$=5.02 TeV pPb and $\sqrt{s}$=2.76 TeV pp collisions". In: *JHEP* 04 (2014), p. 103. DOI: 10.1007/JHEP04(2014)103. arXiv: 1312.6300 [nucl-ex].

[148] Betty Bezverkhny Abelev et al. "J/ψ production and nuclear effects in p-Pb collisions at $\sqrt{S_{NN}}$ = 5.02 TeV". In: *JHEP* 02 (2014), p. 073. DOI: 10.1007/JHEP02(2014)073. arXiv: 1308.6726 [nucl-ex].

[149] Jaroslav Adam et al. "Centrality dependence of inclusive J/ψ production in p-Pb collisions at $\sqrt{s_{\rm NN}} = 5.02$ TeV". In: *JHEP* 11 (2015), p. 127. DOI: 10.1007/JHEP11(2015)127. arXiv: 1506.08808 [nucl-ex].

[150] Jaroslav Adam et al. "Centrality dependence of χ(2S) suppression in p-Pb collisions at $\sqrt{s_{\rm NN}}$ = 5.02 TeV". In: *JHEP* 06 (2016), p. 050. DOI: 10.1007/JHEP06(2016)050. arXiv: 1603.02816 [nucl-ex].

[151] Albert M Sirunyan et al. "Measurement of prompt and nonprompt J/ψ production in pp and pPb collisions at $\sqrt{s_{\rm NN}} = 5.02$ TeV". In: *Eur. Phys. J.* C77.4 (2017), p. 269. DOI: 10.1140/epjc/s10052-017-4828-3. arXiv: 1702.01462 [nucl-ex].

[152] R Arnaldi et al. "J/psi production in proton-nucleus collisions at 158 and 400 GeV". In: *Phys. Lett.* B706 (2012), pp. 263–267. DOI: 10.1016/j.physletb.2011.11.042. arXiv: 1004.5523 [nucl-ex].

[153] Shreyasi Acharya et al. "Inclusive J/ψ production at forward and backward rapidity in p-Pb collisions at $\sqrt{s_{\rm NN}}$ = 8.16 TeV". In: *JHEP* 07 (2018), p. 160. DOI: 10.1007/JHEP07(2018)160. arXiv: 1805.04381 [nucl-ex].

[154] Vardan Khachatryan et al. "Suppression and azimuthal anisotropy of prompt and nonprompt J/ψ production in PbPb collisions at $\sqrt{s_{NN}} = 2.76$ TeV". In: *Eur. Phys. J.* C77.4 (2017), p. 252. DOI: 10.1140/epjc/s10052-017-4781-1. arXiv: 1610.00613 [nucl-ex].

[155] A. Adare et al. "Cold Nuclear Matter Effects on J/ψ Yields as a Function of Rapidity and Nuclear Geometry in Deuteron-Gold Collisions at $\sqrt{s_{NN}} = 200$ GeV". In: *Phys. Rev. Lett.* 107 (2011), p. 142301. DOI: 10.1103/PhysRevLett.107.142301. arXiv: 1010.1246 [nucl-ex].

[156] Z. Conesa del Valle et al. "Quarkonium production in high energy proton-proton and proton-nucleus collisions". In: *Nucl. Phys. Proc. Suppl.* 214 (2011), pp. 3–36. DOI: 10.1016/j.nuclphysbps.2011.03.053. arXiv: 1105.4545 [hep-ph].

[157] Georges Aad et al. "Centrality and rapidity dependence of inclusive jet production in $\sqrt{s_{\mathrm{NN}}} = 5.02$ TeV proton-lead collisions with the ATLAS detector". In: *Phys. Lett.* B748 (2015), pp. 392–413. DOI: 10.1016/j.physletb.2015.07.023. arXiv: 1412.4092 [hep-ex].

[158] Jaroslav Adam et al. "Centrality dependence of charged jet production in p–Pb collisions at $\sqrt{s_{\mathrm{NN}}} = 5.02$ TeV". In: *Eur. Phys. J.* C76.5 (2016), p. 271. DOI: 10.1140/epjc/s10052-016-4107-8. arXiv: 1603.03402 [nucl-ex].

[159] A. Adare et al. "Centrality-dependent modification of jet-production rates in deuteron-gold collisions at $\sqrt{s_{NN}}$=200 GeV". In: *Phys. Rev. Lett.* 116.12 (2016), p. 122301. DOI: 10.1103/PhysRevLett.116.122301. arXiv: 1509.04657 [nucl-ex].

[160] I. Arsene et al. "On the evolution of the nuclear modification factors with rapidity and centrality in d + Au collisions at s(NN)**(1/2) = 200-GeV". In: *Phys. Rev. Lett.* 93 (2004), p. 242303. DOI: 10.1103/PhysRevLett.93.242303. arXiv: nucl-ex/0403005 [nucl-ex].

[161] B. B. Back et al. "Centrality dependence of charged hadron transverse momentum spectra in d + Au collisions at S(NN)**1/2 = 200 GeV". In: *Phys. Rev. Lett.* 91 (2003), p. 072302. DOI: 10.1103/PhysRevLett.91.072302. arXiv: nucl-ex/0306025 [nucl-ex].

[162] S. S. Adler et al. "Absence of suppression in particle production at large transverse momentum in S(NN)**(1/2) = 200-GeV d + Au collisions". In: *Phys. Rev. Lett.* 91 (2003), p. 072303. DOI: 10.1103/PhysRevLett.91.072303. arXiv: nucl-ex/0306021 [nucl-ex].

[163] J. Adams et al. "Identified hadron spectra at large transverse momentum in p+p and d+Au collisions at s(NN)**(1/2) = 200-GeV". In: *Phys. Lett.* B637 (2006), pp. 161–169. DOI: 10.1016/j.physletb.2006.04.032. arXiv: nucl-ex/0601033 [nucl-ex].

[164] CMS Collaboration. "Measurement of inclusive jet nuclear modification factor in pPb collisions at sqrtsNN=5.02 TeV with CMS". In: (2014).

[165] CMS Collaboration. *Nuclear Modification Factor RpA of b jets in pPb collisions*. CMS-PAS-HIN-14-007. 2014.

[166] Miklos Gyulassy and Larry McLerran. "New forms of QCD matter discovered at RHIC". In: *Nucl. Phys.* A750 (2005), pp. 30–63. DOI: 10.1016/j.nuclphysa.2004.10.034. arXiv: nucl-th/0405013 [nucl-th].

[167] Isobel Kolbe. "Short path length pQCD corrections to energy loss in the quark gluon plasmaShort path length pQCD corrections to energy loss in the quark gluon plasma".

In: *J. Phys. Conf. Ser.* 668.1 (2016), p. 012107. DOI: 10.1088/1742-6596/668/1/012107. arXiv: 1509.06122 [hep-ph].

[168] Nestor Armesto et al. "Comparison of Jet Quenching Formalisms for a Quark-Gluon Plasma 'Brick'". In: *Phys. Rev.* C86 (2012), p. 064904. DOI: 10.1103/PhysRevC.86.064904. arXiv: 1106.1106 [hep-ph].

[169] Xilin Zhang and Jinfeng Liao. "Jet Quenching and Its Azimuthal Anisotropy in AA and possibly High Multiplicity pA and dA Collisions". In: (2013). arXiv: 1311.5463 [nucl-th].

[170] Chanwook Park et al. "Rapidity-dependent jet energy loss in small systems with finite-size effects and running coupling". In: *Nucl. Part. Phys. Proc.* 289-290 (2017), pp. 289–292. DOI: 10.1016/j.nuclphysbps.2017.05.066. arXiv: 1612.06754 [nucl-th].

[171] Simon Wicks et al. "Elastic, inelastic, and path length fluctuations in jet tomography". In: *Nucl. Phys.* A784 (2007), pp. 426–442. DOI: 10.1016/j.nuclphysa.2006.12.048. arXiv: nucl-th/0512076 [nucl-th].

[172] Magdalena Djordjevic. "Theoretical formalism of radiative jet energy loss in a finite size dynamical QCD medium". In: *Phys. Rev.* C80 (2009), p. 064909. DOI: 10.1103/PhysRevC.80.064909. arXiv: 0903.4591 [nucl-th].

[173] Magdalena Djordjevic and Ulrich W. Heinz. "Radiative energy loss in a finite dynamical QCD medium". In: *Phys. Rev. Lett.* 101 (2008), p. 022302. DOI: 10.1103/PhysRevLett.101.022302. arXiv: 0802.1230 [nucl-th].

[174] W. A. Horowitz and B. A. Cole. "Systematic theoretical uncertainties in jet quenching due to gluon kinematics". In: *Phys. Rev.* C81 (2010), p. 024909. DOI: 10.1103/PhysRevC.81.024909. arXiv: 0910.1823 [hep-ph].

[175] Bojana Blagojevic, Magdalena Djordjevic, and Marko Djordjevic. "Calculating hard probe radiative energy loss beyond soft-gluon approximation: how valid is the approximation?" In: (2018). arXiv: 1804.07593 [nucl-th].

[176] Magdalena Djordjevic and Miklos Gyulassy. "The Ter-Mikayelian effect on QCD radiative energy loss". In: *Phys. Rev.* C68 (2003), p. 034914. DOI: 10.1103/PhysRevC.68.034914. arXiv: nucl-th/0305062 [nucl-th].

[177] A. Majumder and M. Van Leeuwen. "The Theory and Phenomenology of Perturbative QCD Based Jet Quenching". In: *Prog. Part. Nucl. Phys.* 66 (2011), pp. 41–92. DOI: 10.1016/j.ppnp.2010.09.001. arXiv: 1002.2206 [hep-ph].

[178] Simon Caron-Huot and Charles Gale. "Finite-size effects on the radiative energy loss of a fast parton in hot and dense strongly interacting matter". In: *Phys. Rev.* C82 (2010), p. 064902. DOI: 10.1103/PhysRevC.82.064902. arXiv: 1006.2379 [hep-ph].

[179] A. Adare et al. "Onset of pi0 Suppression Studied in Cu+Cu Collisions at sNN=22.4, 62.4, and 200 GeV". In: *Phys. Rev. Lett.* 101 (2008), p. 162301. DOI: 10.1103/PhysRevLett.101.162301. arXiv: 0801.4555 [nucl-ex].

[180] B. I. Abelev et al. “Spectra of identified high-p_T $\pi^{\pm}$ and $p(\bar{p})$ in Cu+Cu collisions at $\sqrt{s_{NN}} = 200$ GeV”. In: *Phys. Rev.* C81 (2010), p. 054907. DOI: 10.1103/PhysRevC.81.054907. arXiv: 0911.3130 [nucl-ex].

[181] S. Afanasiev et al. “High-pT pi0 Production with Respect to the Reaction Plane in Au + Au Collisions at s(NN)**(1/2) = 200-GeV”. In: *Phys. Rev.* C80 (2009), p. 054907. DOI: 10.1103/PhysRevC.80.054907. arXiv: 0903.4886 [nucl-ex].

[182] B. G. Zakharov. “Parton energy loss in the mini quark-gluon plasma and jet quenching in proton-proton collisions”. In: *J. Phys.* G41 (2014), p. 075008. DOI: 10.1088/0954-3899/41/7/075008. arXiv: 1311.1159 [hep-ph].

[183] Aleksi Kurkela and Egang Lu. “Approach to Equilibrium in Weakly Coupled Non-Abelian Plasmas”. In: *Phys. Rev. Lett.* 113.18 (2014), p. 182301. DOI: 10.1103/PhysRevLett.113.182301. arXiv: 1405.6318 [hep-ph].

[184] Wilke van der Schee, Paul Romatschke, and Scott Pratt. “Fully Dynamical Simulation of Central Nuclear Collisions”. In: *Phys. Rev. Lett.* 111.22 (2013), p. 222302. DOI: 10.1103/PhysRevLett.111.222302. arXiv: 1307.2539 [nucl-th].

[185] Liam Keegan et al. “Initial conditions for hydrodynamics from weakly coupled pre-equilibrium evolution”. In: *JHEP* 08 (2016), p. 171. DOI: 10.1007/JHEP08(2016)171. arXiv: 1605.04287 [hep-ph].

[186] Aleksi Kurkela et al. “Effective kinetic description of event-by-event pre-equilibrium dynamics in high-energy heavy-ion collisions”. In: (2018). arXiv: 1805.00961 [hep-ph].

[187] Aleksi Kurkela et al. “Matching the non-equilibrium initial stage of heavy ion collisions to hydrodynamics with QCD kinetic theory”. In: (2018). arXiv: 1805.01604 [hep-ph].

[188] Aleksi Kurkela. “Thermalization in collisions of large nuclei at high energies”. In: (2013). [PoSConfinementX,174(2012)]. DOI: 10.22323/1.171.0174. arXiv: 1303.4639 [hep-ph].

[189] H. B. G. Casimir. “On the Attraction Between Two Perfectly Conducting Plates”. In: *Indag. Math.* 10 (1948). [Kon. Ned. Akad. Wetensch. Proc.100N3-4,61(1997)], pp. 261–263.

[190] E." "Lifshitz. “"The Theory of Molecular Attractive Forces between Solids"”. In: *"Soviet Physics"* 2.1 (1956).

[191] R. L. Jaffe. “The Casimir effect and the quantum vacuum”. In: *Phys. Rev.* D72 (2005), p. 021301. DOI: 10.1103/PhysRevD.72.021301. arXiv: hep-th/0503158 [hep-th].

[192] N. Graham et al. “The Dirichlet Casimir problem”. In: *Nucl. Phys.* B677 (2004), pp. 379–404. DOI: 10.1016/j.nuclphysb.2003.11.001. arXiv: hep-th/0309130 [hep-th].

[193] M. Bordag et al. “Advances in the Casimir effect”. In: *Int. Ser. Monogr. Phys.* 145 (2009), pp. 1–768.

[194] R. D. M. De Paola, R. B. Rodrigues, and N. F. Svaiter. "Casimir energy of massless fermions in the slab bag". In: *Mod. Phys. Lett.* A14 (1999), pp. 2353–2362. DOI: 10.1142/S0217732399002431. arXiv: hep-th/9905039 [hep-th].

[195] M. De Francia. "Free energy for massless confined fields". In: *Phys. Rev.* D50 (1994), pp. 2908–2919. DOI: 10.1103/PhysRevD.50.2908.

[196] Dieter H E Gross. *Microcanonical Thermodynamics*. WORLD SCIENTIFIC, 2001. DOI: 10.1142/4340. eprint: https://www.worldscientific.com/doi/pdf/10.1142/4340. URL: https://www.worldscientific.com/doi/abs/10.1142/4340.

[197] Hongbo Cheng. "The Casimir energy for a rectangular cavity at finite temperature". In: *Journal of Physics A: Mathematical and General* 35.9 (2002), p. 2205. URL: http://stacks.iop.org/0305-4470/35/i=9/a=310.

[198] N. F. Svaiter. "Finite size effects in thermal field theory". In: *J. Math. Phys.* 45 (2004), pp. 4524–4538. DOI: 10.1063/1.1808485. arXiv: hep-th/0410016 [hep-th].

[199] Loris Ferrari. "Comparing Boltzmann and Gibbs definitions of entropy in small systems". In: *The European Physical Journal Plus* 132.11 (Nov. 2017), p. 487. ISSN: 2190-5444. DOI: 10.1140/epjp/i2017-11756-5. URL: https://doi.org/10.1140/epjp/i2017-11756-5.

[200] Terrell L. Hill. "Thermodynamics of Small Systems". In: *The Journal of Chemical Physics* 36.12 (1962), pp. 3182–3197. DOI: 10.1063/1.1732447. eprint: https://doi.org/10.1063/1.1732447. URL: https://doi.org/10.1063/1.1732447.

[201] Hugo Touchette, Richard S. Ellis, and Bruce Turkington. "An introduction to the thermodynamic and macrostate levels of nonequivalent ensembles". In: *Physica A: Statistical Mechanics and its Applications* 340.1 (2004). News and Expectations in Thermostatistics, pp. 138–146. ISSN: 0378-4371. DOI: https://doi.org/10.1016/j.physa.2004.03.088. URL: http://www.sciencedirect.com/science/article/pii/S037843710400408X.

[202] Jörn Dunkel and Stefan Hilbert. "Phase transitions in small systems: Microcanonical vs. canonical ensembles". In: *Physica A: Statistical Mechanics and its Applications* 370.2 (2006), pp. 390–406. ISSN: 0378-4371. DOI: https://doi.org/10.1016/j.physa.2006.05.018. URL: http://www.sciencedirect.com/science/article/pii/S0378437106006005.

[203] Alessandro Campa, Thierry Dauxois, and Stefano Ruffo. "Statistical mechanics and dynamics of solvable models with long-range interactions". In: *Physics Reports* 480.3 (2009), pp. 57–159. ISSN: 0370-1573. DOI: https://doi.org/10.1016/j.physrep.2009.07.001. URL: http://www.sciencedirect.com/science/article/pii/S0370157309001586.

[204] Philippe Chomaz and Francesca Gulminelli. "Phase Transitions in Finite Systems". In: *Dynamics and Thermodynamics of Systems with Long-Range Interactions*. Ed. by Thierry Dauxois et al. Berlin, Heidelberg: Springer Berlin Heidelberg, 2002, pp. 68–129.

[205] Joseph V. Pulé and Valentin A. Zagrebnov. "The canonical perfect Bose gas in Casimir boxes". In: *Journal of Mathematical Physics* 45.9 (2004), pp. 3565–3583. DOI: 10.1063/1.1777402. eprint: https://doi.org/10.1063/1.1777402. URL: https://doi.org/10.1063/1.1777402.

[206] Johannes Bausch et al. "Size-driven quantum phase transitions". In: *Proceedings of the National Academy of Sciences* 115.1 (2018), pp. 19–23. ISSN: 0027-8424. DOI: 10.1073/pnas.1705042114. eprint: http://www.pnas.org/content/115/1/19.full.pdf. URL: http://www.pnas.org/content/115/1/19.

[207] Sylvain Mogliacci, Isobel Kolbé, and W. A. Horowitz. "From Heavy-Ion Collisions to Compact Stars: Equation of State and Relevance of the System Size". In: *Universe* 4.1 (2018), p. 14. DOI: 10.3390/universe4010014. arXiv: 1801.08187 [hep-ph].

[208] Constantino Tsallis. "Possible Generalization of Boltzmann-Gibbs Statistics". In: *J. Statist. Phys.* 52 (1988), pp. 479–487. DOI: 10.1007/BF01016429.

[209] C. Tsallis, R. S. Mendes, and A. R. Plastino. "The Role of constraints within generalized nonextensive statistics". In: *Physica* A261 (1998), p. 534. DOI: 10.1016/S0378-4371(98)00437-3.

[210] R. H. Swendsen. "Thermodynamics, statistical mechanics and entropy". In: *Entropy* 19.11 (Nov. 2017), p. 603. DOI: 10.3390/e19110603. URL: https://doi.org/10.3390/e19110603.

[211] Yukinao Akamatsu, Aleksas Mazeliauskas, and Derek Teaney. "A kinetic regime of hydrodynamic fluctuations and long time tails for a Bjorken expansion". In: *Phys. Rev.* C95.1 (2017), p. 014909. DOI: 10.1103/PhysRevC.95.014909. arXiv: 1606.07742 [nucl-th].

[212] Shyamal Biswas. "Bose-Einstein condensation and Casimir effect of trapped ideal Bose gas in between two slabs". In: *The European Physical Journal D* 42.1 (Apr. 2007), pp. 109–112. ISSN: 1434-6079. DOI: 10.1140/epjd/e2007-00007-y. URL: https://doi.org/10.1140/epjd/e2007-00007-y.

[213] Jeong-Hyuck Park and Sang-Woo Kim. "Thermodynamic instability and first-order phase transition in an ideal Bose gas". In: *Phys. Rev.* A81 (2010), p. 063636. DOI: 10.1103/PhysRevA.81.063636. arXiv: 0809.4652 [cond-mat.stat-mech].

[214] Harvey B. Meyer. "Finite Volume Effects in Thermal Field Theory". In: *JHEP* 07 (2009), p. 059. DOI: 10.1088/1126-6708/2009/07/059. arXiv: 0905.1663 [hep-th].

[215] Leonardo Giusti and Harvey B. Meyer. "Thermodynamic potentials from shifted boundary conditions: the scalar-field theory case". In: *JHEP* 11 (2011), p. 087. DOI: 10.1007/JHEP11(2011)087. arXiv: 1110.3136 [hep-lat].

[216] Jens Braun, Bertram Klein, and Bernd-Jochen Schaefer. "On the Phase Structure of QCD in a Finite Volume". In: *Phys. Lett.* B713 (2012), pp. 216–223. DOI: 10.1016/j.physletb.2012.05.053. arXiv: 1110.0849 [hep-ph].

[217] Johan Bijnens, Emil Boström, and Timo A. Lähde. "Two-loop Sunset Integrals at Finite Volume". In: *JHEP* 01 (2014), p. 019. DOI: 10.1007/JHEP01(2014)019. arXiv: 1311.3531 [hep-lat].

[218] Leonard Fister and Jan Martin Pawlowski. "Functional renormalization group in a finite volume". In: *Phys. Rev.* D92.7 (2015), p. 076009. DOI: 10.1103/PhysRevD.92.076009. arXiv: 1504.05166 [hep-ph].

[219] A. S. Parvan. "Finite size effects in the thermodynamics of a free neutral scalar field". In: *Physica* A496 (2018), pp. 410–433. DOI: 10.1016/j.physa.2017.12.107. arXiv: 1505.05838 [hep-ph].

[220] Eduardo S. Fraga, Daniel Kroff, and Jorge Noronha. "Linde problem in Yang-Mills theory compactified on $\mathbb{R}^2 \times \mathbb{T}^2$". In: *Phys. Rev.* D95.3 (2017), p. 034031. DOI: 10.1103/PhysRevD.95.034031. arXiv: 1610.01130 [hep-th].

[221] Ana Juričić and Bernd-Jochen Schaefer. "Chiral Thermodynamics in a finite box". In: *Acta Phys. Polon. Supp.* 10 (2017), p. 609. DOI: 10.5506/APhysPolBSupp.10.609. arXiv: 1611.03653 [hep-ph].

[222] Gabor Almasi, Robert Pisarski, and Vladimir Skokov. "Volume dependence of baryon number cumulants and their ratios". In: *Phys. Rev.* D95.5 (2017), p. 056015. DOI: 10.1103/PhysRevD.95.056015. arXiv: 1612.04416 [hep-ph].

[223] Alexei Bazavov and Bernd A. Berg. "Deconfining Phase Transition on Lattices with Boundaries at Low Temperature". In: *Phys. Rev.* D76 (2007), p. 014502. DOI: 10.1103/PhysRevD.76.014502. arXiv: hep-lat/0701007 [hep-lat].

[224] Antonino Flachi. "Interacting Fermions, Boundaries, and Finite Size Effects". In: *Phys. Rev.* D86 (2012), p. 104047. DOI: 10.1103/PhysRevD.86.104047. arXiv: 1209.4754 [hep-th].

[225] Bernd A. Berg and Hao Wu. "SU(3) deconfining phase transition with finite volume corrections due to a confined exterior". In: *Phys. Rev.* D88 (2013), p. 074507. DOI: 10.1103/PhysRevD.88.074507. arXiv: 1305.2975 [hep-lat].

[226] Carl M. Bender and P. Hays. "Zero Point Energy of Fields in a Finite Volume". In: *Phys. Rev.* D14 (1976), pp. 2622–2632. DOI: 10.1103/PhysRevD.14.2622.

[227] Siegfried Grossmann and Martin Holthaus. "Bose-Einstein condensation in a cavity". In: *Zeitschrift für Physik B Condensed Matter* 97.2 (June 1995), pp. 319–326. DOI: 10.1007/BF01307482. URL: https://doi.org/10.1007/BF01307482.

[228] Klaus Kirsten and David J. Toms. "Bose-Einstein condensation in arbitrarily shaped cavities". In: *Phys. Rev.* E59 (1999), pp. 158–167. DOI: 10.1103/PhysRevE.59.158.

[229] Klaus Kirsten. "Grand thermodynamic potential in a static space-time with boundary". In: *Class. Quant. Grav.* 8 (1991), pp. 2239–2255. DOI: 10.1088/0264-9381/8/12/009.

[230] M. N. Chernodub, V. A. Goy, and A. V. Molochkov. "Casimir effect and deconfinement phase transition". In: *Phys. Rev.* D96.9 (2017), p. 094507. DOI: 10.1103/PhysRevD.96.094507. arXiv: 1709.02262 [hep-lat].

[231] N. Graham et al. "Casimir energies in light of quantum field theory". In: *Phys. Lett.* B572 (2003), pp. 196–201. DOI: 10.1016/j.physletb.2003.03.003. arXiv: hep-th/0207205 [hep-th].

[232] E. Elizalde. "On the issue of imposing boundary conditions on quantum fields". In: *J. Phys.* A36 (2003), p. L567. DOI: 10.1088/0305-4470/36/45/L01. arXiv: hep-th/0309075 [hep-th].

[233] A. Chodos et al. "A New Extended Model of Hadrons". In: *Phys. Rev.* D9 (1974), pp. 3471–3495. DOI: 10.1103/PhysRevD.9.3471.

[234] G. Boyd et al. "Thermodynamics of SU(3) lattice gauge theory". In: *Nucl. Phys.* B469 (1996), pp. 419–444. DOI: 10.1016/0550-3213(96)00170-8. arXiv: hep-lat/9602007 [hep-lat].

[235] F. Karsch, E. Laermann, and A. Peikert. "The Pressure in two flavor, (2+1)-flavor and three flavor QCD". In: *Phys. Lett.* B478 (2000), pp. 447–455. DOI: 10.1016/S0370-2693(00)00292-6. arXiv: hep-lat/0002003 [hep-lat].

[236] C. R. Allton et al. "The QCD thermal phase transition in the presence of a small chemical potential". In: *Phys. Rev.* D66 (2002), p. 074507. DOI: 10.1103/PhysRevD.66.074507. arXiv: hep-lat/0204010 [hep-lat].

[237] Y. Aoki et al. "The QCD transition temperature: Results with physical masses in the continuum limit". In: *Phys. Lett.* B643 (2006), pp. 46–54. DOI: 10.1016/j.physletb.2006.10.021. arXiv: hep-lat/0609068 [hep-lat].

[238] A. Bazavov et al. "Equation of state and QCD transition at finite temperature". In: *Phys. Rev.* D80 (2009), p. 014504. DOI: 10.1103/PhysRevD.80.014504. arXiv: 0903.4379 [hep-lat].

[239] Szabolcs Borsanyi et al. "Is there still any T_c mystery in lattice QCD? Results with physical masses in the continuum limit III". In: *JHEP* 09 (2010), p. 073. DOI: 10.1007/JHEP09(2010)073. arXiv: 1005.3508 [hep-lat].

[240] Claudia Ratti et al. "Are there hadronic bound states above the QCD transition temperature?" In: *Phys. Rev.* D85 (2012), p. 014004. DOI: 10.1103/PhysRevD.85.014004. arXiv: 1109.6243 [hep-ph].

[241] A. Bazavov et al. "The chiral and deconfinement aspects of the QCD transition". In: *Phys. Rev.* D85 (2012), p. 054503. DOI: 10.1103/PhysRevD.85.054503. arXiv: 1111.1710 [hep-lat].

[242] A. Bazavov et al. "Strangeness at high temperatures: from hadrons to quarks". In: *Phys. Rev. Lett.* 111 (2013), p. 082301. DOI: 10.1103/PhysRevLett.111.082301. arXiv: 1304.7220 [hep-lat].

[243] S. Borsanyi et al. "Freeze-out parameters: lattice meets experiment". In: *Phys. Rev. Lett.* 111 (2013), p. 062005. DOI: 10.1103/PhysRevLett.111.062005. arXiv: 1305.5161 [hep-lat].

[244] Masakiyo Kitazawa et al. "Equation of State for SU(3) Gauge Theory via the Energy-Momentum Tensor under Gradient Flow". In: *Phys. Rev.* D94.11 (2016), p. 114512. DOI: 10.1103/PhysRevD.94.114512. arXiv: 1610.07810 [hep-lat].

[245] Sz. Borsanyi et al. "Calculation of the axion mass based on high-temperature lattice quantum chromodynamics". In: *Nature* 539.7627 (2016), pp. 69–71. DOI: 10.1038/nature20115. arXiv: 1606.07494 [hep-lat].

[246] Yusuke Taniguchi et al. "Exploring N_f = 2+1 QCD thermodynamics from the gradient flow". In: *Phys. Rev.* D96.1 (2017), p. 014509. DOI: 10.1103/PhysRevD.96.014509. arXiv: 1609.01417 [hep-lat].

[247] Christian Schmidt and Sayantan Sharma. "The phase structure of QCD". In: *J. Phys.* G44.10 (2017), p. 104002. DOI: 10.1088/1361-6471/aa824a. arXiv: 1701.04707 [hep-lat].

[248] Takeo Matsubara. "A New approach to quantum statistical mechanics". In: *Prog. Theor. Phys.* 14 (1955), pp. 351–378. DOI: 10.1143/PTP.14.351.

[249] R. P. Feynman. "Space-time approach to nonrelativistic quantum mechanics". In: *Rev. Mod. Phys.* 20 (1948), pp. 367–387. DOI: 10.1103/RevModPhys.20.367.

[250] N. P. Landsman and C. G. van Weert. "Real and Imaginary Time Field Theory at Finite Temperature and Density". In: *Phys. Rept.* 145 (1987), p. 141. DOI: 10.1016/0370-1573(87)90121-9.

[251] Ulrike Kraemmer and Anton Rebhan. "Advances in perturbative thermal field theory". In: *Rept. Prog. Phys.* 67 (2004), p. 351. DOI: 10.1088/0034-4885/67/3/R05. arXiv: hep-ph/0310337 [hep-ph].

[252] Jens O. Andersen and Michael Strickland. "Resummation in hot field theories". In: *Annals Phys.* 317 (2005), pp. 281–353. DOI: 10.1016/j.aop.2004.09.017. arXiv: hep-ph/0404164 [hep-ph].

[253] J. I. Kapusta and Charles Gale. *Finite-temperature field theory: Principles and applications*. Cambridge Monographs on Mathematical Physics. Cambridge University Press, 2011. ISBN: 9780521173223, 9780521820820, 9780511222801. DOI: 10.1017/CBO9780511535130.

[254] Michel Le Bellac. *Thermal Field Theory*. Cambridge Monographs on Mathematical Physics. Cambridge University Press, 2011. ISBN: 9780511885068, 9780521654777. DOI: 10.1017/CBO9780511721700. URL: http://www.cambridge.org/mw/academic/subjects/physics/theoretical-physics-and-mathematical-physics/thermal-field-theory?format=AR.

[255] Mikko Laine and Aleksi Vuorinen. "Basics of Thermal Field Theory". In: *Lect. Notes Phys.* 925 (2016), pp.1–281. DOI: 10.1007/978-3-319-31933-9. arXiv: 1701.01554 [hep-ph].

[256] Klaus Kirsten. "Basic zeta functions and some applications in physics". In: *MSRI Publ.* 57 (2010), pp. 101–143. arXiv: 1005.2389 [hep-th].

[257] Claude W. Bernard. "Feynman Rules for Gauge Theories at Finite Temperature". In: *Phys. Rev.* D9 (1974), p. 3312. DOI: 10.1103/PhysRevD.9.3312.

[258] M. W. Zemansky. *Heat and Thermodynamics*. 7th. Mc Graw Hill, 1997.

[259] H. B. Callen. *Thermodynamics and an introduction to thermostatistics*. John Wiley & Sons, Inc, 1985.

[260] M. Le Bellac, F. Mortessagne, and G. G. Batrouni. *Equilibrium and non-equiibrium statistical thermodynamics*. Cambridge University Press, 2004.

[261] Hugo Touchette. "When is a quantity additive, and when is it extensive?" In: *Physica A: Statistical Mechanics and its Applications* 305 (2002), pp. 84–88. DOI: 10.1073/pnas.1705042114. arXiv: 0201134 [cond-mat]. URL: https://doi.org/10.1016/S0378-4371(01)00644-6.

[262] G. L. Klimchitskaya, U. Mohideen, and V. M. Mostepanenko. "The Casimir force between real materials: Experiment and theory". In: *Rev. Mod. Phys.* 81 (2009), pp. 1827–1885. DOI: 10.1103/RevModPhys.81.1827. arXiv: 0902.4022 [cond-mat.other].

[263] J. S. Hoye et al. "Does the transverse electric zero mode contribute to the Casimir effect for a metal?" In: *Phys. Rev.* E67 (2003), p. 056116. DOI: 10.1103/PhysRevE.67.056116. arXiv: quant-ph/0212125 [quant-ph].

[264] Luca Peliti. *Statistical Mechanics in a nutshell*. Princeton University Press, 2011.

[265] T. C. Dorlas. *Statistical Mechanics: Fundamentals and Model Solutions*. Institute of Physics Publishing, 1999. ISBN: 0750305398.

[266] H. "Touchette, R. S. Ellis, and B." Turkington. ""An introduction to the thermodynamic and macrostate levels of nonequivalent ensembles"". In: *"Physica A: Statistical Mechanics and its Applications"* 340 (2004).

[267] A. Widom et al. "The Casimir effect and thermodynamic instability". In: (1998). arXiv: quant-ph/9803013 [quant-ph].

[268] T. Christodoulakis et al. "Casimir effect in 2-D stringy black hole backgrounds". In: *Phys. Rev.* D64 (2001), p. 124022. DOI: 10.1103/PhysRevD.64.124022. arXiv: hep-th/0107049 [hep-th].

[269] H. Mitter and D. Robaschik. "Thermodynamics of the Casimir effect". In: *Eur. Phys. J.* B13 (2000), pp. 335–340. DOI: 10.1007/s100510050039. arXiv: quant-ph/9902074 [quant-ph].

[270] F. Caruso et al. "On the attractive or repulsive nature of Casimir force in D-dimensional Minkowski space-time". In: *Phys. Rev.* D43 (1991), pp. 1300–1306. DOI: 10.1103/PhysRevD.43.1300.

[271] A. Altland and B. Simons. *Condensed matter field theory*. 2006.

[272] Paul Romatschke. "Do nuclear collisions create a locally equilibrated quark–gluon plasma?" In: *Eur. Phys. J.* C77.1 (2017), p. 21. DOI: 10.1140/epjc/s10052-016-4567-x. arXiv: 1609.02820 [nucl-th].

[273] Jonah E. Bernhard et al. "Applying Bayesian parameter estimation to relativistic heavy-ion collisions: simultaneous characterization of the initial state and quark-gluon plasma medium". In: *Phys. Rev.* C94.2 (2016), p. 024907. DOI: 10.1103/PhysRevC.94.024907. arXiv: 1605.03954 [nucl-th].

[274] Johannes Bausch et al. "Size-driven quantum phase transitions". In: *Proceedings of the National Academy of Sciences* 115.1 (2018), pp. 19–23. ISSN: 0027-8424. DOI: 10.1073/pnas.1705042114. eprint: http://www.pnas.org/content/115/1/19.full.pdf. URL: http://www.pnas.org/content/115/1/19.

[275] Andrei D. Linde. "Infrared Problem in Thermodynamics of the Yang-Mills Gas". In: *Phys. Lett.* 96B (1980), pp. 289–292. DOI: 10.1016/0370-2693(80)90769-8.

[276] Yu. A. Simonov. "Magnetic confinement and the Linde problem". In: *Phys. Rev.* D96.9 (2017), p. 096002. DOI: 10.1103/PhysRevD.96.096002. arXiv: 1605.07060 [hep-ph].

[277] Raghav Kunnawalkam Elayavalli and Korinna Christine Zapp. "Medium response in JEWEL and its impact on jet shape observables in heavy ion collisions". In: *JHEP* 07 (2017), p. 141. DOI: 10.1007/JHEP07(2017)141. arXiv: 1707.01539 [hep-ph].

[278] Raktim Abir. "Jet-parton inelastic interaction beyond eikonal approximation". In: *Phys. Rev.* D87.3 (2013), p. 034036. DOI: 10.1103/PhysRevD.87.034036. arXiv: 1301.1839 [hep-ph].

[279] Trambak Bhattacharyya, Surasree Mazumder, and Raktim Abir. "Soft Gluon Radiation off Heavy Quarks beyond Eikonal Approximation". In: *Adv. High Energy Phys.* 2016 (2016), p. 1298986. DOI: 10.1155/2016/1298986. arXiv: 1307.6931 [hep-ph].

[280] George Leibbrandt. "Introduction to the Technique of Dimensional Regularization". In: *Rev. Mod. Phys.* 47 (1975), p. 849. DOI: 10.1103/RevModPhys.47.849.

[281] William A. Bardeen et al. "Deep Inelastic Scattering Beyond the Leading Order in Asymptotically Free Gauge Theories". In: *Phys. Rev.* D18 (1978), p. 3998. DOI: 10.1103/PhysRevD.18.3998.

[282] Boris M. Kastening. "Four loop vacuum energy beta function in O(N) symmetric scalar theory". In: *Phys. Rev.* D54 (1996), pp. 3965–3975. DOI: 10.1103/PhysRevD.54.3965. arXiv: hep-ph/9604311 [hep-ph].

[283] Jan Ambjorn and Stephen Wolfram. "Properties of the Vacuum. 1. Mechanical and Thermodynamic". In: *Annals Phys.* 147 (1983), p. 1. DOI: 10.1016/0003-4916(83)90065-9.

[284] Jan Ambjorn and Stephen Wolfram. "Properties of the Vacuum. 2. Electrodynamic". In: *Annals Phys.* 147 (1983), p. 33. DOI: 10.1016/0003-4916(83)90066-0.

[285] E. Elizalde and A. Romeo. "Regularization of General Multidimensional Epstein Zeta Functions". In: *Rev. Math. Phys.* 1 (1989), pp. 113–128. DOI: 10.1142/S0129055X89000055.

[286] K. Kirsten. "Generalized multidimensional Epstein zeta functions". In: *J. Math. Phys.* 35 (1994), pp. 459–470. DOI: 10.1063/1.530793.

[287] E. Elizalde. "Analysis of an inhomogeneous generalized Epstein-Hurwitz zeta function with physical applications". In: *J. Math. Phys.* 35 (1994), pp. 6100–6122. DOI: 10.1063/1.530731.

[288] E. Elizalde. "Multidimensional extension of the generalized Chowla-Selberg formula". In: *Commun. Math. Phys.* 198 (1998), pp. 83–95. DOI: 10.1007/s002200050472. arXiv: hep-th/9707257 [hep-th].

[289] Emilio Elizalde. "Zeta Function Methods and Quantum Fluctuations". In: *J. Phys.* A41 (2008), p. 304040. DOI: 10.1088/1751-8113/41/30/304040. arXiv: 0712.1346 [hep-th].

[290] E. Elizalde. "Ten physical applications of spectral zeta functions". In: *Lect. Notes Phys.* 855 (2012), pp. 1–225. DOI: 10.1007/978-3-642-29405-1.

[291] Michael Bordag, U. Mohideen, and V. M. Mostepanenko. "New developments in the Casimir effect". In: *Phys. Rept.* 353 (2001), pp. 1–205. DOI: 10.1016/S0370-1573(01)00015-1. arXiv: quant-ph/0106045 [quant-ph].